EQUATION OF STATE CONSTRAINS THROUGH BINARY NEUTRON STAR MERGERS

NIKOLAOS STERGIOULAS

DEPARTMENT OF PHYSICS
ARISTOTLE UNIVERSITY OF THESSALONIKI

Tuebingen, November 14, 2019

GW170817 Binary Neutron Star (BNS) merger

GW + EM follow up

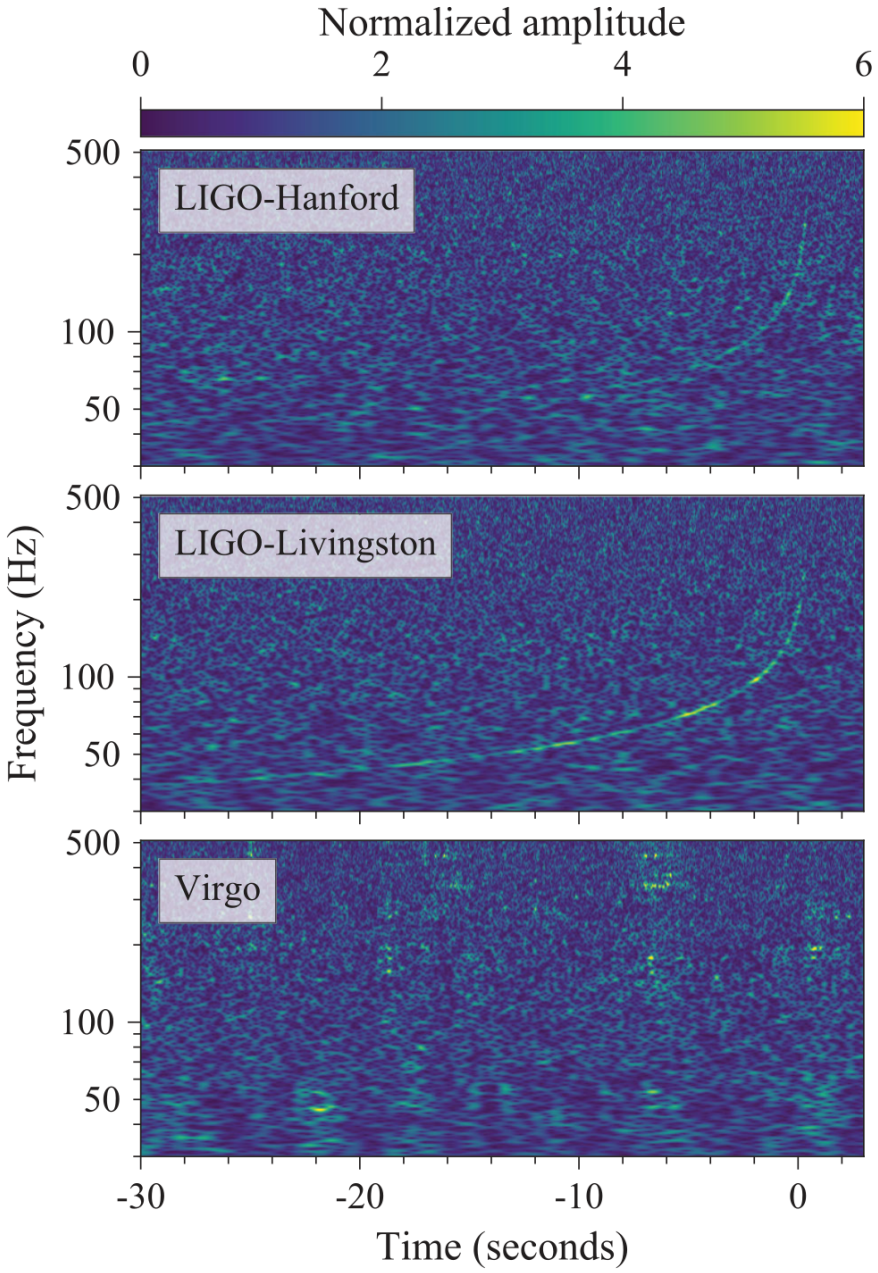

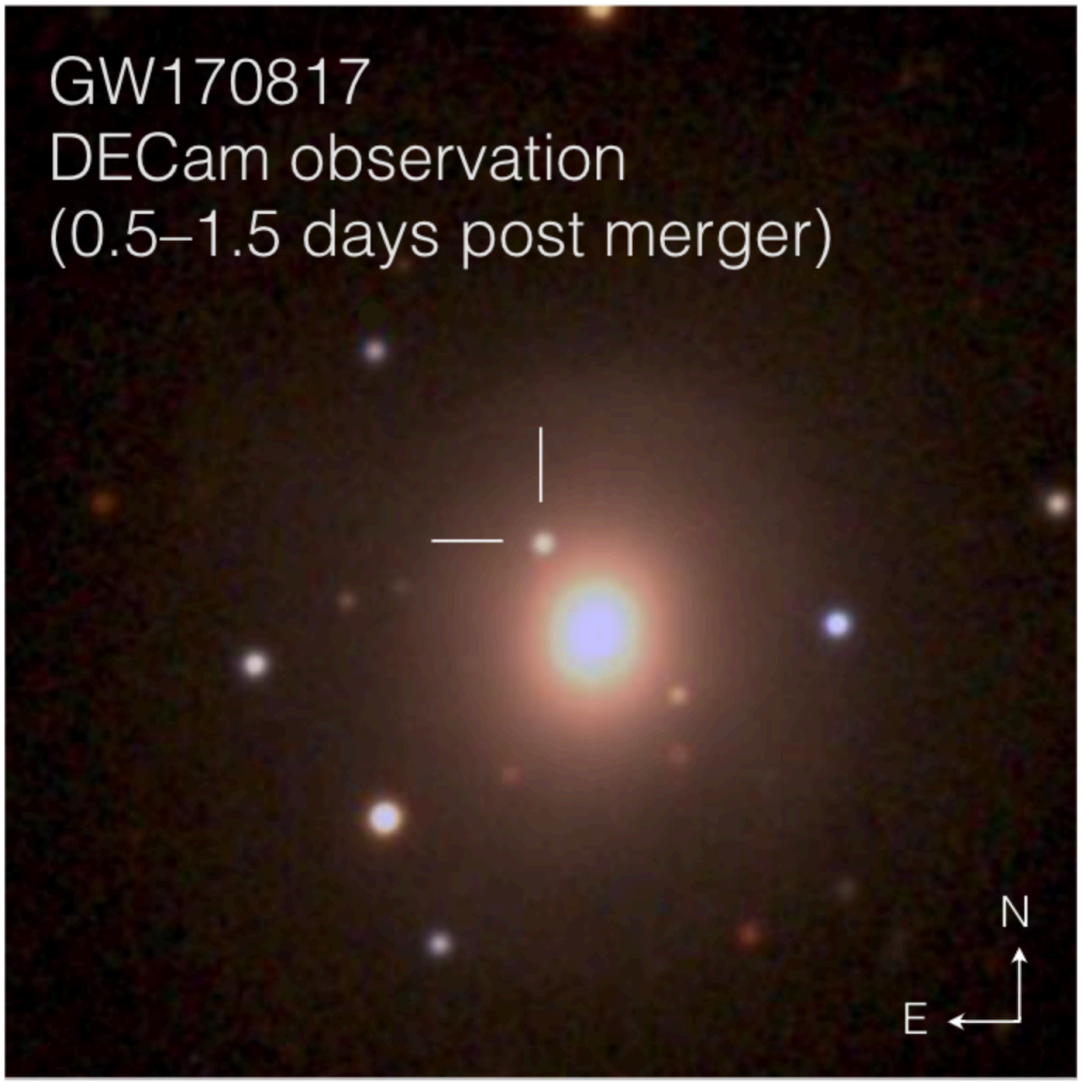

Rence BNS merger candidates

So far in O3 LVC run:

S190910h	BNS (61%), Terrestrial (39%)	Sept. 10, 2019 08:29:58 UTC	GCN Circulars Notices | VOE	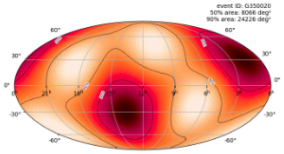	1.1312 per year
S190901ap	BNS (86%), Terrestrial (14%)	Sept. 1, 2019 23:31:01 UTC	GCN Circulars Notices | VOE	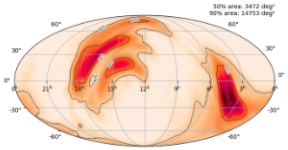	1 per 4.5093 years
S190426c	BNS (49%), MassGap (24%), Terrestrial (14%), NSBH (13%)	April 26, 2019 15:21:55 UTC	GCN Circulars Notices | VOE	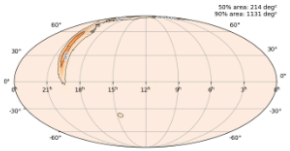	1 per 1.6276 years
S190425z	BNS (>99%)	April 25, 2019 08:18:05 UTC	GCN Circulars Notices | VOE	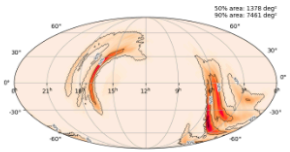	1 per 69834 years

DB: rho.xy_merged.h5
Cycle: 21504 Time:252

Pseudocolor
Var: HYDROBASE--rho
0.001103
6.053e-06
3.321e-08
1.822e-10
1.000e-12
Max: 0.001103
Min: 1.000e-12

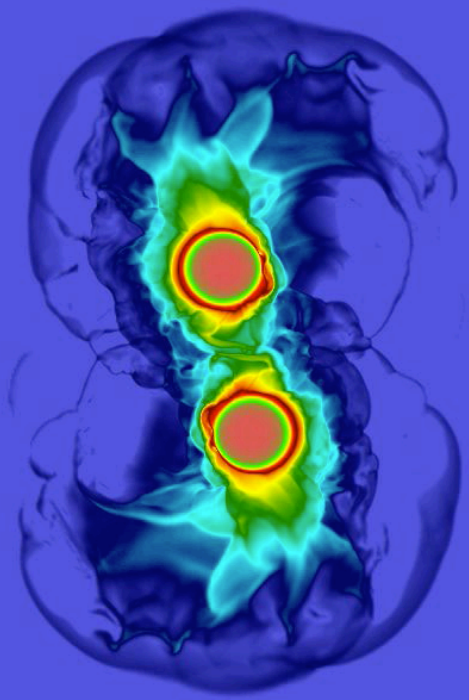

Simulation: Th. Soultanis & NS
Visualization: K. Zagkouris

user: c3po
Sat Mar 16 00:22:11 2019

Gravitational Waves

Soultanis & NS (2018)

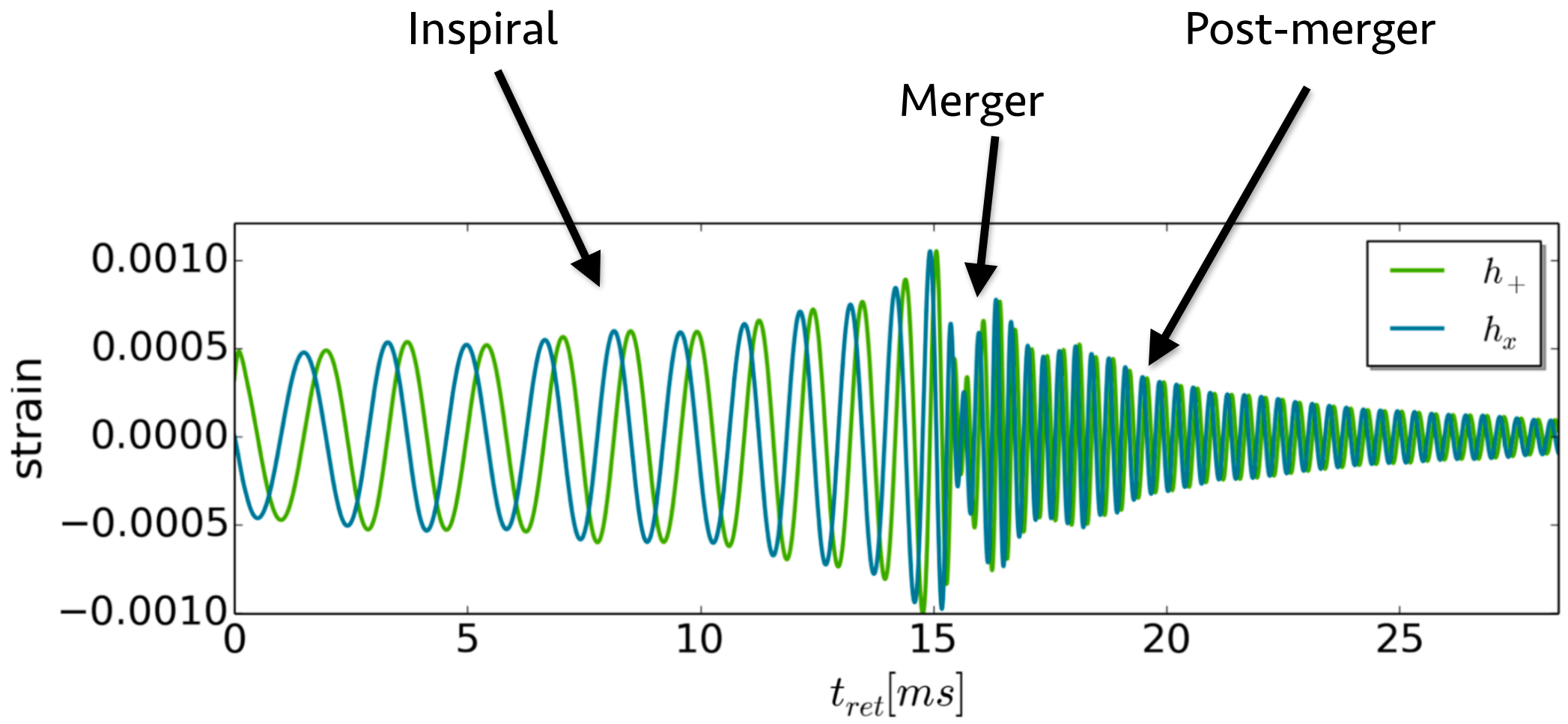

Gravitational Waves

Soultanis & NS (2018)

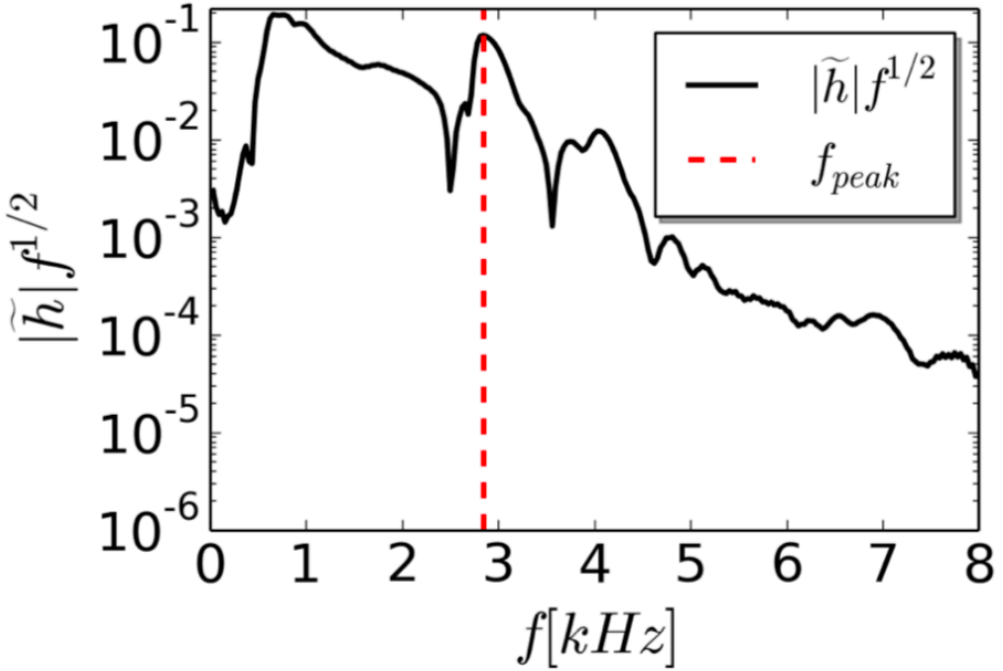

GW spectrum

GW strain

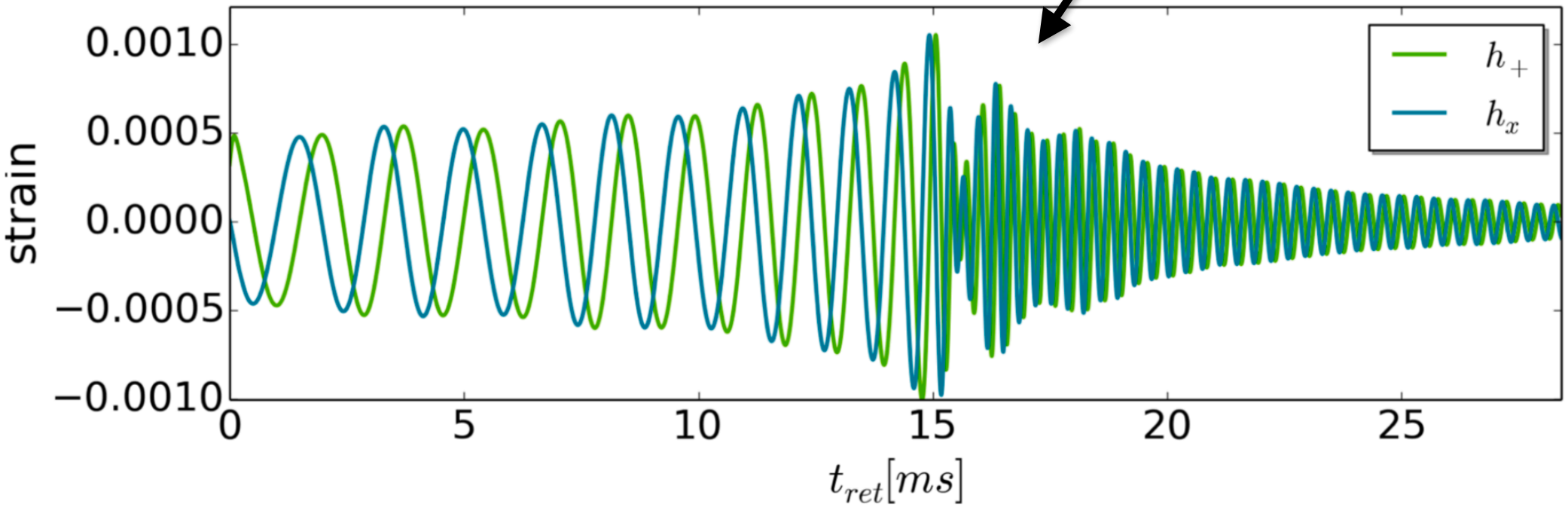

Cold Neutron Star Equation of State (EOS)

The interior of isolated, cold neutron stars is described in different approximations:

1) **Microphysical** (tabulated) EOS (needs high-order interpolation)
2) **Piecewise Polytropic** approximation
3) **Spectral** approximation
   (in terms of basis functions)

Problems of Piecewise Polytropes:

1) *sound speed is not continuous*
2) shock waves and rarefactions waves may not be described correctly in a time evolution

Spectral representation does not have the above problems

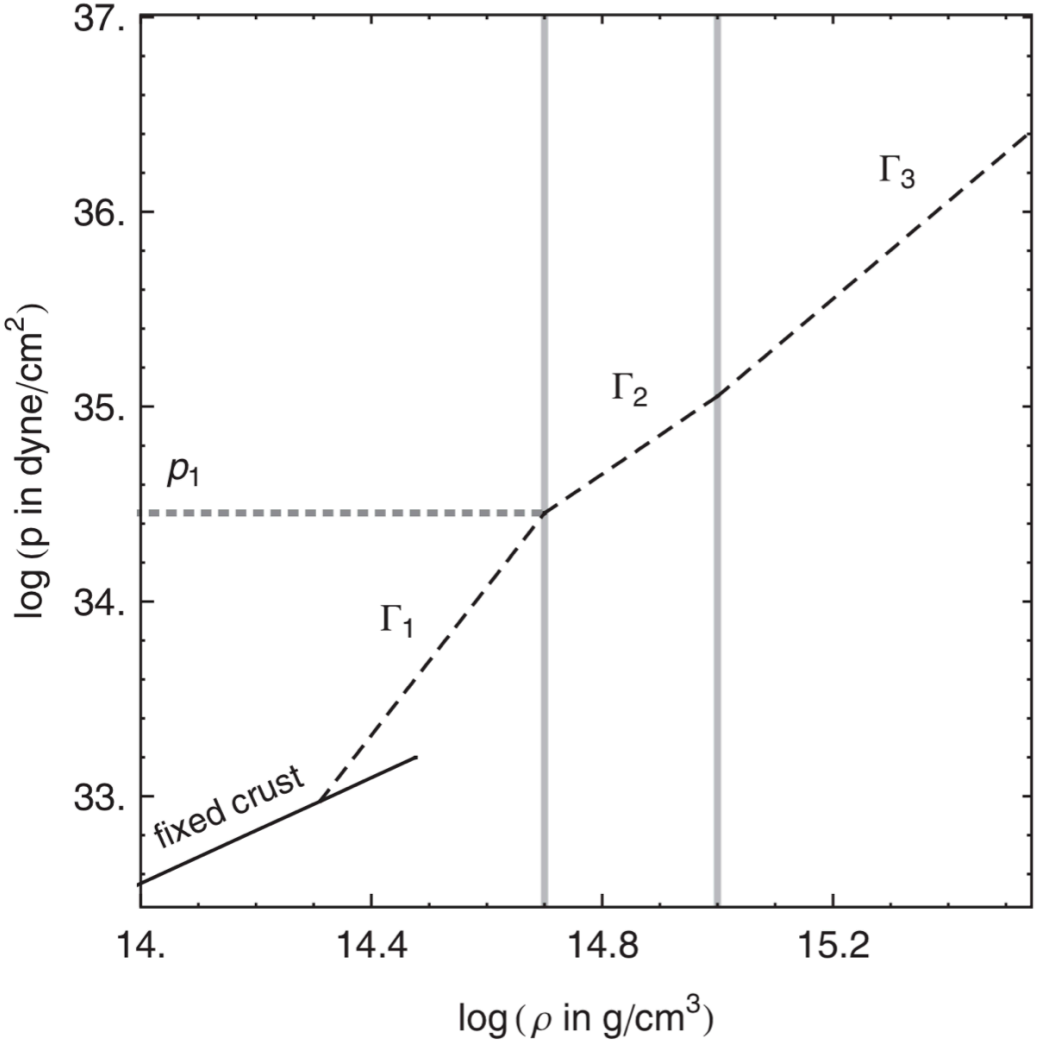

Phase Transitions

Both piecewise and spectral are problematic when there are phase transitions.

If hadrons undergo **deconfinement** at high densities

-> quark-matter core

Several **effective models** to describe phase transitions:

1) simple MIT bag model (massless quarks confined in a bag of finite dimension)
2) more complicated Nambu–Jona-Lasinio model
3) assume a density-independent speed of sound (constant-speed-of-sound parameterisation)

More generally, assume that:

- EoS is known at low densities
- pressure approaches that of deconfined quark matter at high densities

Thermal Structure of BNS Merger Remnant

Parts of the remnant reach temperatures of several tens MeV.

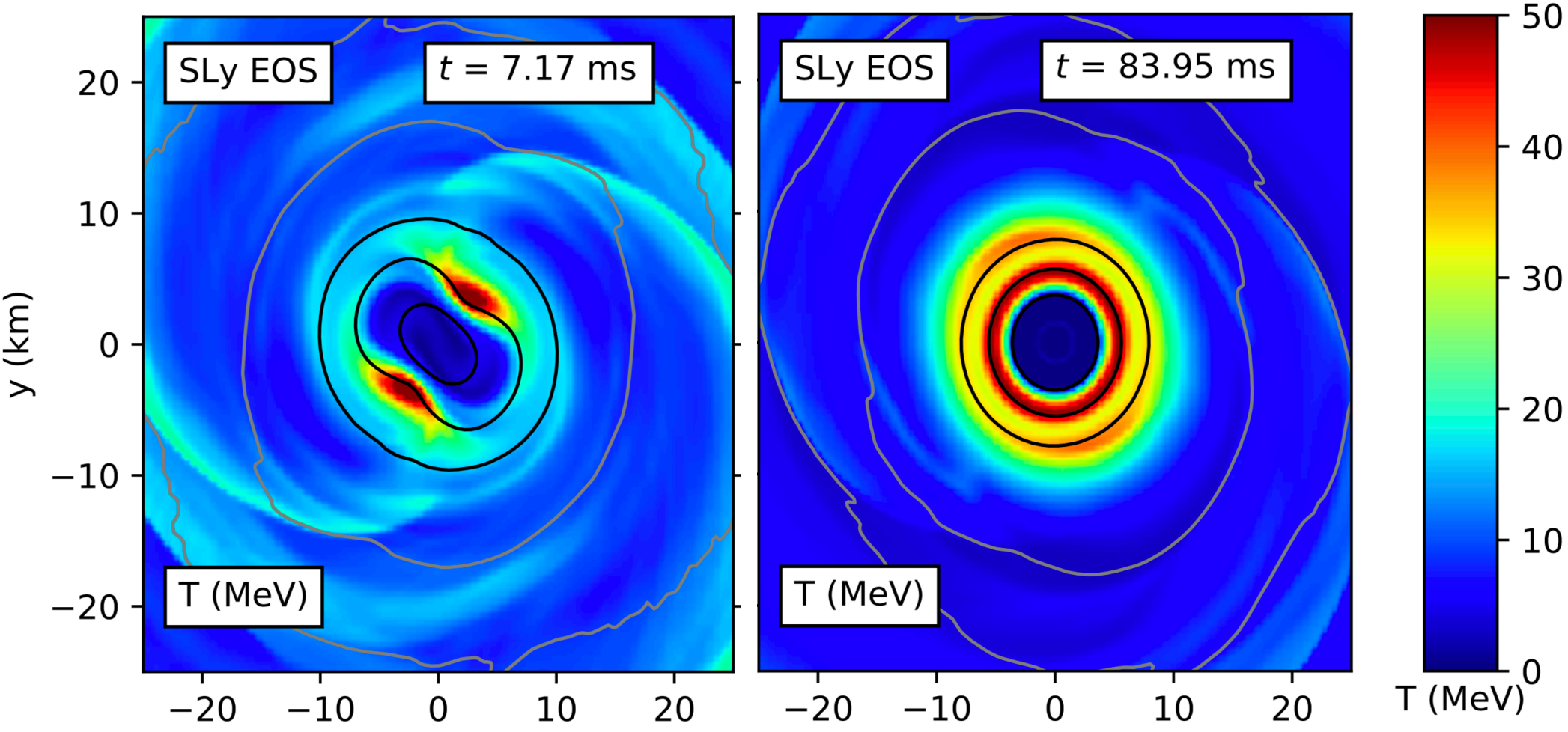

De Pietri et al. (2019)

Hot Neutron Star Equation of State (EOS)

Description of **shock heating** in the BNS remnant requires high-T EOS

1) Hot Microphysical, $P = P(\rho, s, Y_e, \ldots)$

2) Cold EOS + thermal part e.g. $P_{\rm thermal} = (\gamma\text{-}1)\rho\varepsilon$ (ideal fluid)

3) Approximate *Taylor expansions* of temperature dependence:

   a) of the energy per nucleon E

   b) of the proton fraction $x_p = \rho_p/(\rho_n + \rho_p)$ from pure neutron matter to symmetric neutron matter

EOS Constraints through BNS mergers

1) GW @ inspiral (already achieved with GW170817)

2) GW @ post-merger (expected with A+ and 3G detectors)

3) EM emission

4) GW + EM (multimessenger)

5) all of the above + laboratory experiments

Tidal Deformability

Tidal deformation of NS in the field of a companion:

$$Q_{ij} = -\lambda \mathcal{E}_{ij}$$

Induced quadrupole deformation

Proportionality constant

External tidal field

Dimensionless tidal deformability

$$\Lambda \equiv \frac{\lambda}{M^5} = \frac{2}{3}\kappa_2 \left(\frac{R}{M}\right)^5$$

Quadrupole Love number

Calculating the Tidal Deformability

Assume a spherically symmetric, static background spacetime

$$ds_0^2 = -e^{\nu(r)}dt^2 + e^{\gamma(r)}dr^2 + r^2\left(d\theta^2 + \sin^2\theta d\varphi^2\right)$$

Then

$$\begin{aligned}\Lambda =& \frac{16}{15}(1-2C)^2[2+2C(y(R)-1)-y(R)] \\ & \{2C[6-3y(R)+3C(5y(R)-8)] \\ & +4C^3\left[13-11y(R)+C(3y(R)-2)+2C^2(1+y(R))\right] \\ & +3(1-2C)^2[2-y(R)+2C(y(R)-1)]\ln(1-2C)\}^{-1}\end{aligned}$$

where

$$C \equiv M/R$$

and

$$\frac{dy}{dr} = \frac{4\left(m+4\pi r^3 p\right)^2}{r(r-2m)^2} + \frac{6}{r-2m} - \frac{y^2}{r} - \frac{r+4\pi r^3(p-\rho)}{r(r-2m)}y - \frac{4\pi r^2}{r-2m}\left\{5\rho+9p+\frac{\rho+p}{(dp/d\rho)}\right\}$$

Effect of Λ on GWs

Binary system with masses m_A and m_B

the waveform is affected simultaneously by Λ_A and Λ_B

However, to lowest post-Newtonian order, the waveform is to a good approximation influenced by a *single parameter*, the mass-weighted **effective tidal deformability**

where

$$\tilde{\Lambda} = \frac{16}{13}\frac{(1+12q)\Lambda_A + (12+q)q^4\Lambda_B}{(1+q)^5}$$

$$q \equiv m_B/m_A (\leq 1)$$

is the mass ratio of the binary.

From Λ to Radius

One of the main observables of the inspiral GW waveform is the **chirp mass**

$$\mathcal{M}_c = \frac{(m_1 m_2)^{3/5}}{(m_1+m_2)^{1/5}} = m_1 \frac{q^{3/5}}{(1+q)^{1/5}}$$

For GW170817 $\mathcal{M}_c = 1.188^{+0.004}_{-0.002}\ M_\odot$

For fixed M_c ->
nearly mass-independent
empirical relation

Raithel, Oezel
& Psaltis (2018)

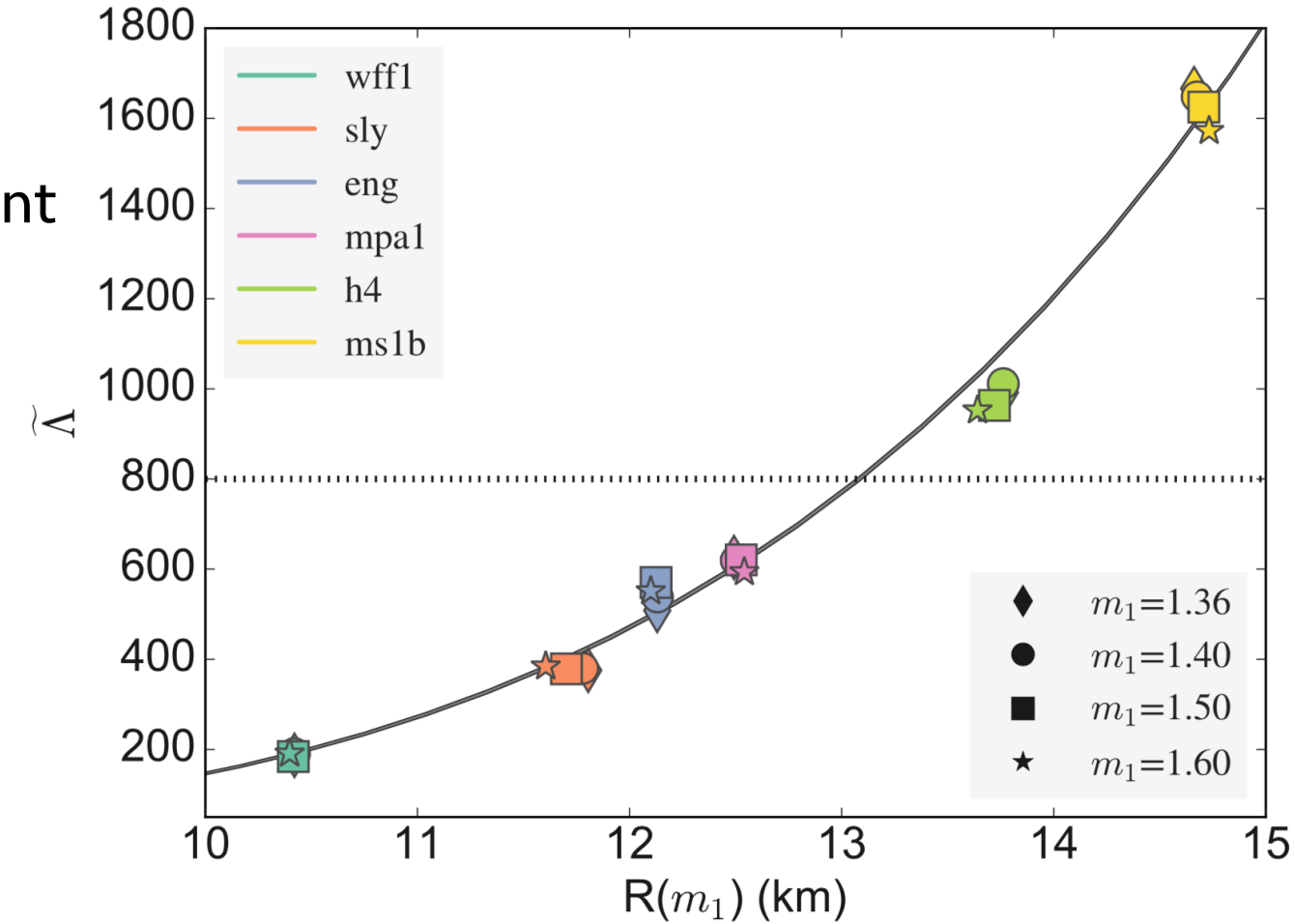

Λ through GW @ Inspiral

For NS binaries with individual masses around $1.4M_\odot$, the dimensionless tidal deformability Λ could be realistically determined with about **10% accuracy** by combining information from about 20 – 100 sources.

Additional effects (may become relevant for next-generation detectors)

1) tidal excitations of *resonant modes*

2) gravitomagnetic excitations of resonant modes

3) resonant shattering of the NS crust by tides

4) nonlinear tidal effects

Empirical Relation for Λ @ Specific Mass

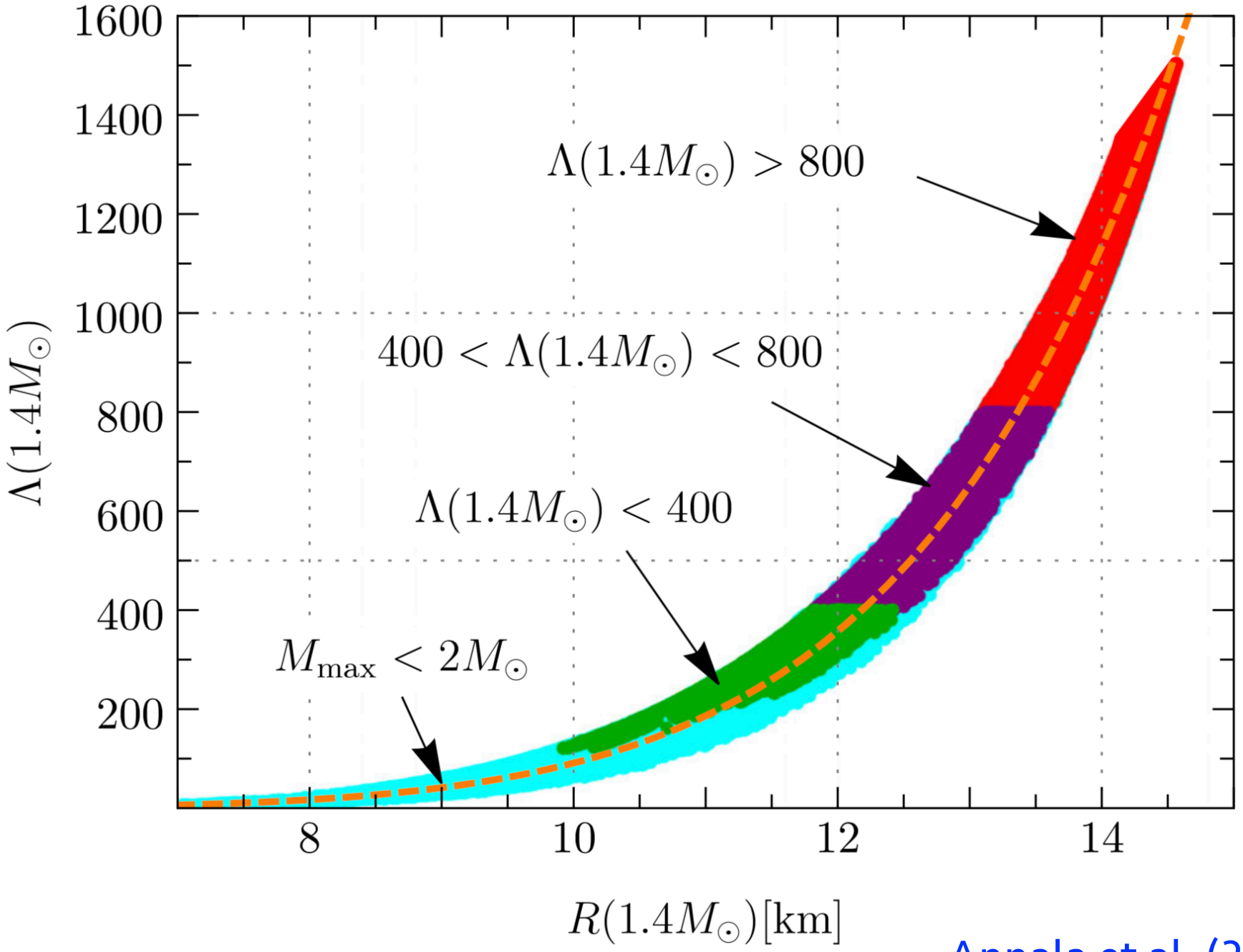

Annala et al. (2018)

EOS Constraints

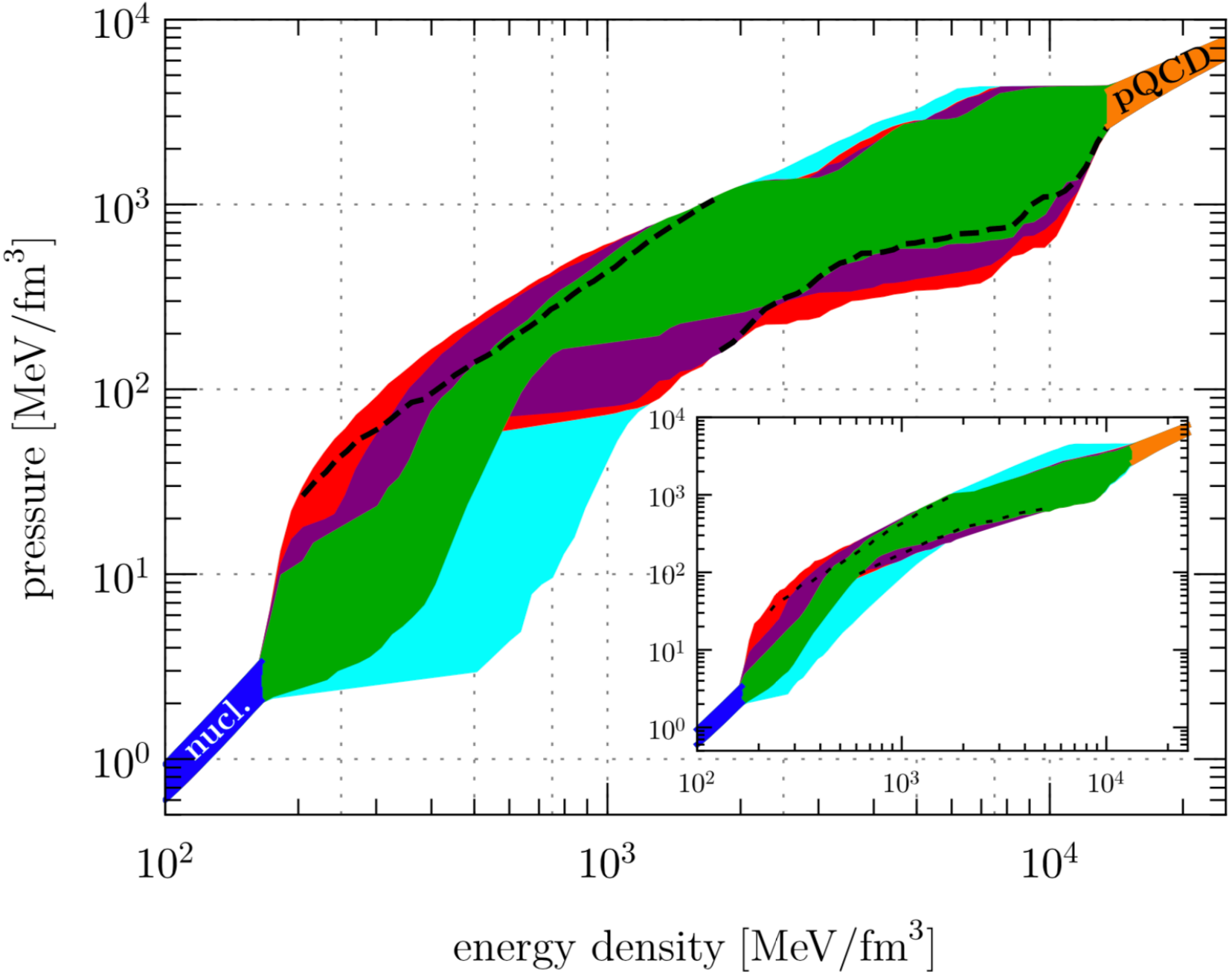

Annala et al. (2018)

Radius uncertainties before GW170817

Bauswein, Janka, Hebeler & Schwenk (2012)

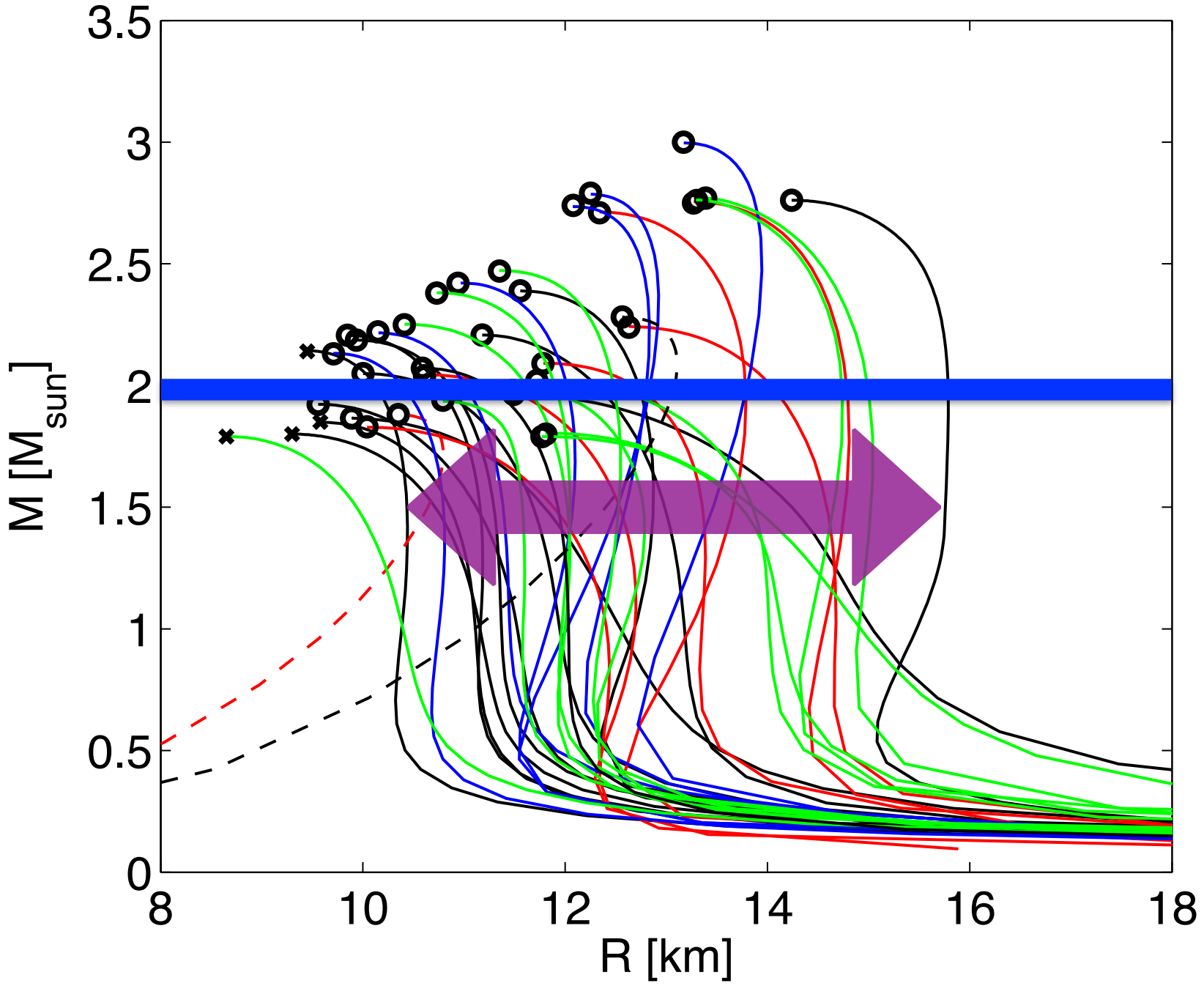

Constraints from the inspiral of GW170817

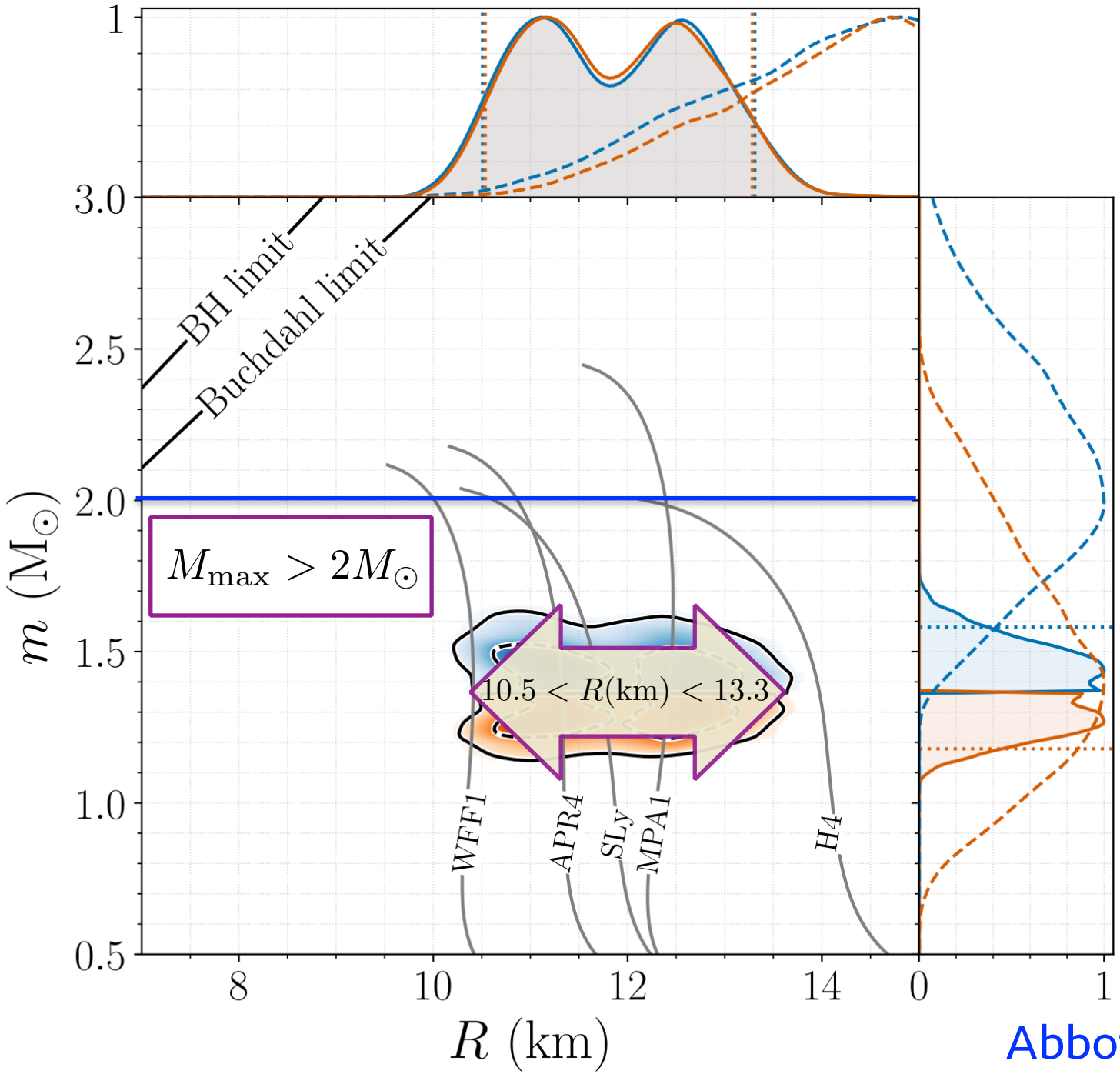

Abbot et al. (2018)

Various Radius Constraints based on GW170817

Montana et al. (2018)

Reference	R_i [km]
Without a phase transition	
Bauswein et al. [42]	$10.68^{+0.15}_{-0.03} \leq R_{1.6}$
Most et al. [51]	$12.00 \leq R_{1.4} \leq 13.45$
Burgio et al. [54]	$11.8 \leq R_{1.5} \leq 13.1$
Tews et al. [55]	$11.3 \leq R_{1.4} \leq 13.6$
De et al. [56]	$8.9 \leq R_{1.4} \leq 13.2$
LIGO/Virgo [57]	$10.5 \leq R_{1.4} \leq 13.3$
With a phase transition	
Annala et al. [46]	$R_{1.4} \leq 13.6$
Most et al. [51]	$8.53 \leq R_{1.4} \leq 13.74$
Burgio et al. [54]	$R_{1.5} = 10.7$
Tews et al. [55]	$9.0 \leq R_{1.4} \leq 13.6$
This work	
NS	$R_{1.4} = 13.11$
HS `Model-2`	$12.9 \leq R_{1.4} \leq 13.11$
HS_T `Model-1`	$10.1 \leq R_{1.4} \leq 12.9$
HS_T `Model-2`	$10.4 \leq R_{1.4} \leq 11.9$

Various Radius Constraints based on GW170817

Montana et al. (2018)

Reference	R_i [km]
Without a phase transition	
Bauswein et al. [42]	$10.68^{+0.15}_{-0.03} \leq R_{1.6}$
Most et al. [51]	$12.00 \leq R_{1.4} \leq 13.45$
Burgio et al. [54]	$11.8 \leq R_{1.5} \leq 13.1$
Tews et al. [55]	$11.3 \leq R_{1.4} \leq 13.6$
De et al. [56]	$8.9 \leq R_{1.4} \leq 13.2$
LIGO/Virgo [57]	$10.5 \leq R_{1.4} \leq 13.3$
With a phase transition	
Annala et al. [46]	$R_{1.4} \leq 13.6$
Most et al. [51]	$8.53 \leq R_{1.4} \leq 13.74$
Burgio et al. [54]	$R_{1.5} = 10.7$
Tews et al. [55]	$9.0 \leq R_{1.4} \leq 13.6$
This work	
NS	$R_{1.4} = 13.11$
HS `Model-2`	$12.9 \leq R_{1.4} \leq 13.11$
HS_T `Model-1`	$10.1 \leq R_{1.4} \leq 12.9$
HS_T `Model-2`	$10.4 \leq R_{1.4} \leq 11.9$

A Minimal Set of Assumptions

Bauswein, Just, Janka, NS (2017)
ApJ Letters

1) GR is valid.

2) A hypermassive neutron star (HMNS) was formed as a result of the GW170817 merger event, lasting for at least 10ms.

3) $M_{\rm max} > 2M_\odot$

4) Causality holds $(v_s < c)$

5) $M_{\rm tot}^{\rm GW170817} = 2.74^{+0.04}_{-0.01}\, M_\odot$

Differentially Rotating Models

(Bauswein & NS 2017)

hypermassive stars

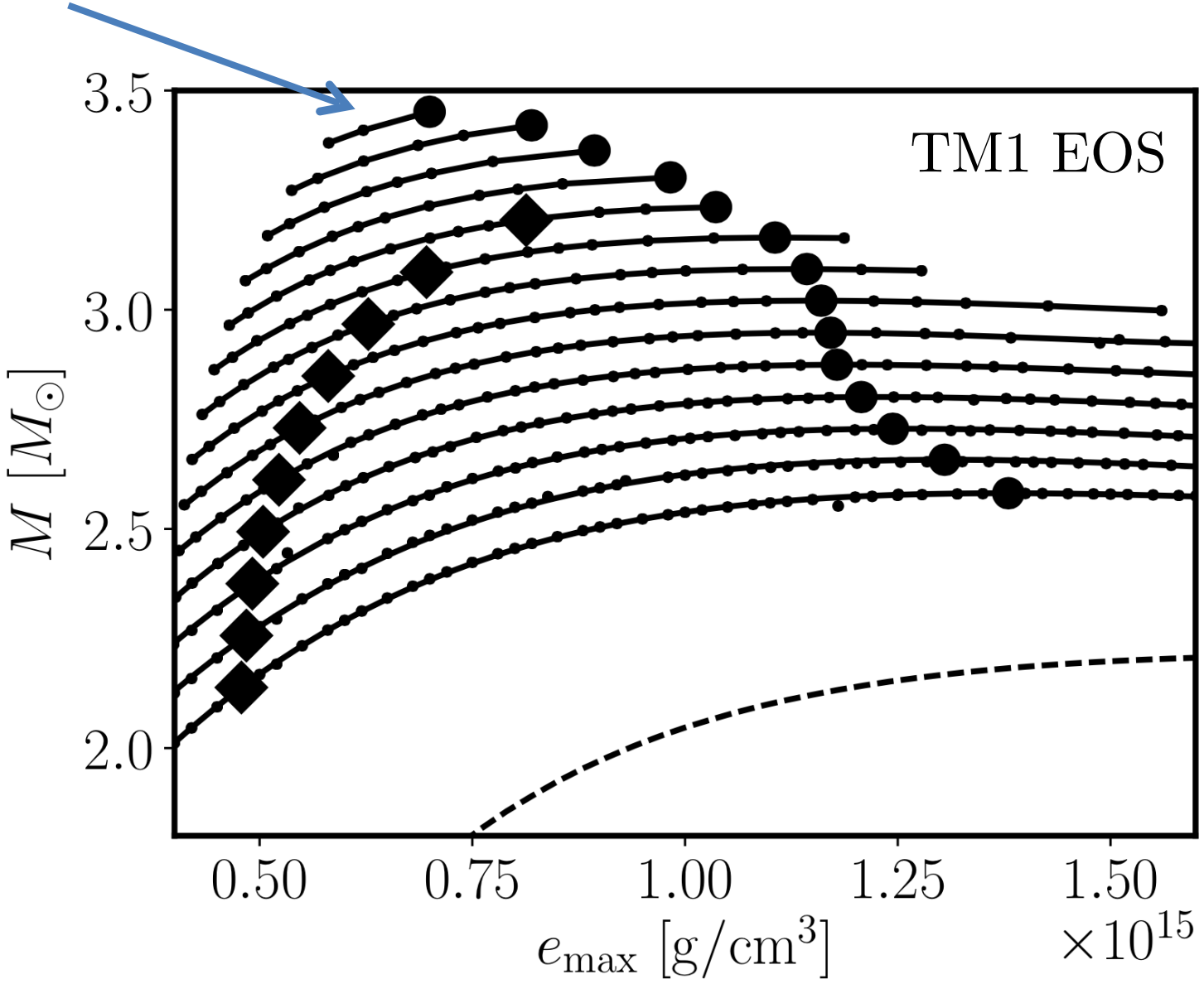

Differentially Rotating Models

(Bauswein & NS 2017)

hypermassive stars

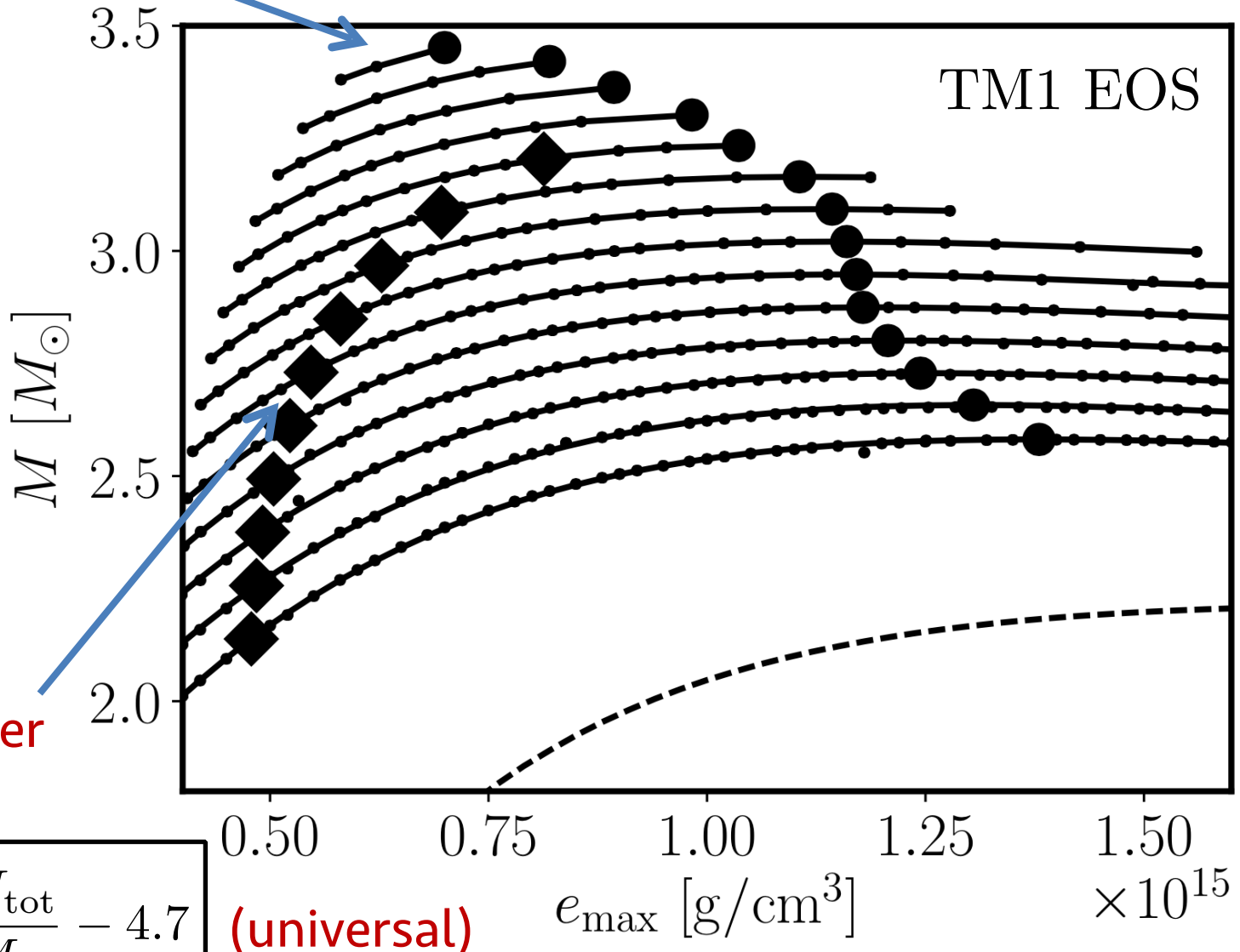

BNS merger remnants

$$\frac{cJ}{M_\odot^2} \simeq 4\frac{M_{\rm tot}}{M_\odot} - 4.7$$

(universal)

Differentially Rotating Models

(Bauswein & NS 2017)

hypermassive stars

Threshold mass

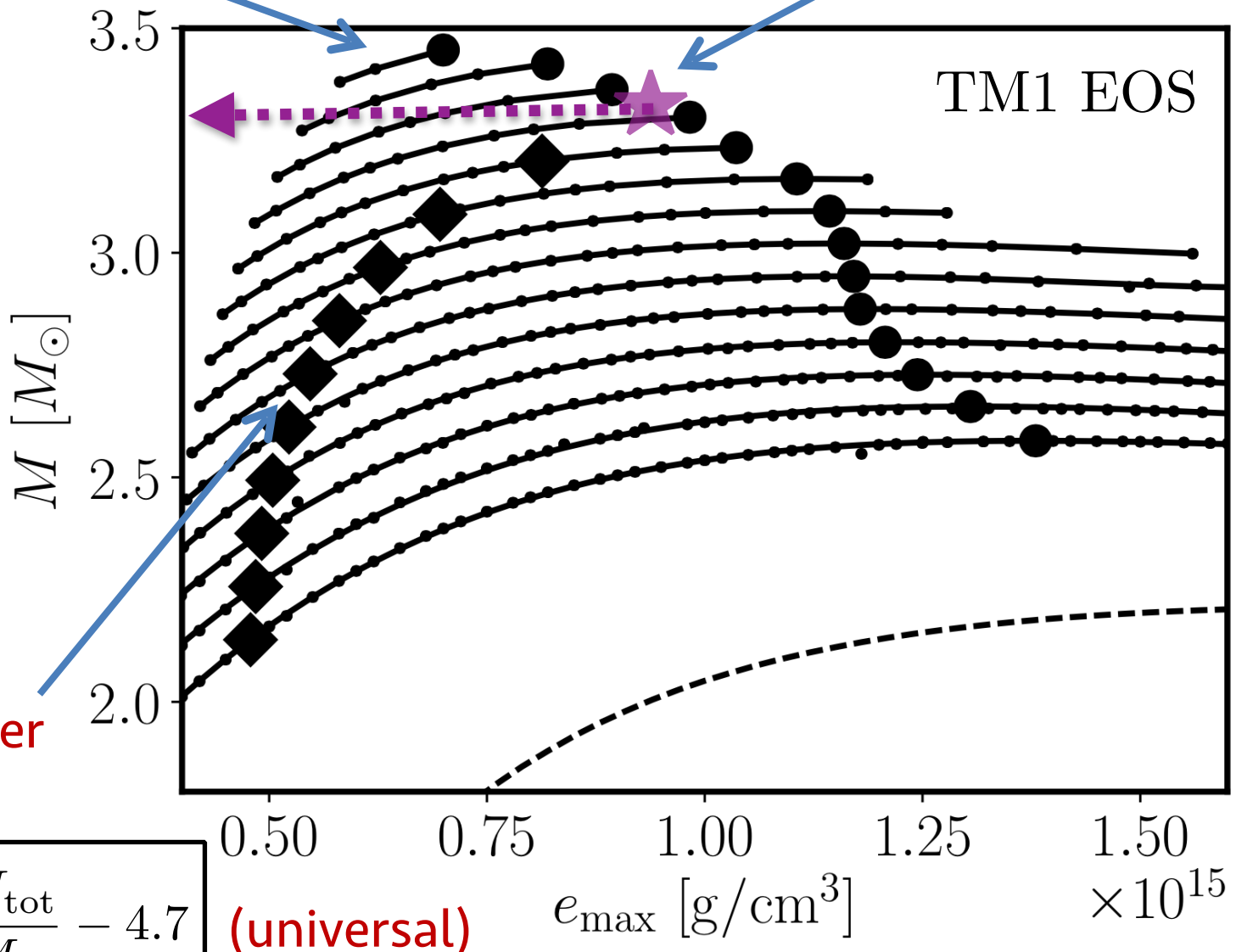

BNS merger remnants

$$\frac{cJ}{M_\odot^2} \simeq 4\frac{M_{\rm tot}}{M_\odot} - 4.7$$

(universal)

Differentially Rotating Models

(Bauswein & NS 2017)

hypermassive stars

Threshold mass

$$M_{\rm thres} > M_{\rm tot}^{\rm GW170817} = 2.74^{+0.04}_{-0.01}\, M_\odot$$

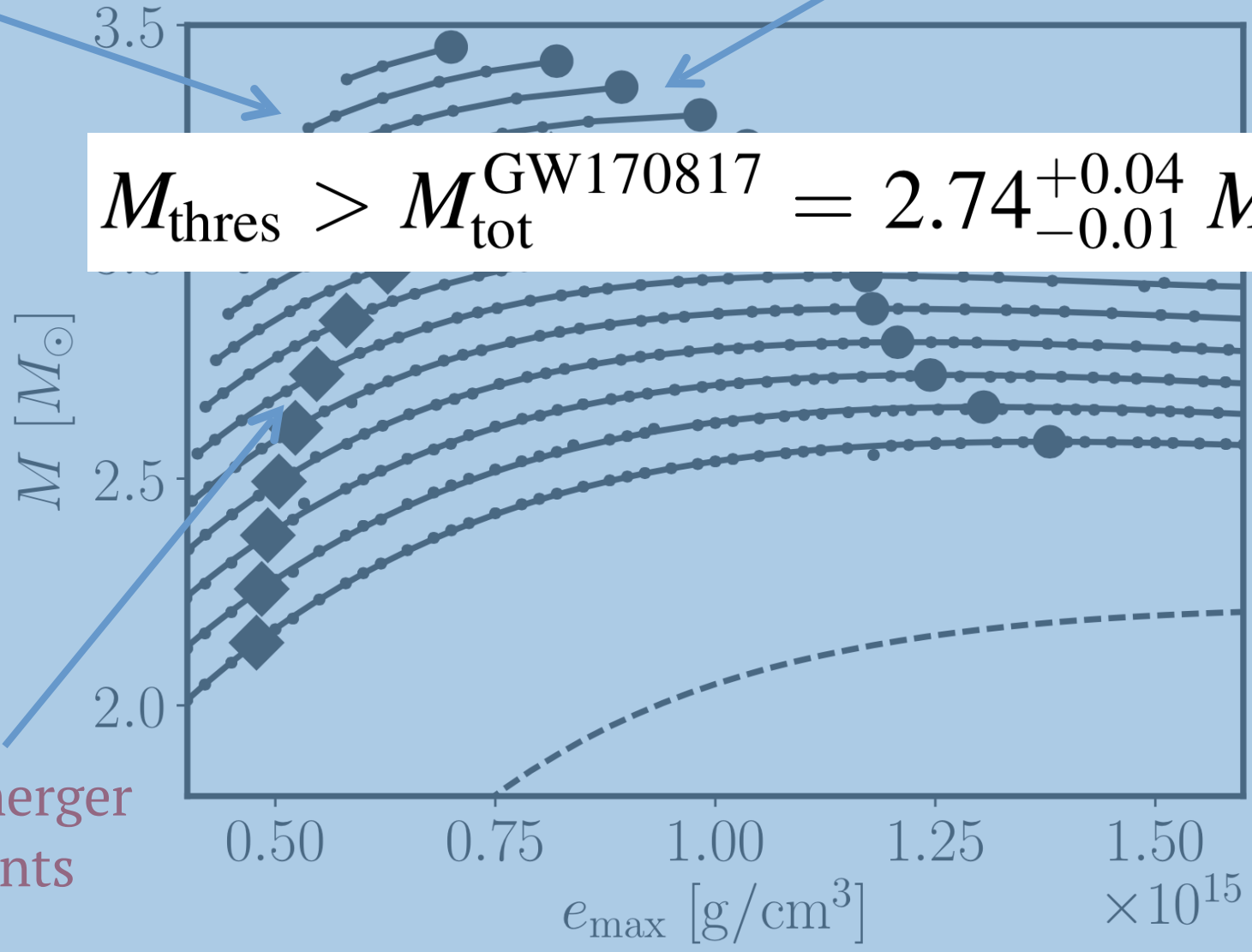

BNS merger remnants

M_thres vs. M_max correlation

Bauswein, Baumgarte, Janka PRL (2013)

The threshold mass is related to the maximum TOV mass as

$$M_{\rm thres} = k(C_{\rm max}) \cdot M_{\rm max} \qquad C_{\rm max} = \frac{M_{\rm max}}{R_{\rm max}}$$

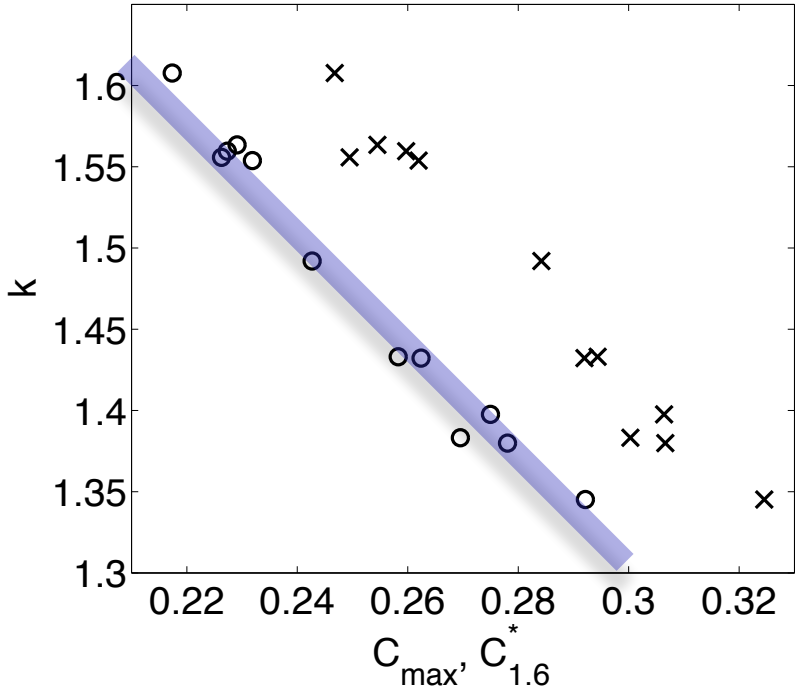

M_thres vs. M_max correlation

Bauswein, Baumgarte, Janka PRL (2013)

The threshold mass is related to the maximum TOV mass as

$$M_{\rm thres} = k(C_{\rm max}) \cdot M_{\rm max} \qquad C_{\rm max} = \frac{M_{\rm max}}{R_{\rm max}}$$

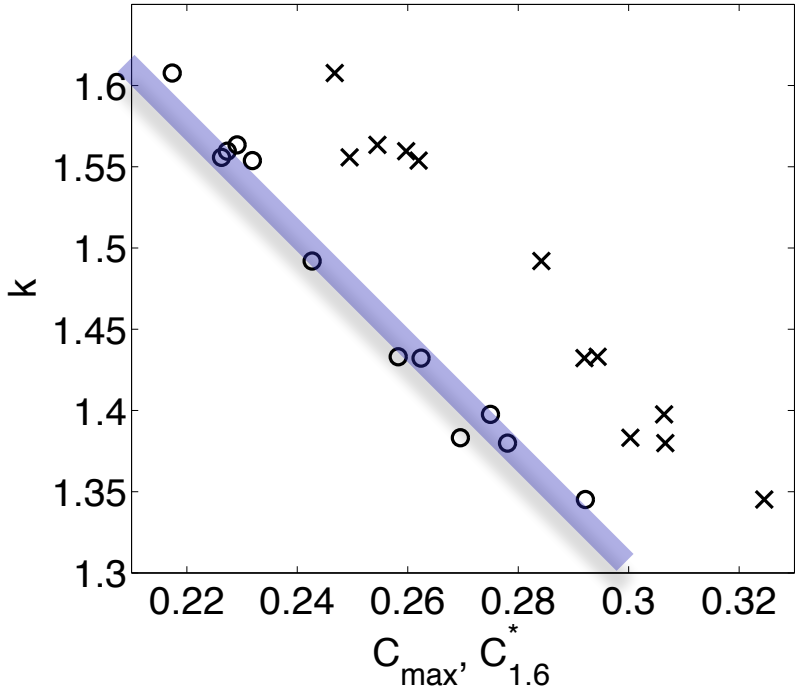

This leads to the relation

$$M_{\rm thres} = \left(-3.606 \frac{G M_{\rm max}}{c^2 R_{1.6}} + 2.38 \right) \cdot M_{\rm max} \; > 2.74 M_\odot$$

Maximally Compact EOS

Maximal compactness $\Leftrightarrow$ Maximally stiff core + maximally soft crust

Koranda, NS & Friedman (1997)

Core is at the causal limit

$$v_s = c$$

$$M_{\rm max} \leq \frac{1}{2.82}\frac{c^2 R_{\rm max}}{G}$$

(Lattimer & Prakash)

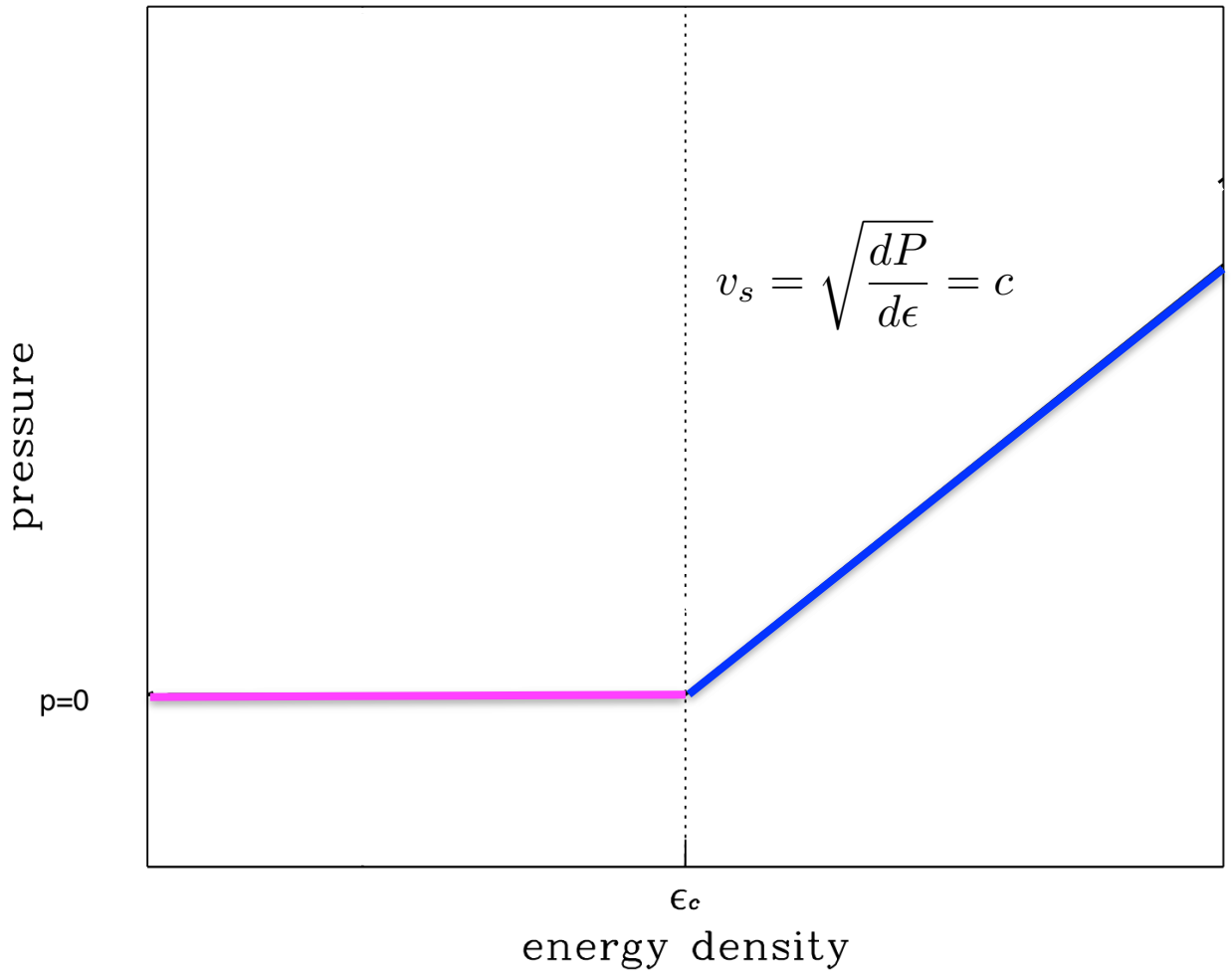

Maximally Compact EOS

Maximal compactness $\Leftrightarrow$ Maximally stiff core + maximally soft crust

Assume causal limit above

$$M > 1.6 M_\odot$$

for each EOS

$$M_{\rm max} \leq \frac{1}{3.10} \frac{c^2 R_{1.6}}{G}$$

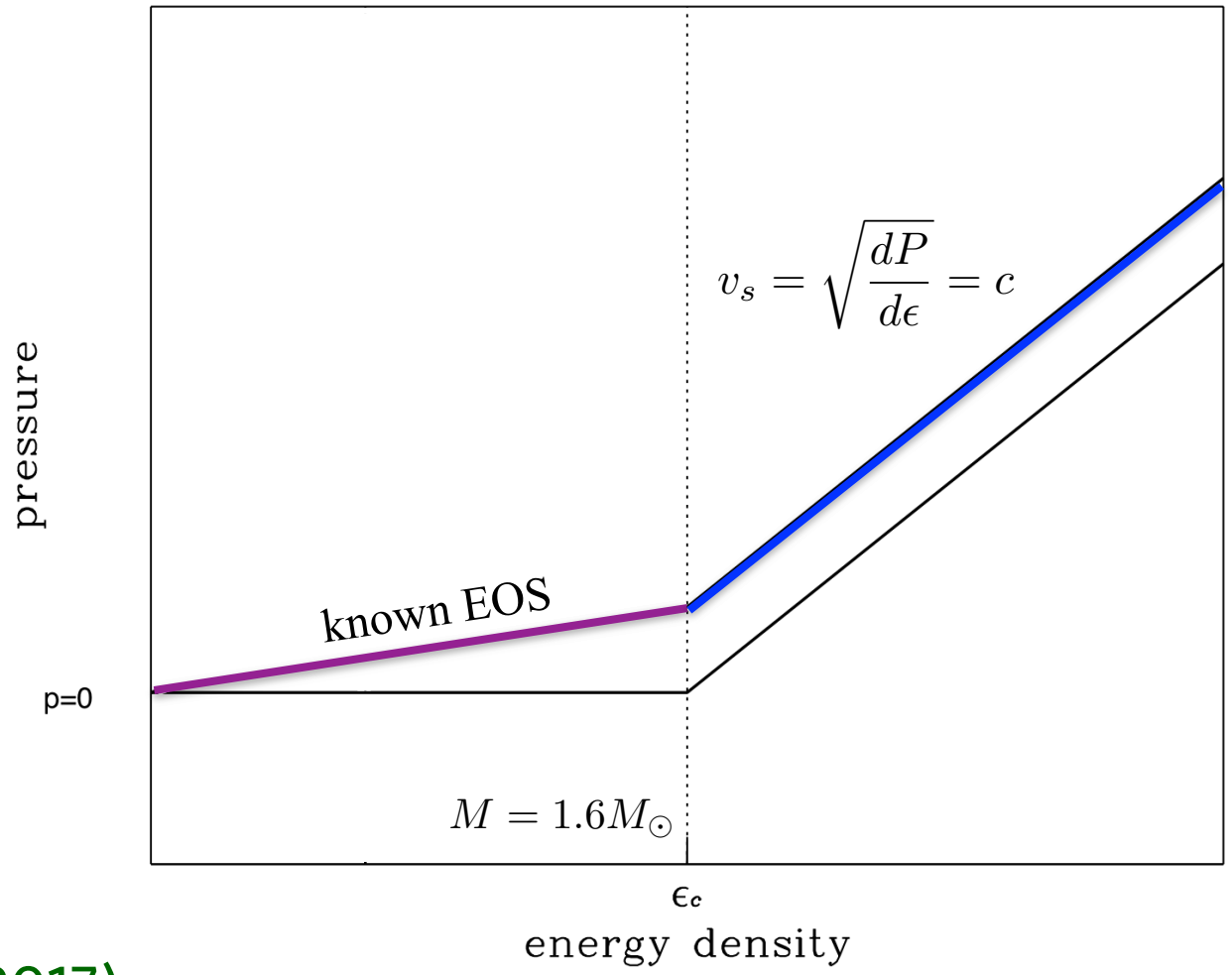

Bauswein, Just, Janka & NS (2017)

Radius Constraints from Minimal Assumptions

Bauswein, Just, Janka & NS (2017)

The combination of the minimal set of assumptions leads to a strict constraint on the radius:

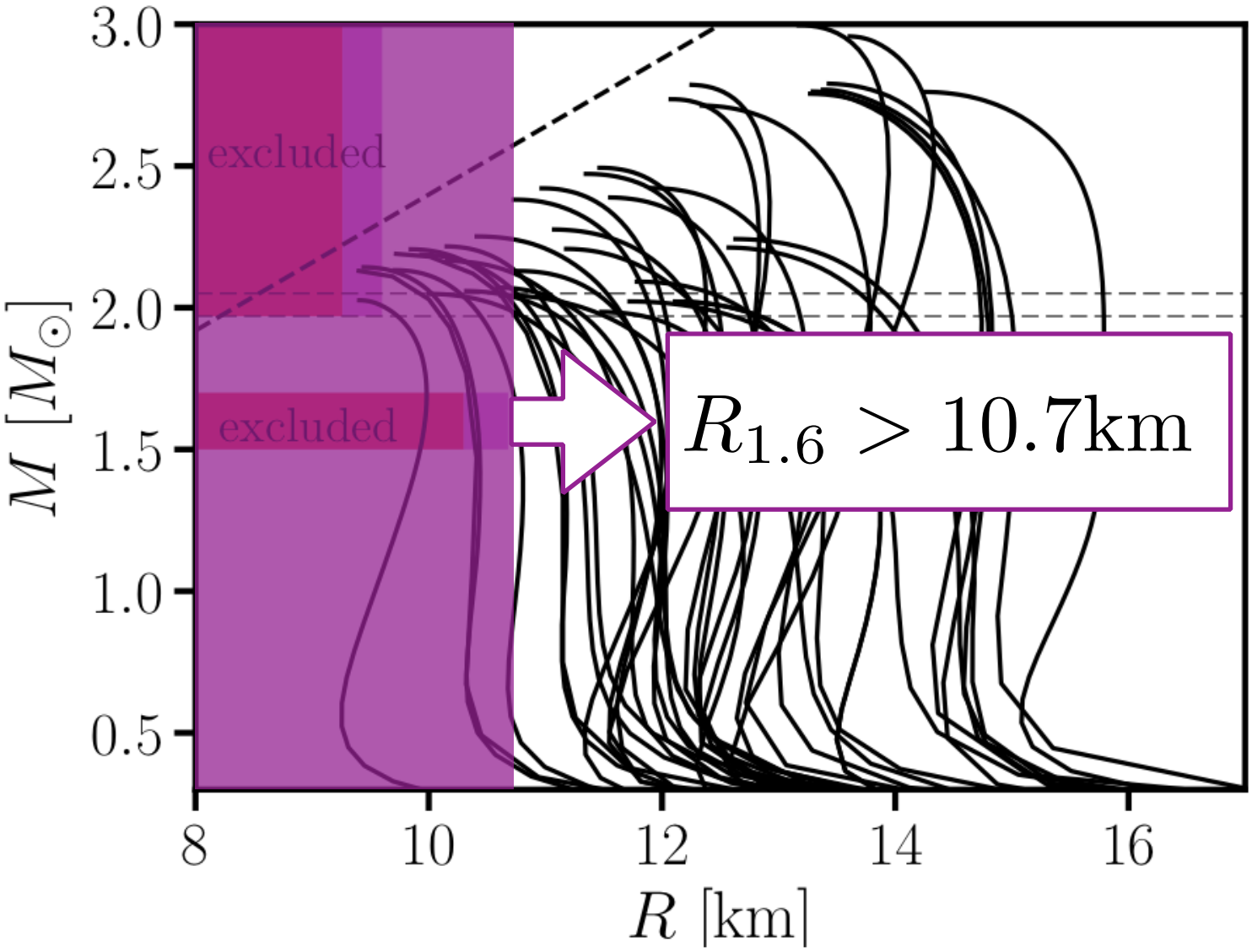

Comparison to Abbot et al. (2008)

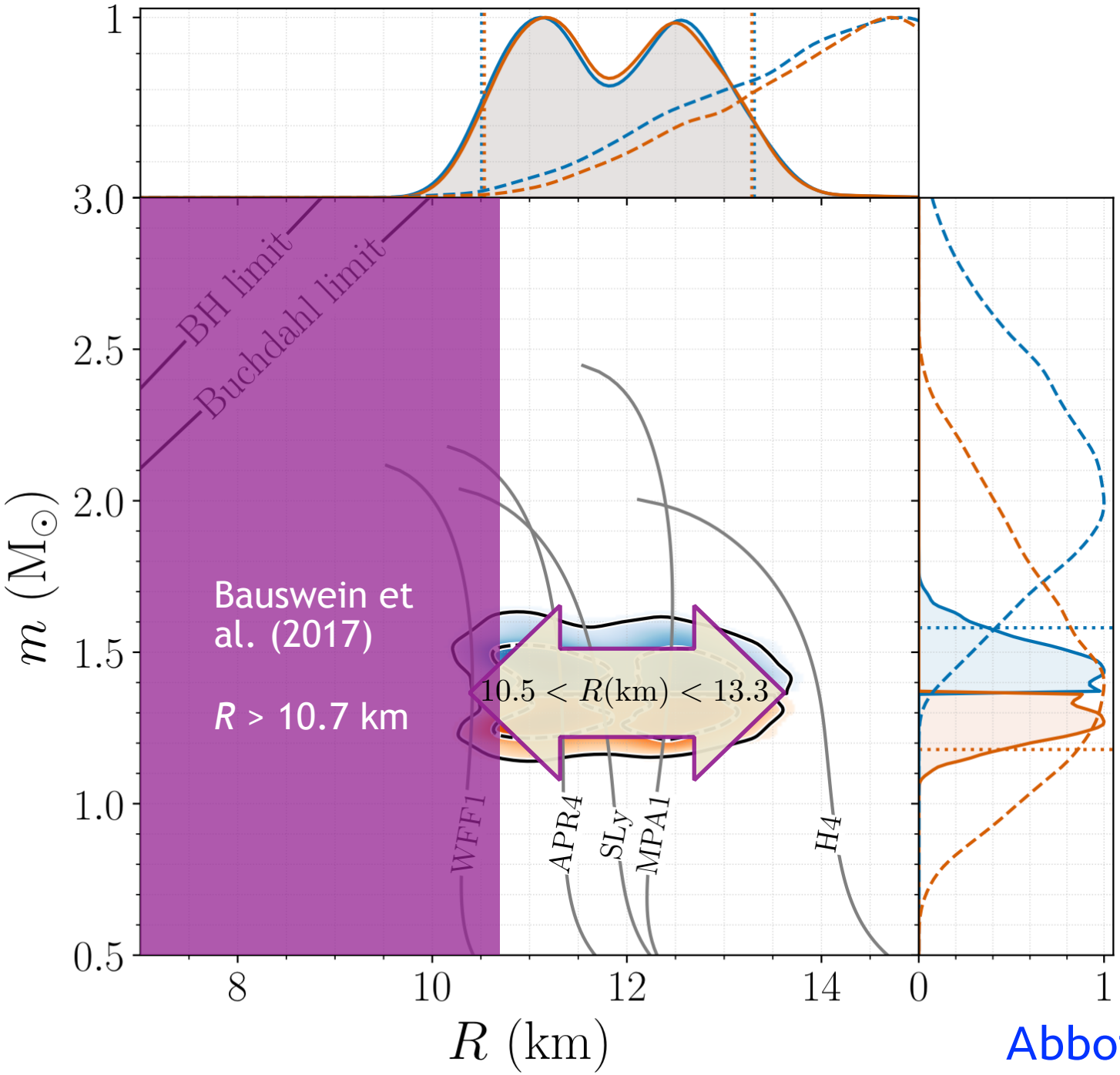

Abbot et al. (2018)

Constraints on M-R Relation

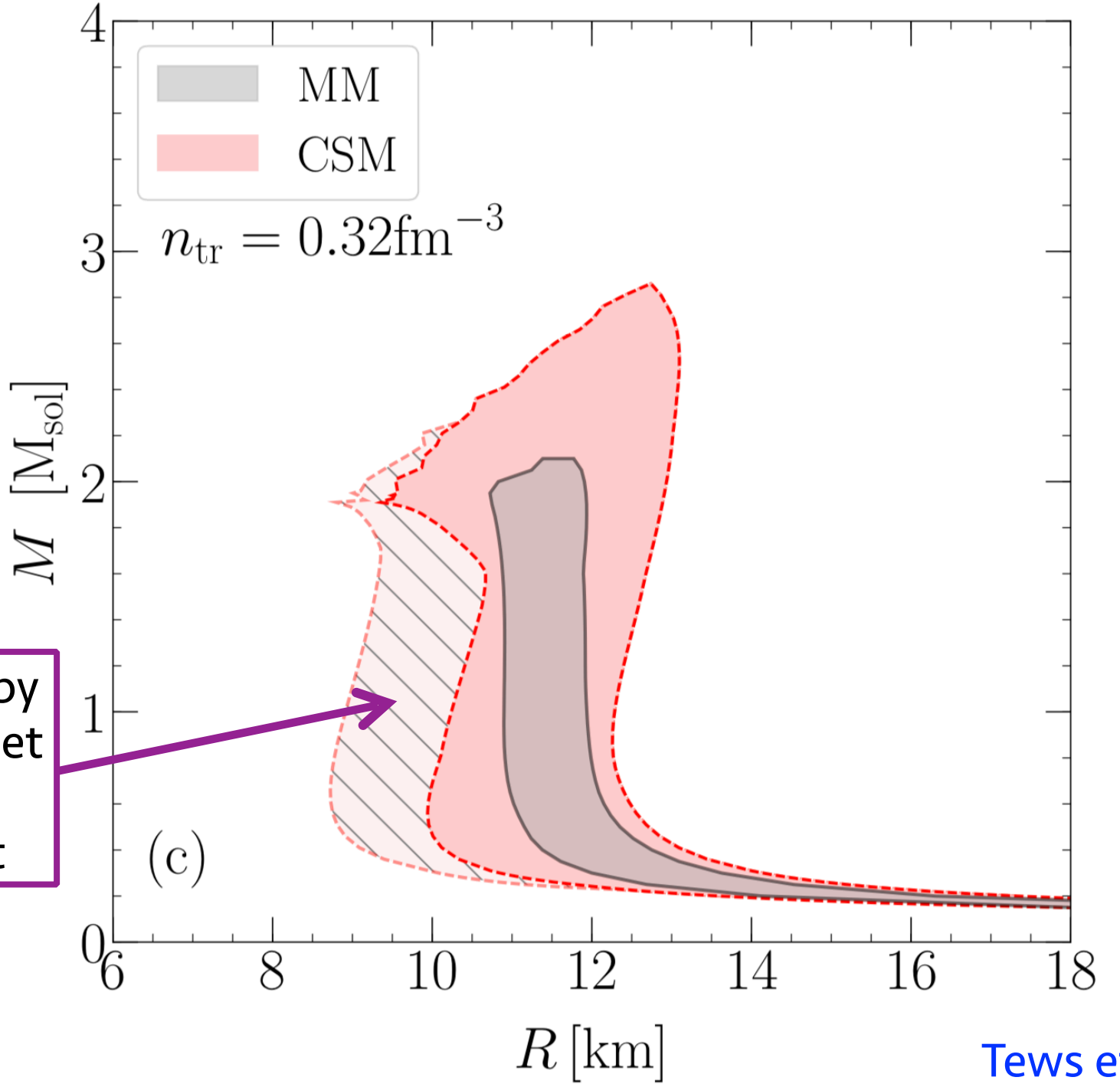

Excluded by Bauswein et al. (2017) constraint

Tews et al. (2019)

Constraints on EOS

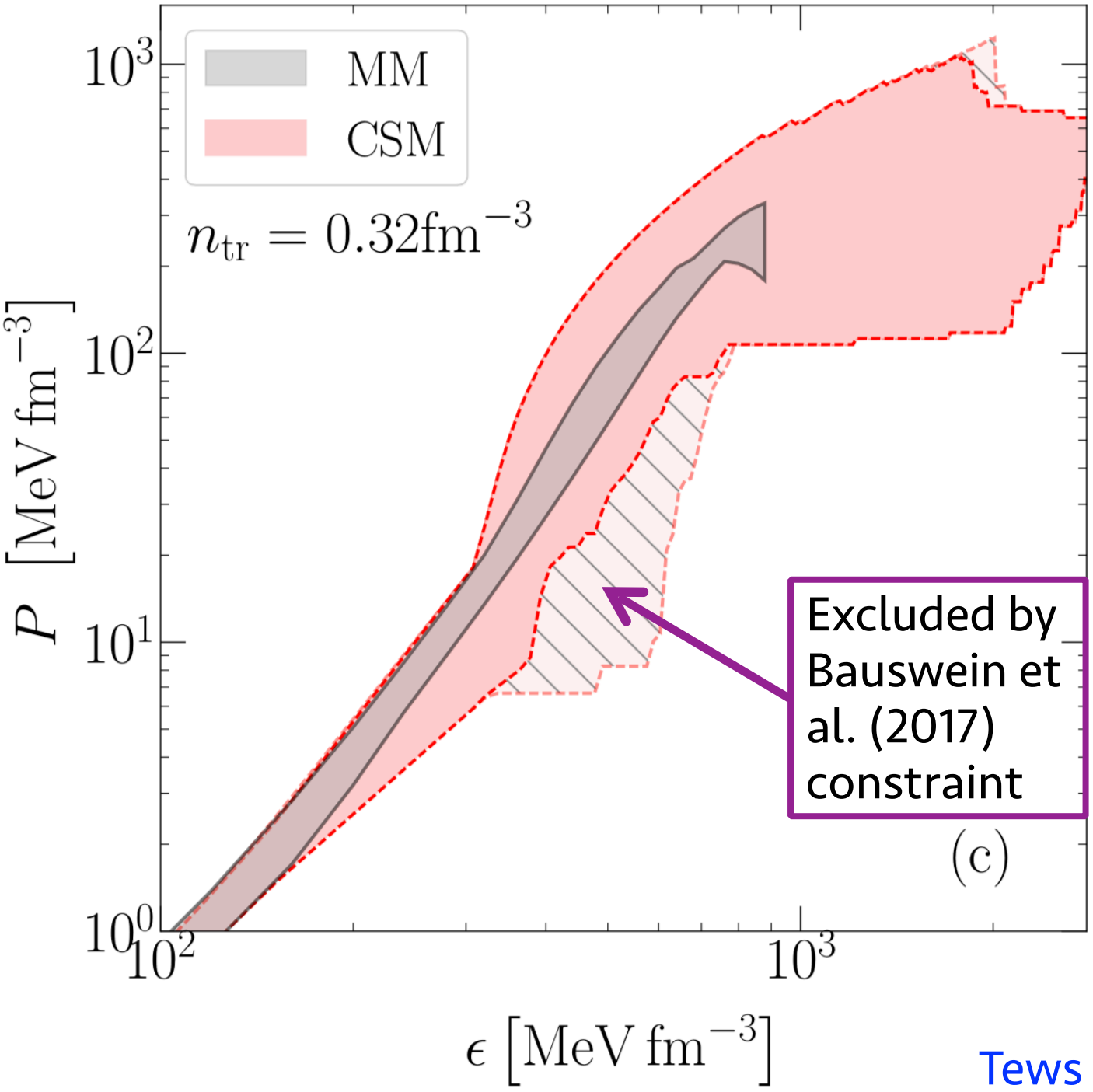

Tews et al. (2019)

Constraints From Future Detections

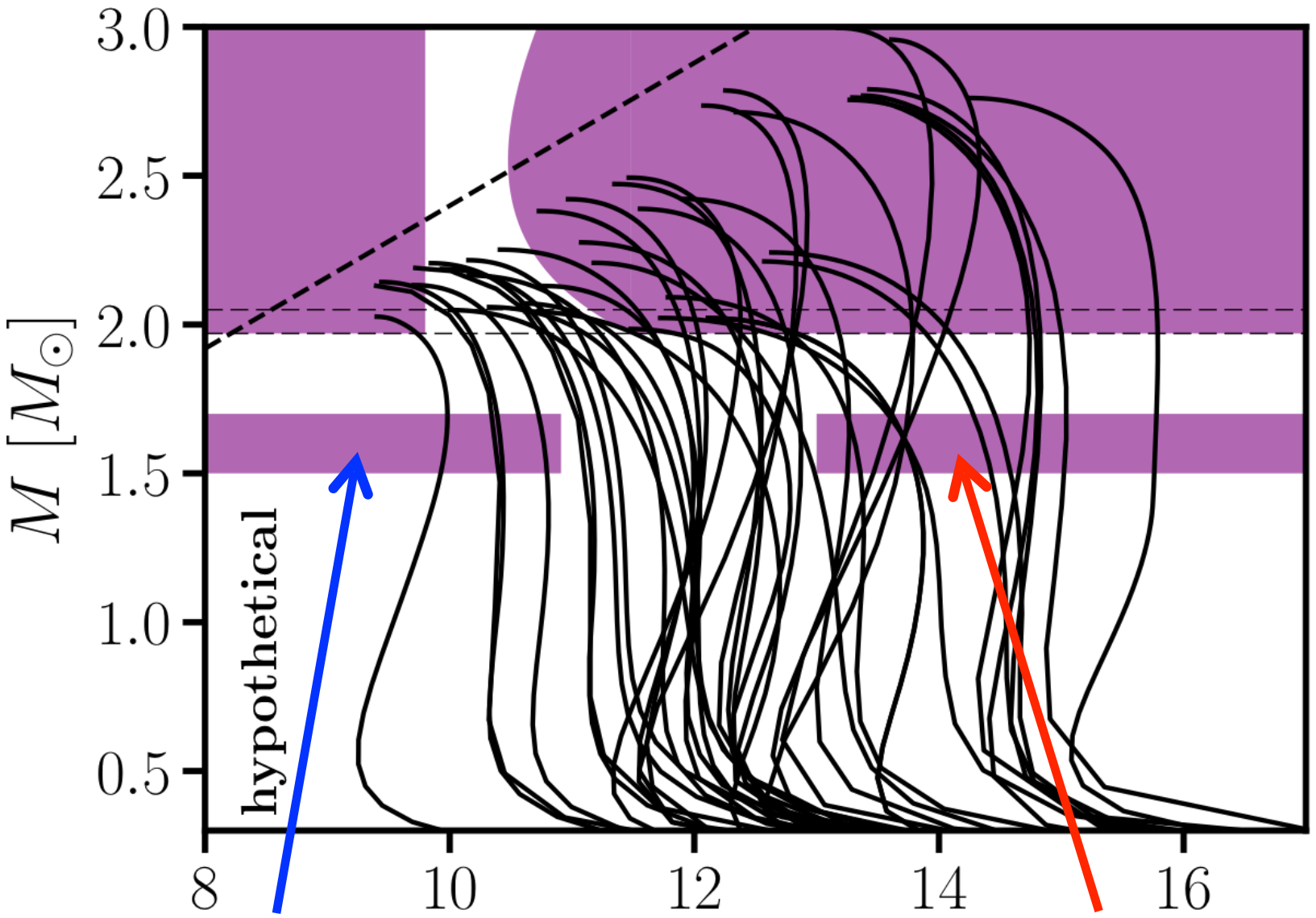

No collapse with
$M_{\rm tot} = 2.9 M_\odot$

Collapse with
$M_{\rm tot} = 3.1 M_\odot$

Post-Merger Gravitational Waves

The GW signal can be divided into three distinct phases:
inspiral, *merger* and *post-merger ringdown*.

Stergioulas et al. (2011)

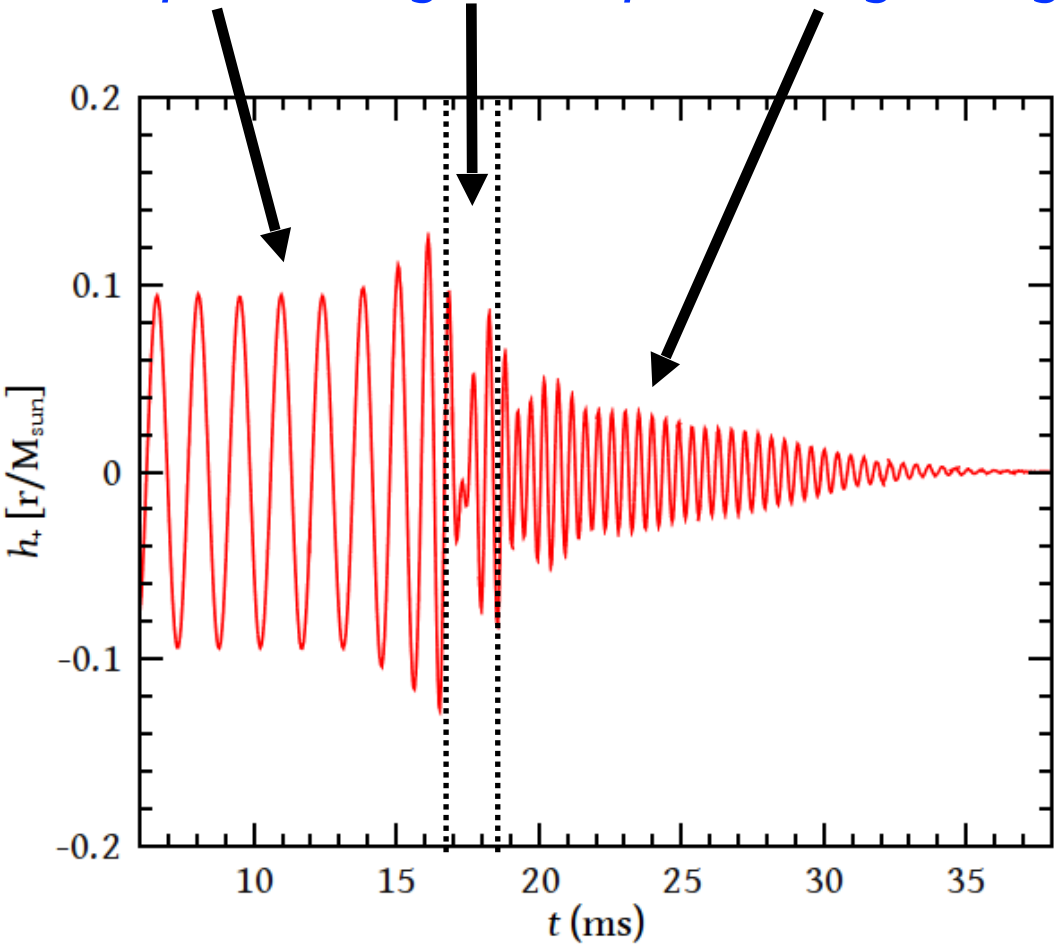

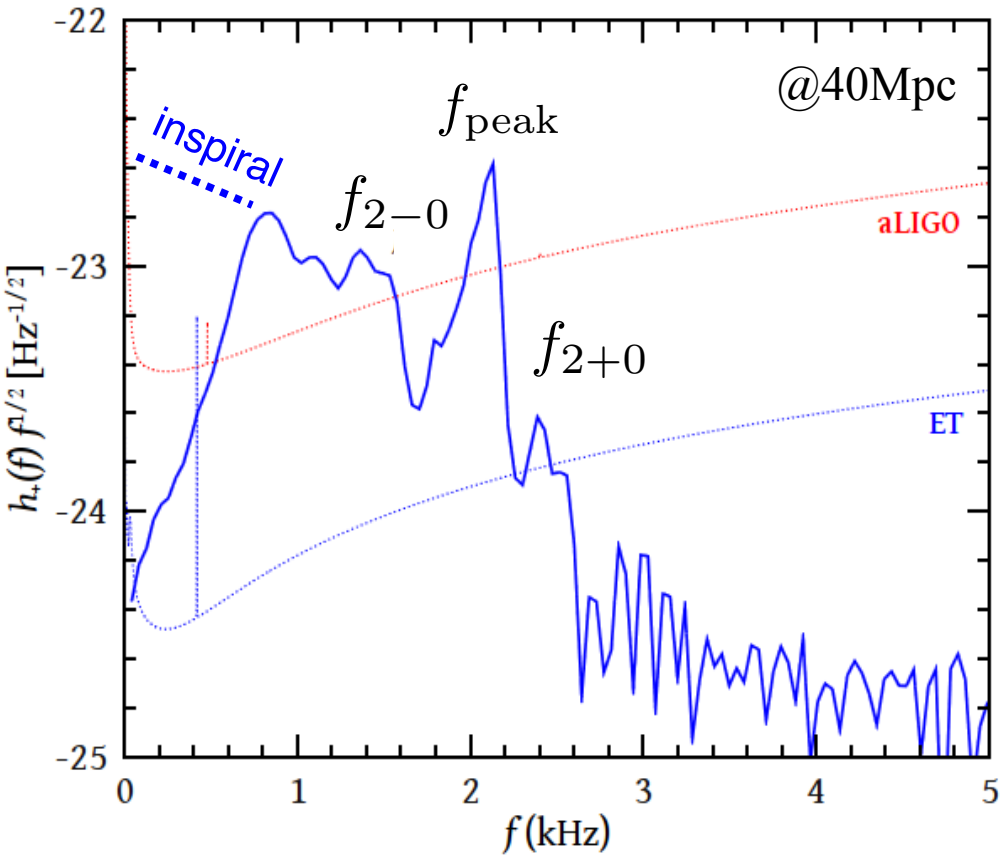

$$f_{\rm peak} = f_2$$

is due to the fundamental *l=m=2 f*-mode oscillation

$$f_{2-0} = f_2 - f_0$$
$$f_{2+0} = f_2 + f_0$$

are quasi-linear combination tones -> (Tartini tones)

Sorge (1745), Tartini (1754)

Post-Merger GW Oscillations

Stergioulas et al. (2011)

GRAVITATIONAL WAVES

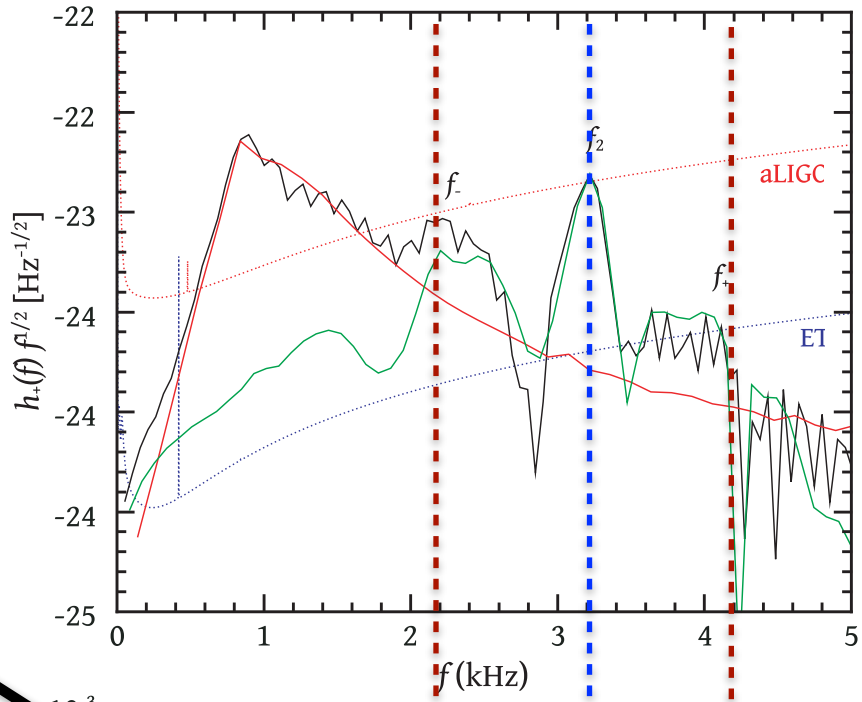

m=0 radial mode

HYDRODYNAMICS

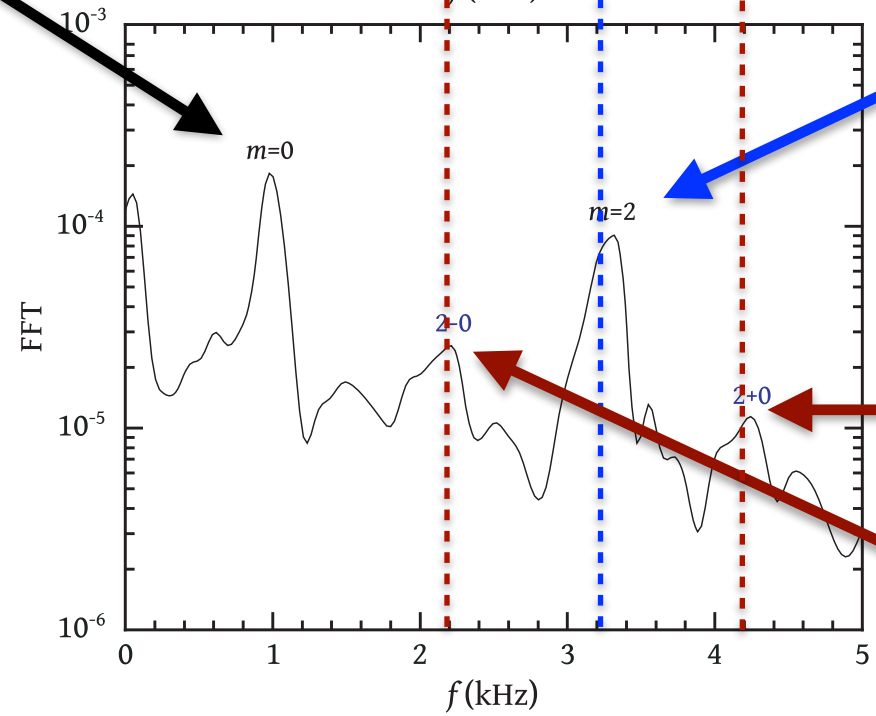

m=2 quadrupole mode

"2-0" and "2+0" quasi-linear combination frequency

Spiral Deformation

Bauswein & NS (2015)

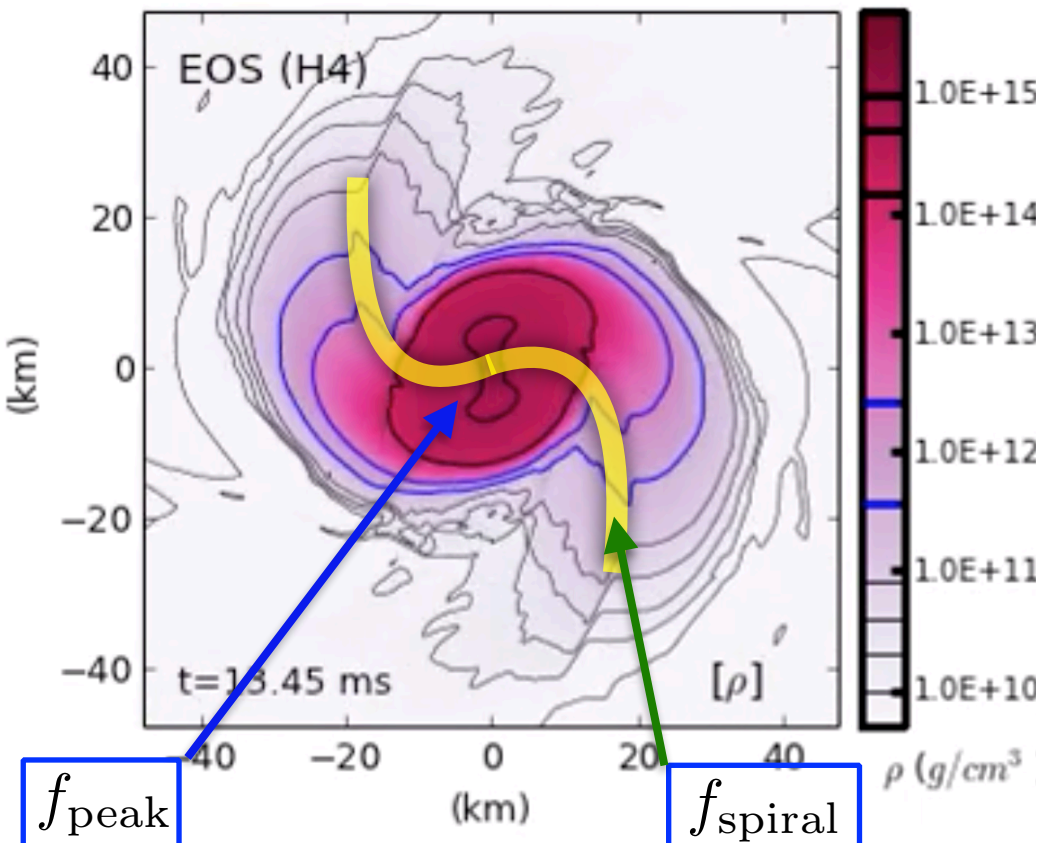

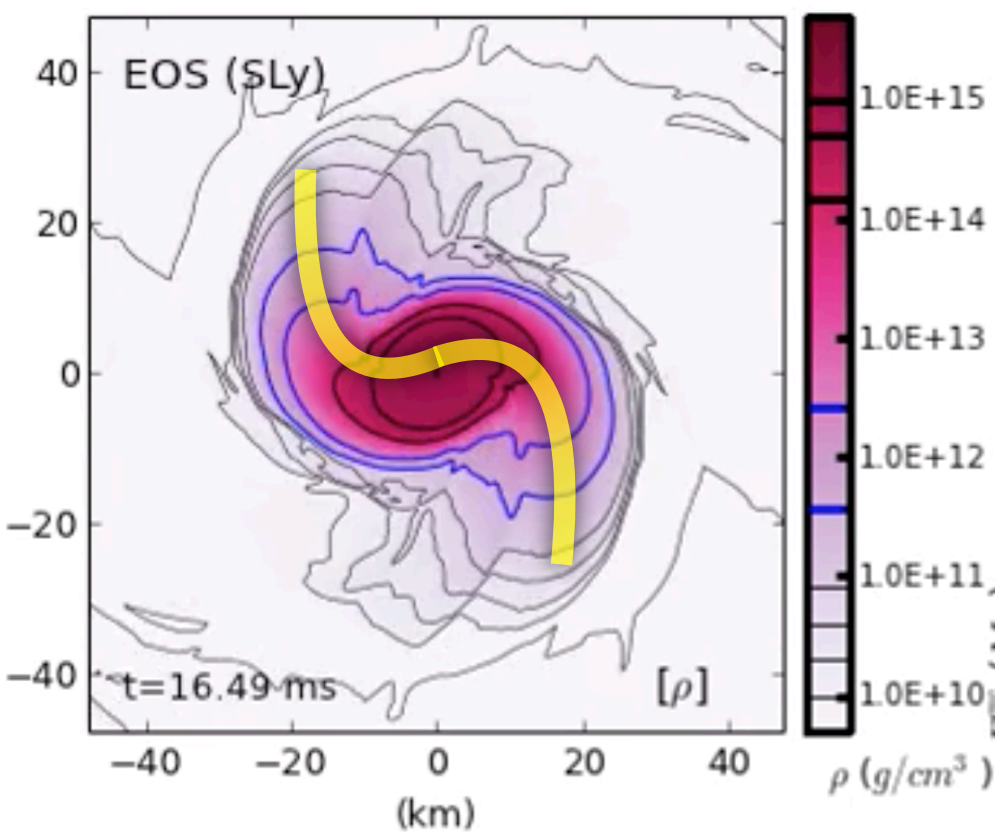

$f_{\rm peak}$

$f_{\rm spiral}$

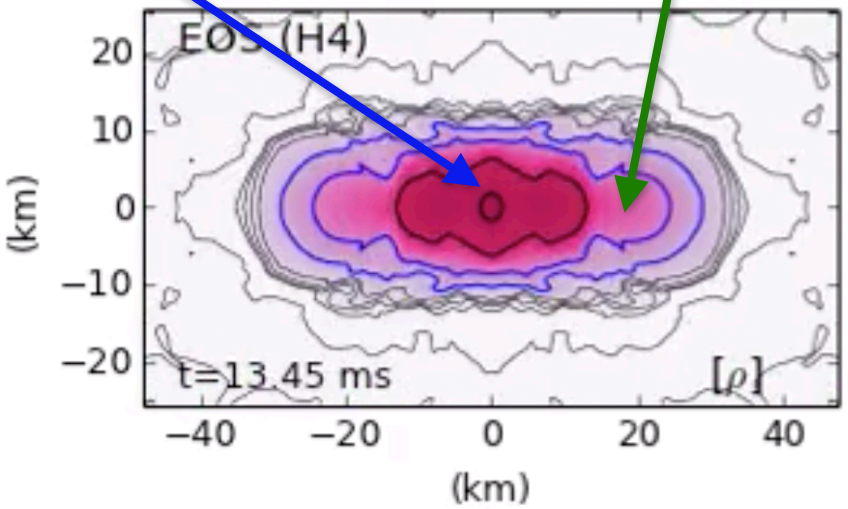

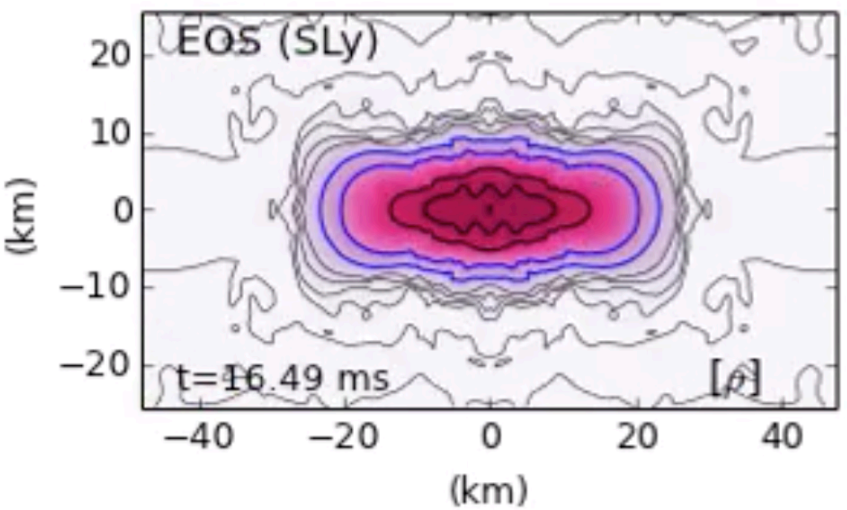

Three Detectable Post-Merger Frequencies

Vretinaris, NS & Bauswein (2019)

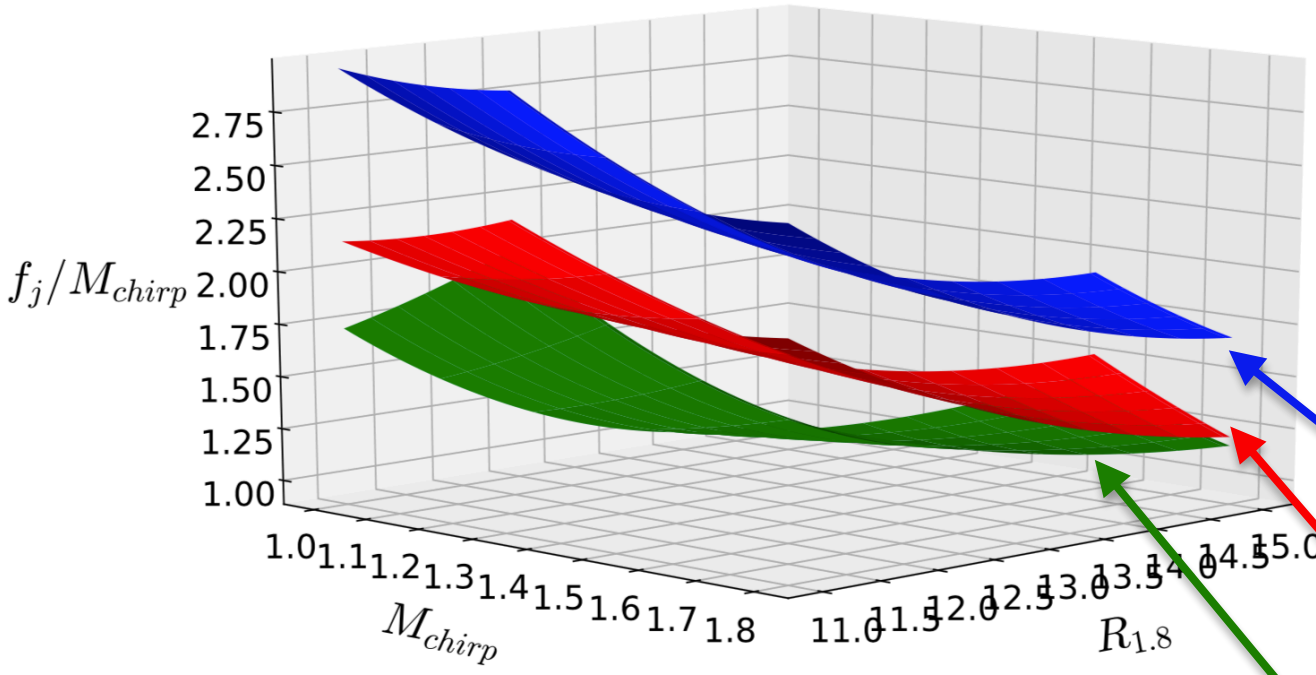

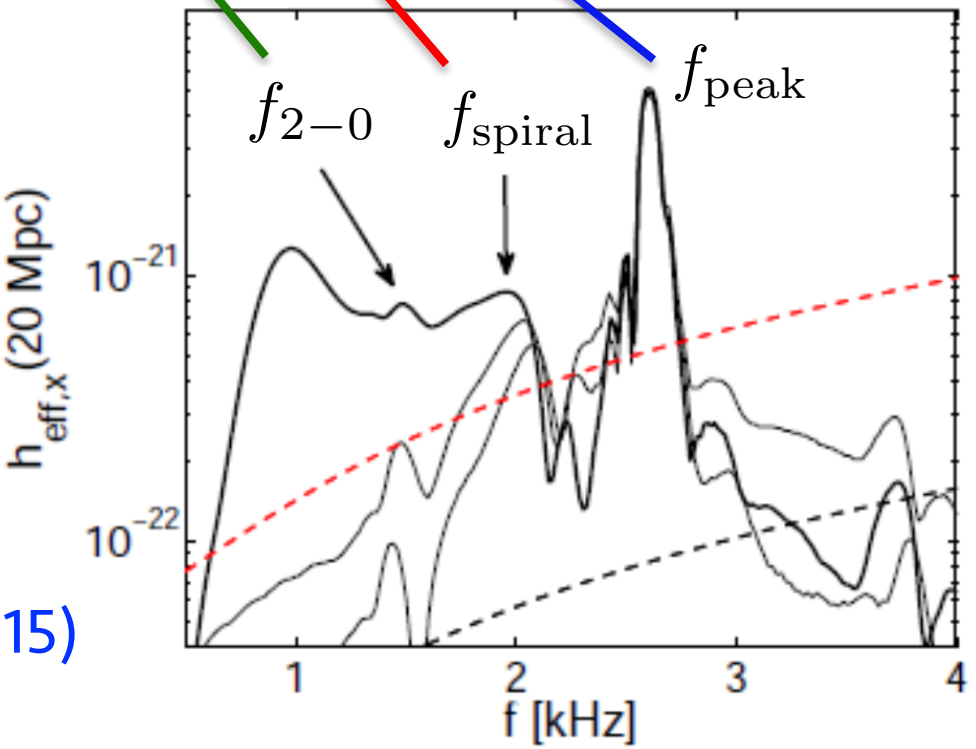

Bauswein & NS (2015)

Spectral Classification Scheme

Bauswein & NS (2015)

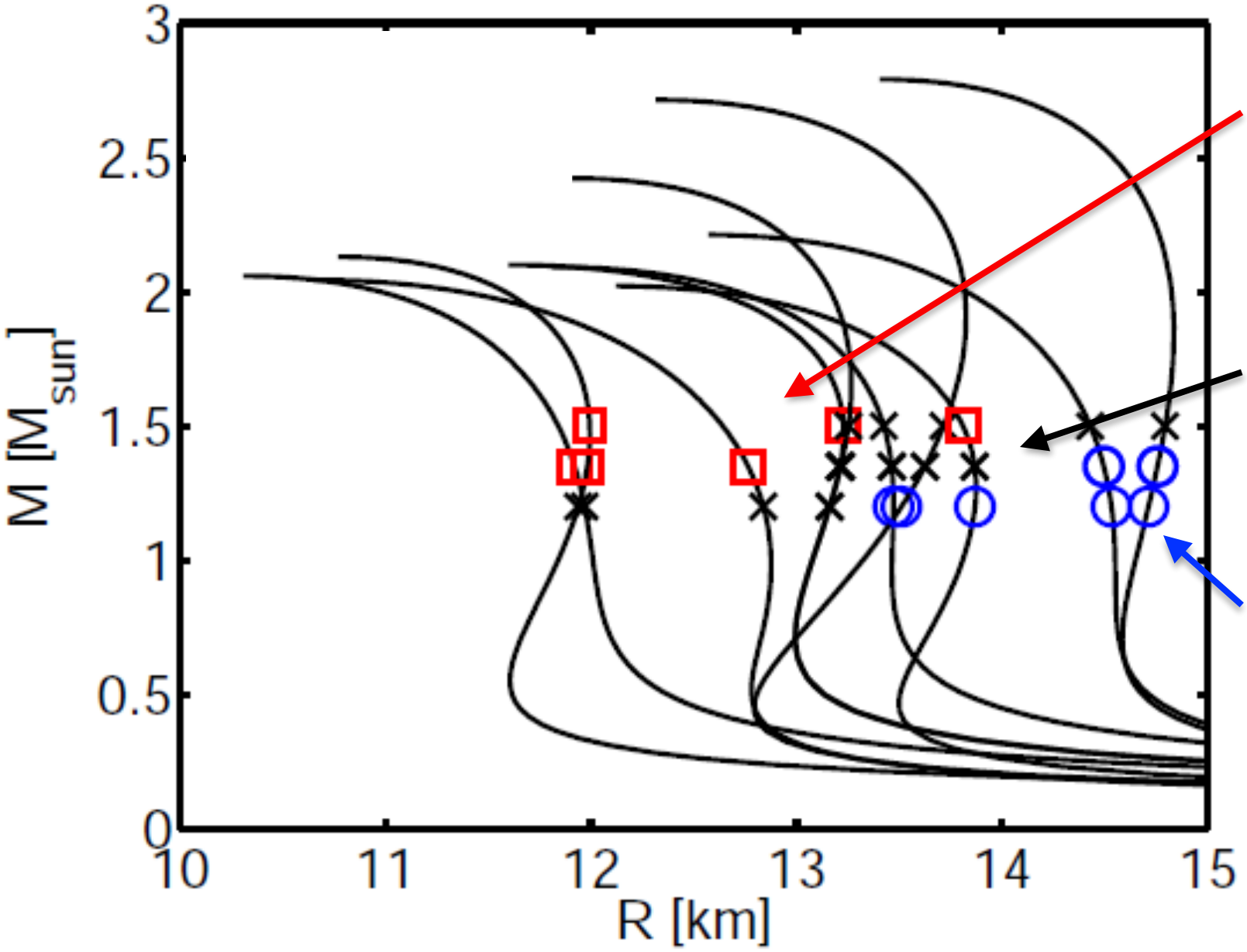

Type I:

$A_{2-0} > A_{\rm spiral}$

Type II:

$A_{2-0} \sim A_{\rm spiral}$

Type III:

$A_{2-0} < A_{\rm spiral}$

Spectral Classification using Machine Learning

Vretinaris, NS & Bauswein (2019)

Clustering: *Affinity Propagation* (Scikit-Learn)
Classification via neural network: *Multi-layer Perceptron (MLP) supervised learning*

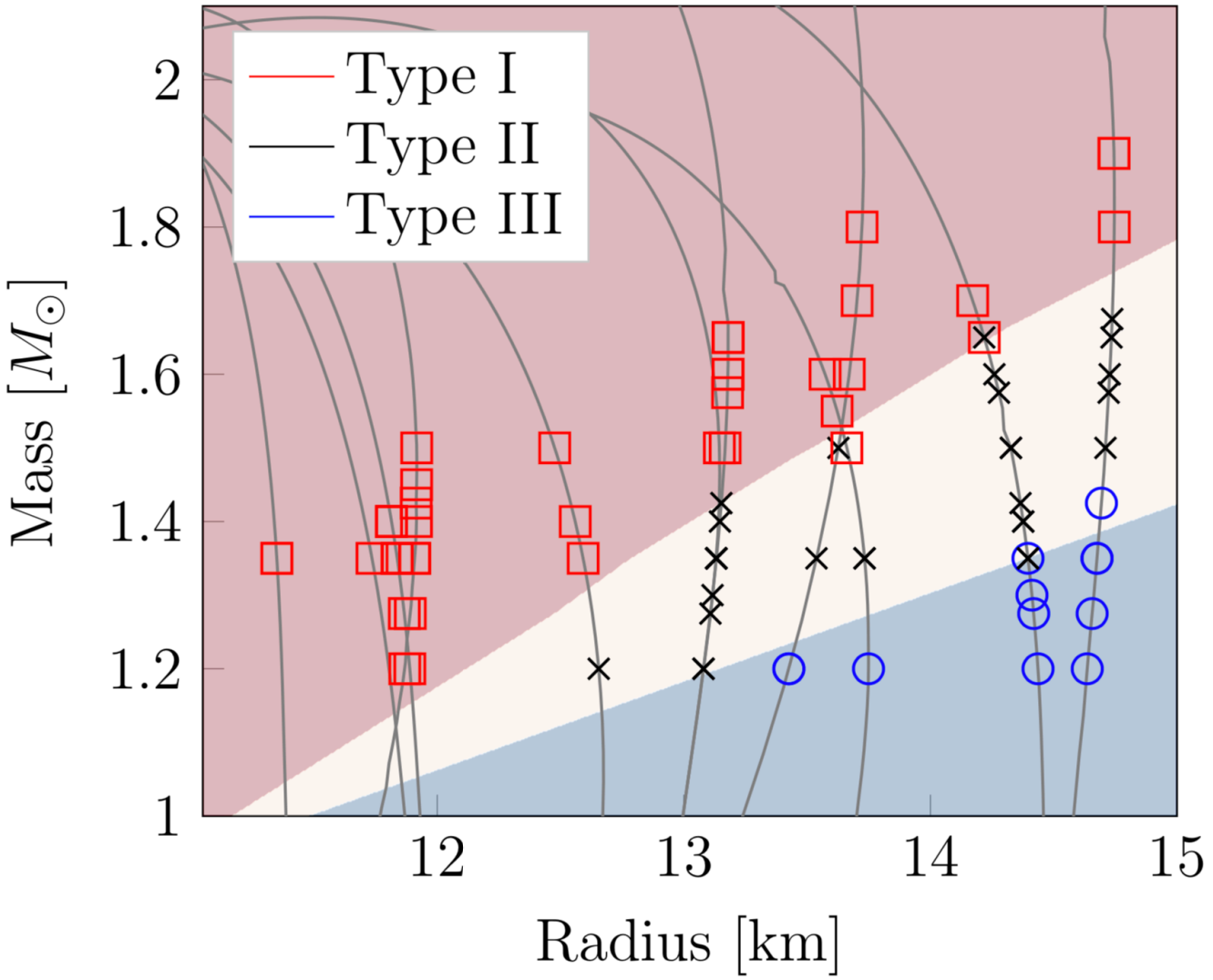

Quadrupole Frequencies for Nonrotating Stars

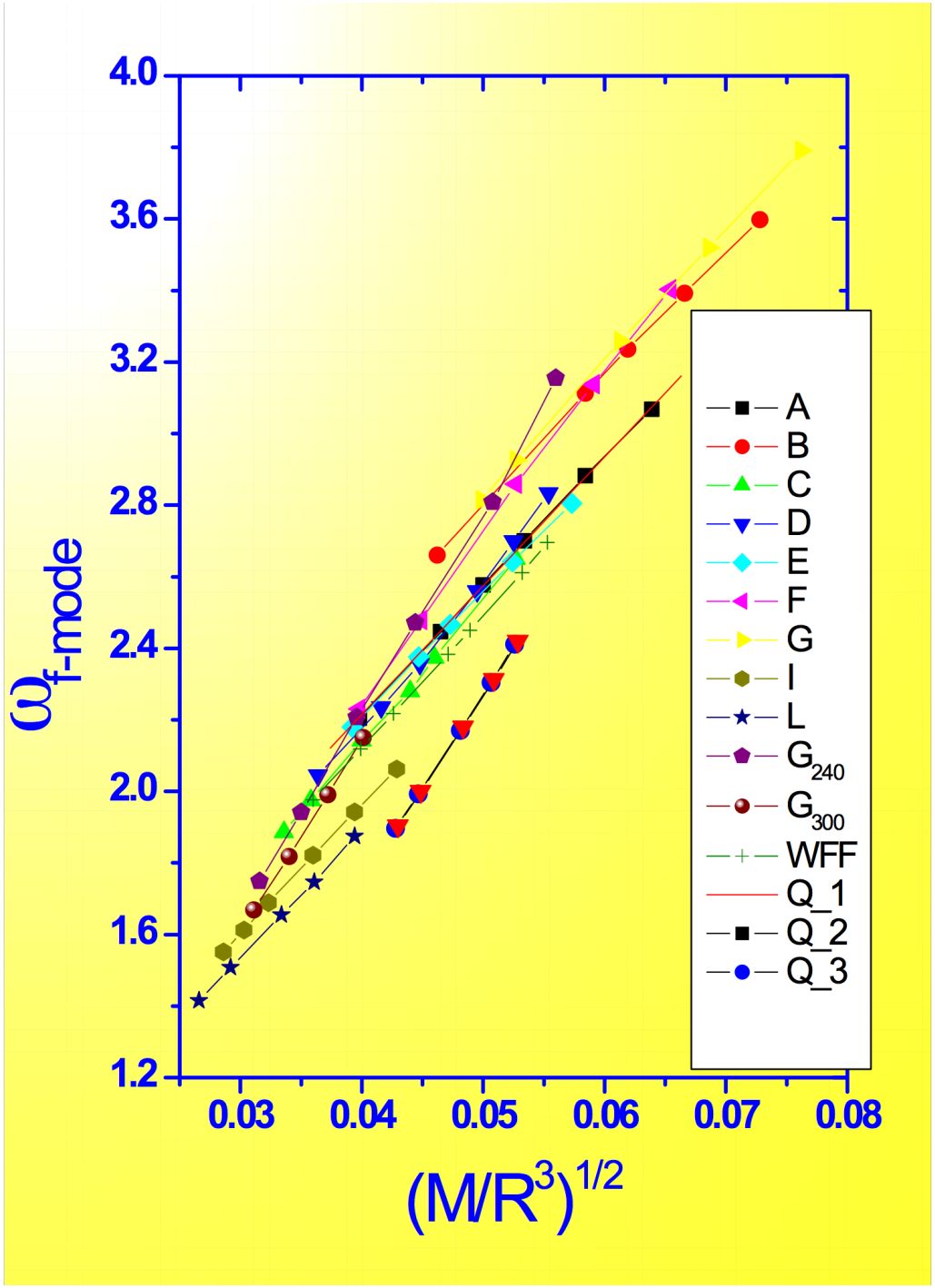

Empirical relations for GW asteroseismology:

$$\omega_f\,(kHz) \approx 0.78 + 1.637\left(\frac{M_{1.4}}{R_{10}^{\ 3}}\right)^{1/2}$$

Andersson & Kokkotas (1998)

Recently extended to fast rotation by Krueger and Kokkotas (2019) !

Radius Determination from Post-Merger Signal

Bauswein et al. (2012)

Bauswein, NS, Janka (2016)

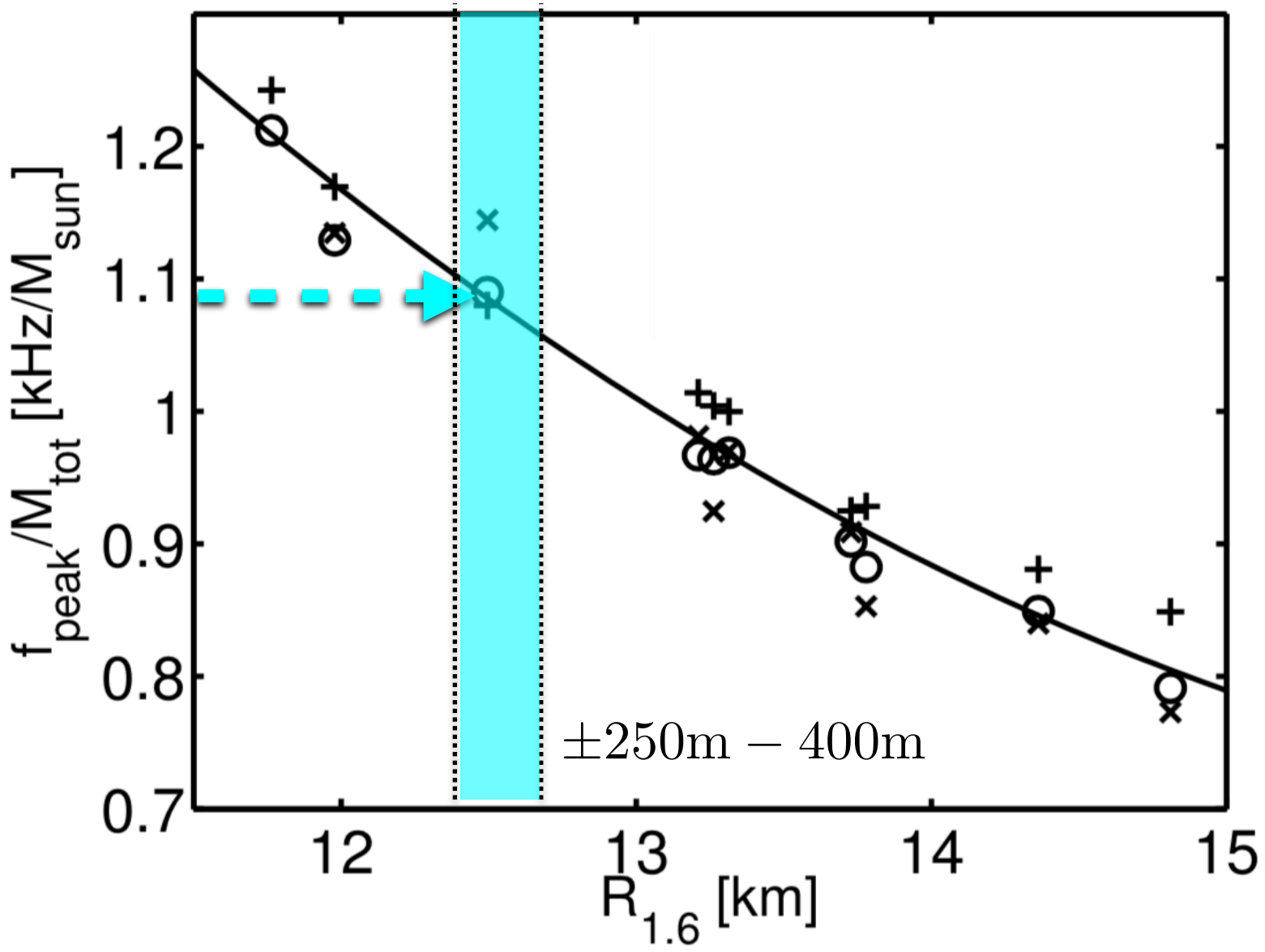

Asymmetric Mergers

Bauswein, NS & Janka (2016)

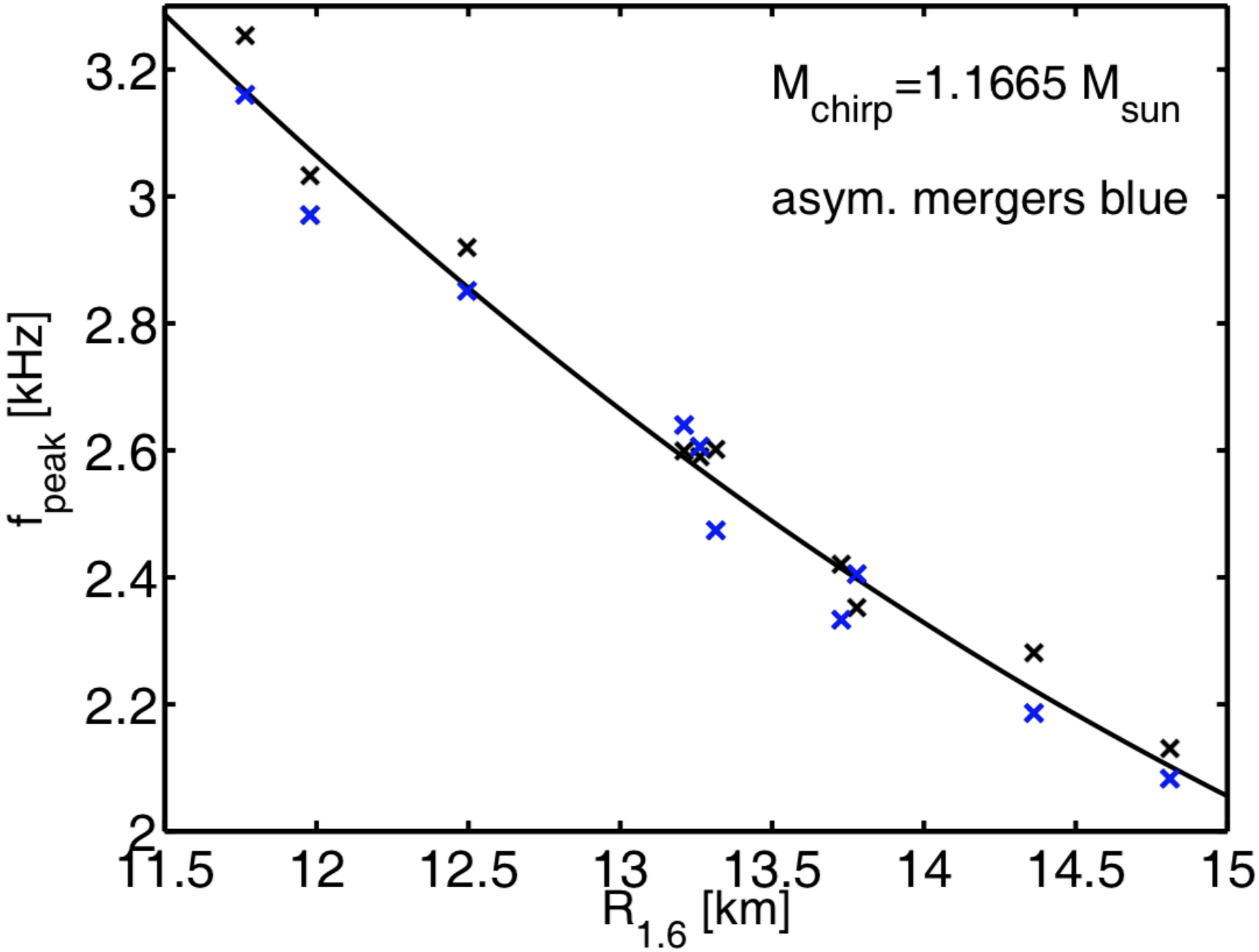

EOS with Strong Phase Transition

Bauswein et al. (2018)

A strong first-order phase transition will have a significant effect on radius extraction.

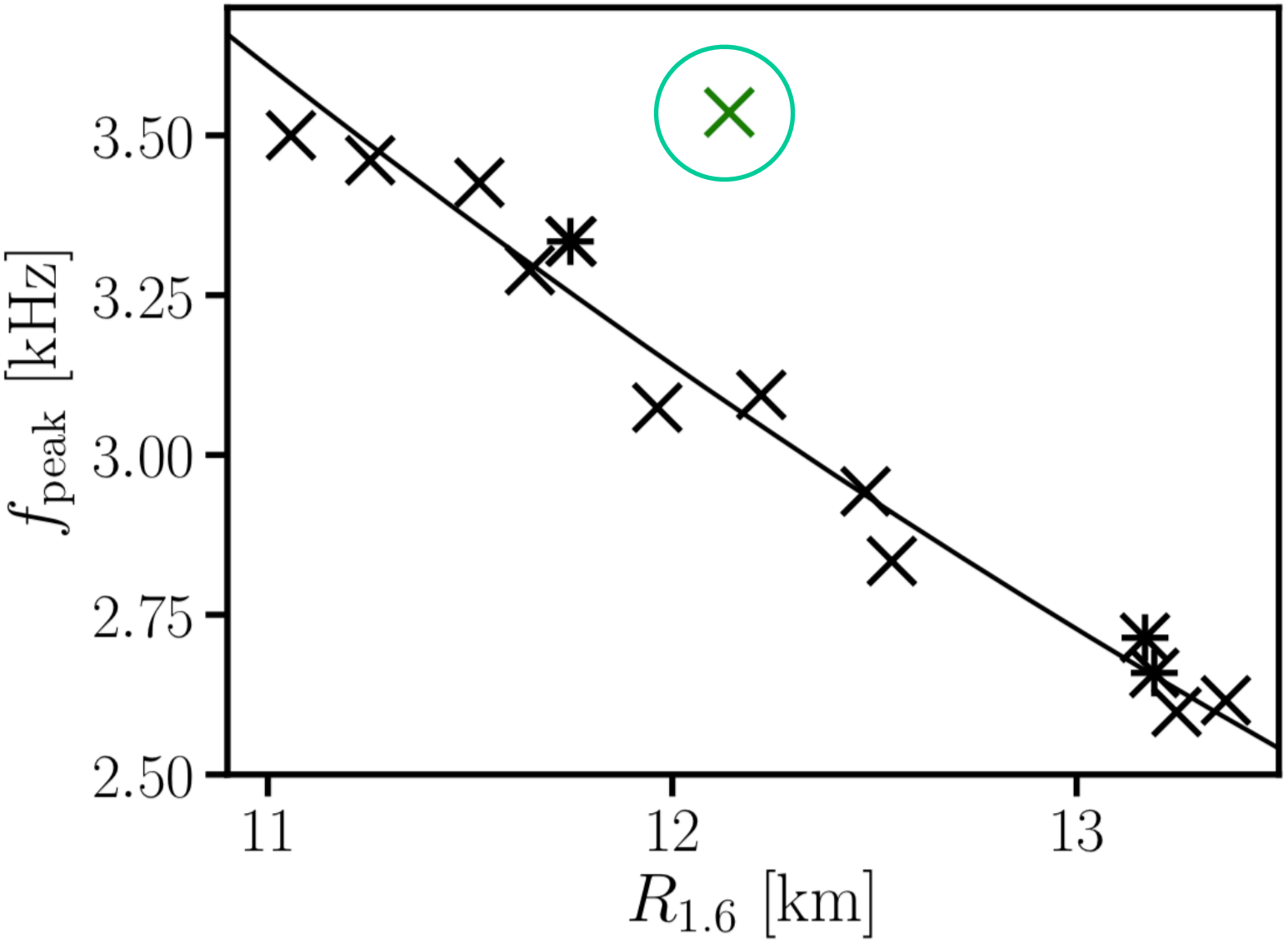

Optimized Empirical Relations

Vretinaris, NS & Bauswein (2019)

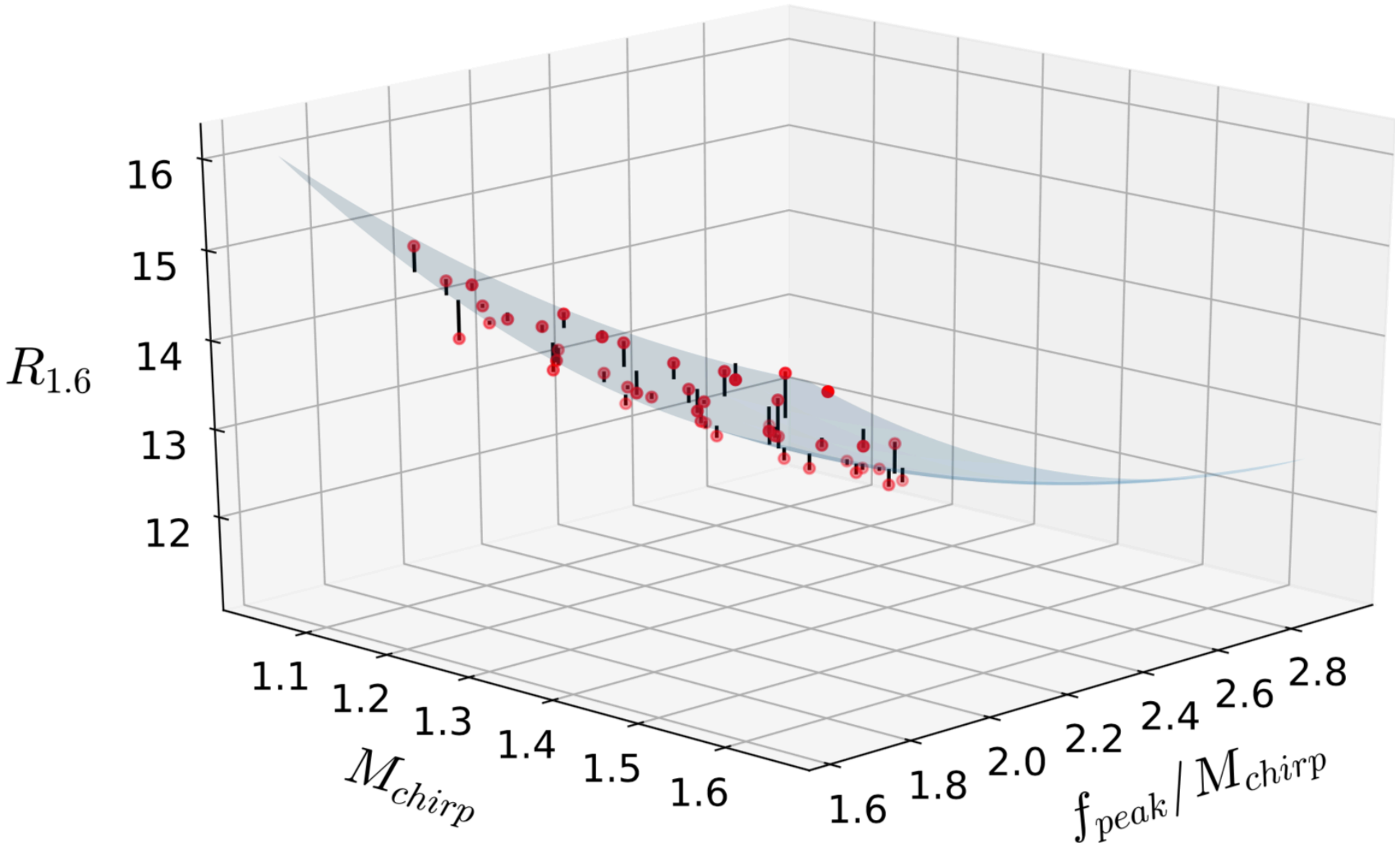

Optimized Empirical Relations

Vretinaris, NS & Bauswein (2019)

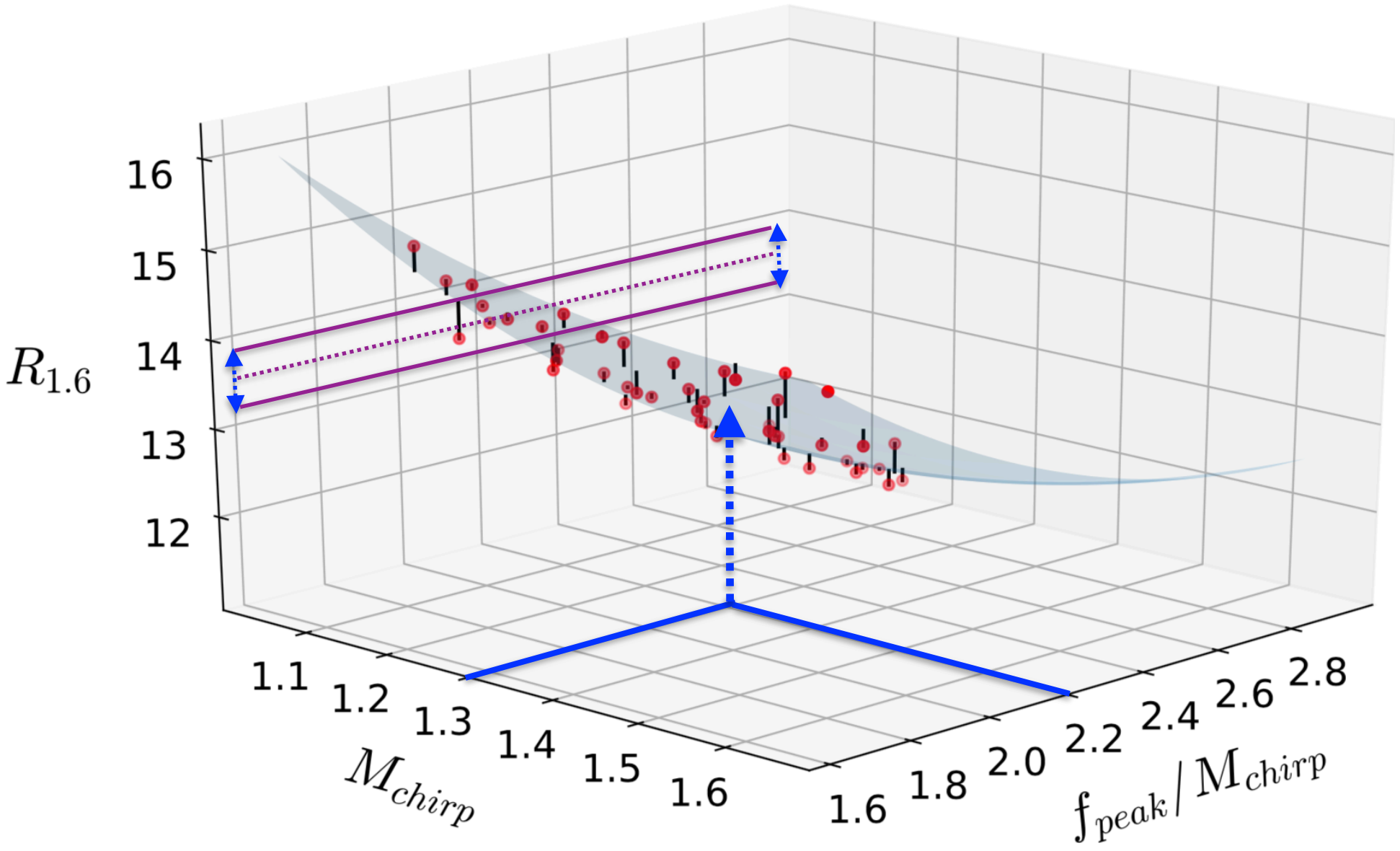

Reconstructing the M-R Diagram

Vretinaris, NS & Bauswein (2019)

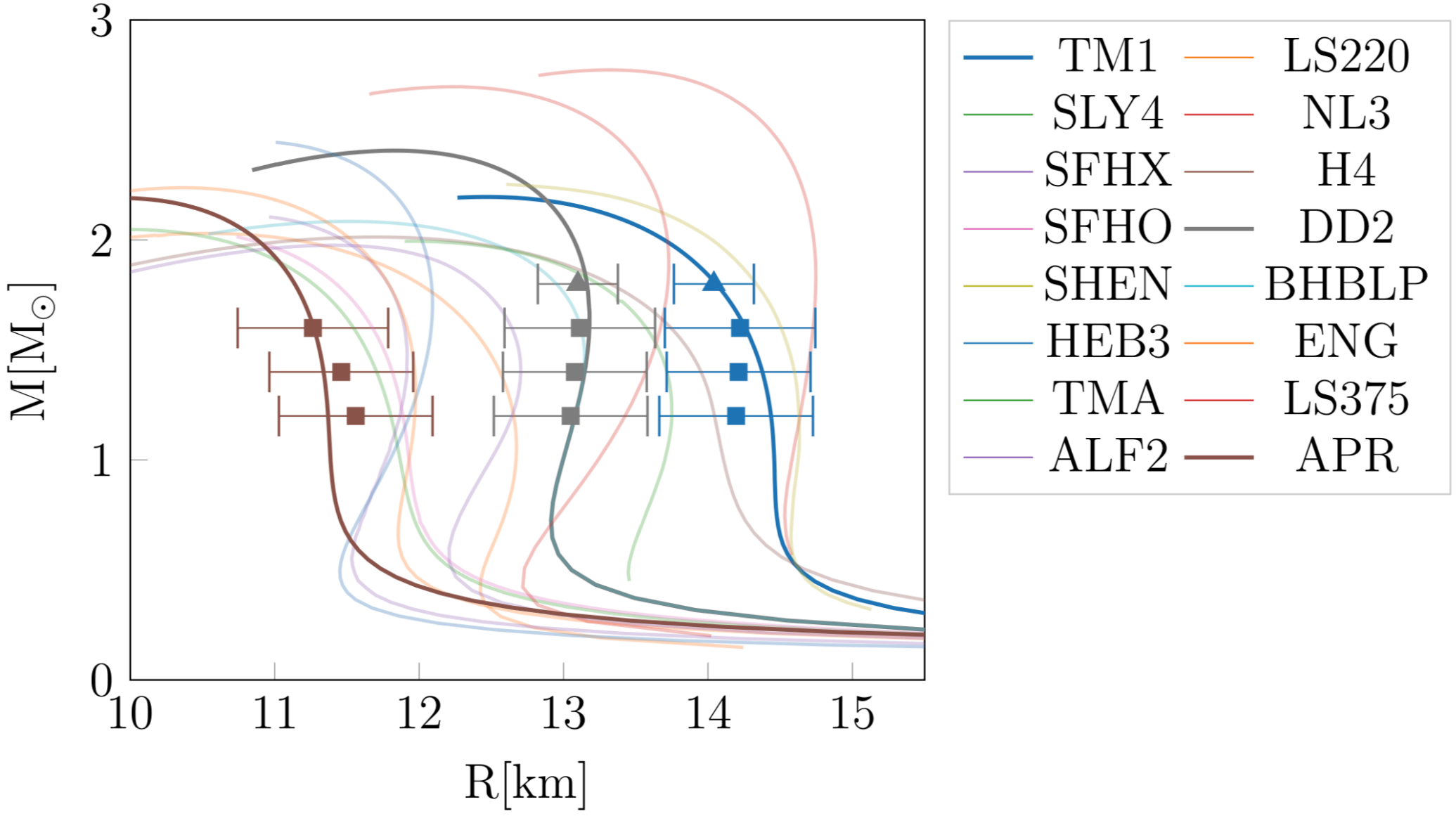

Λ through Post-merger Oscillations

Vretinaris, NS & Bauswein (2019)

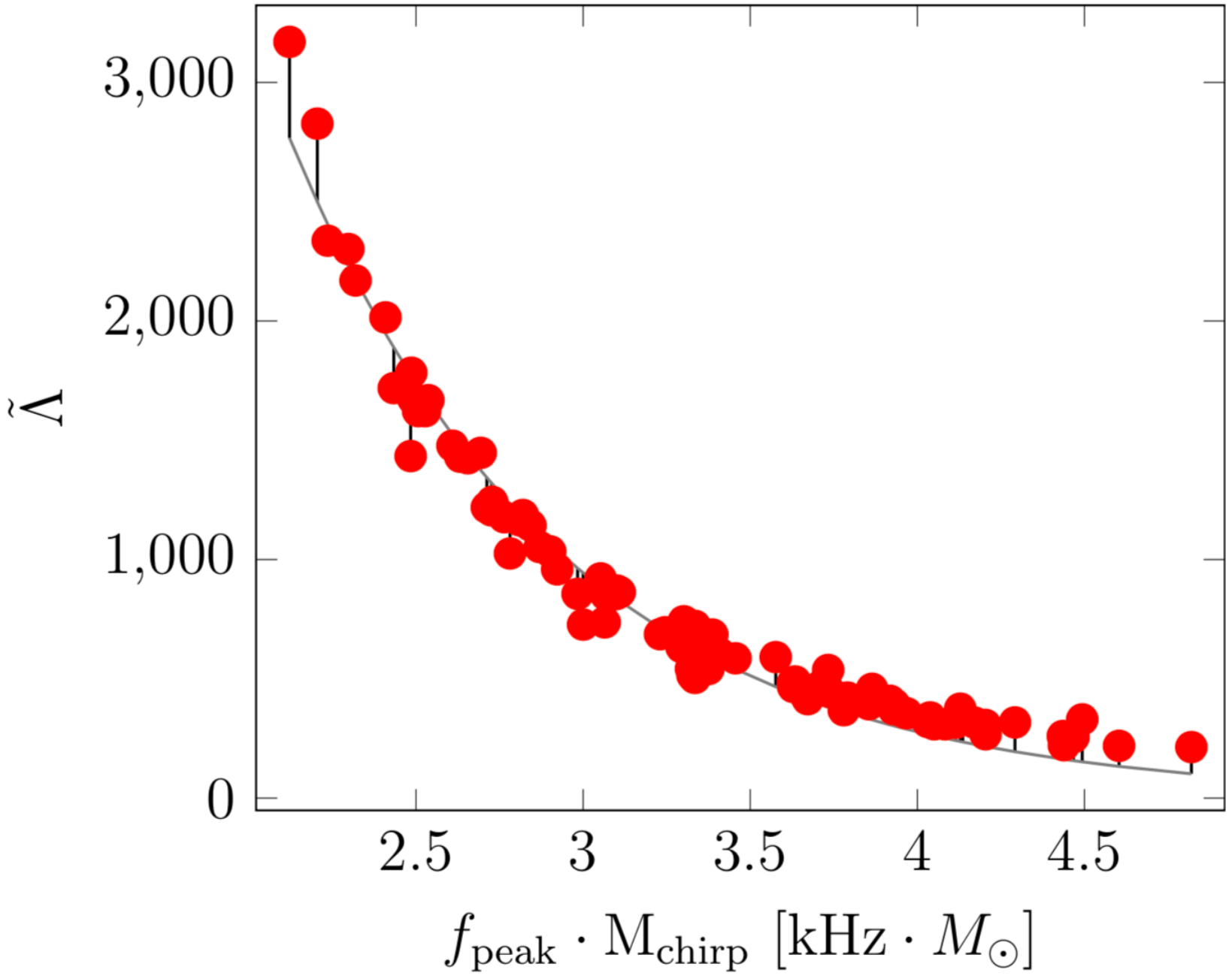

Λ through Post-merger Oscillations

Vretinaris, NS & Bauswein (2019)

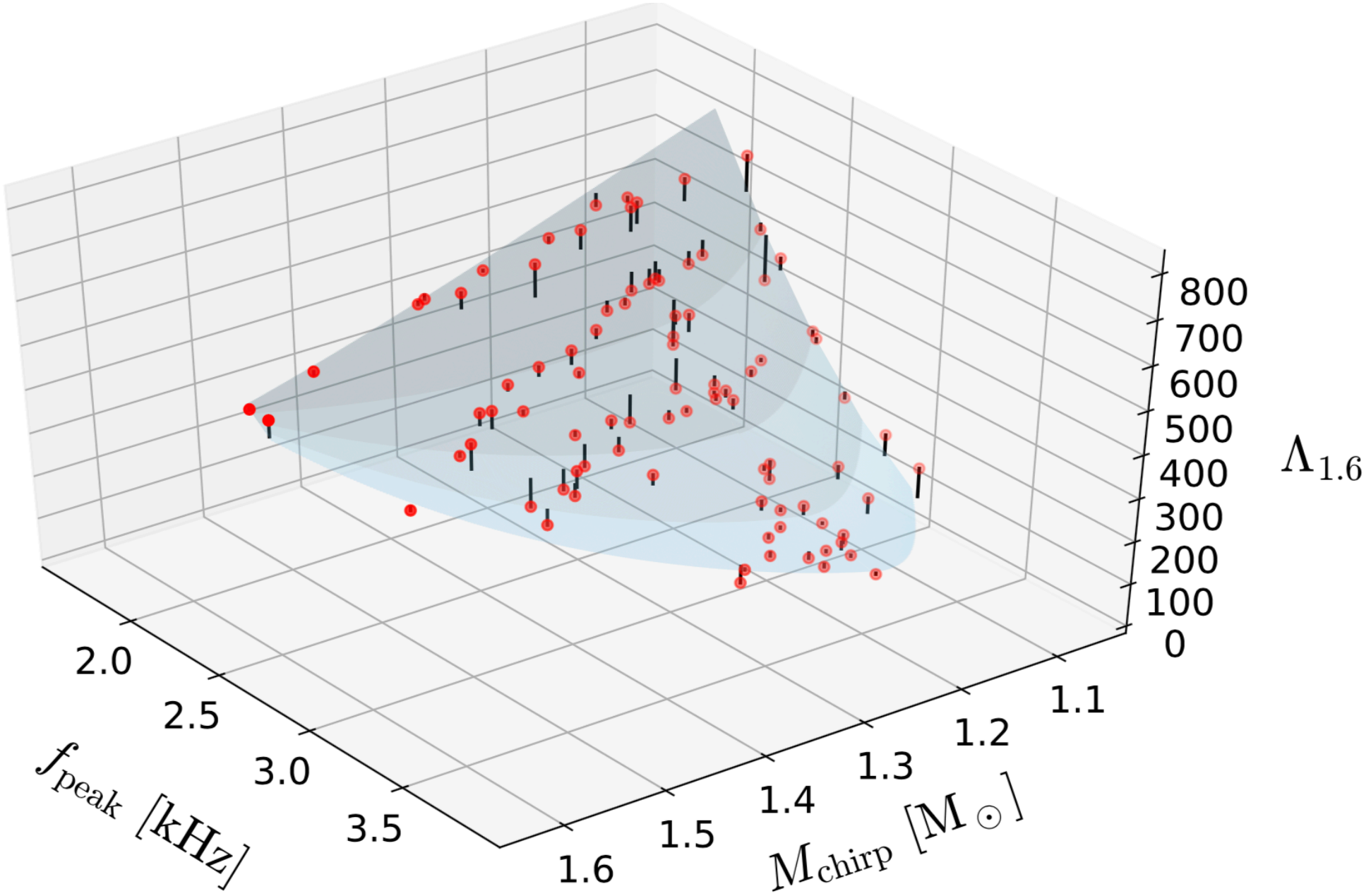

2G, 2+G & 3G Detectors

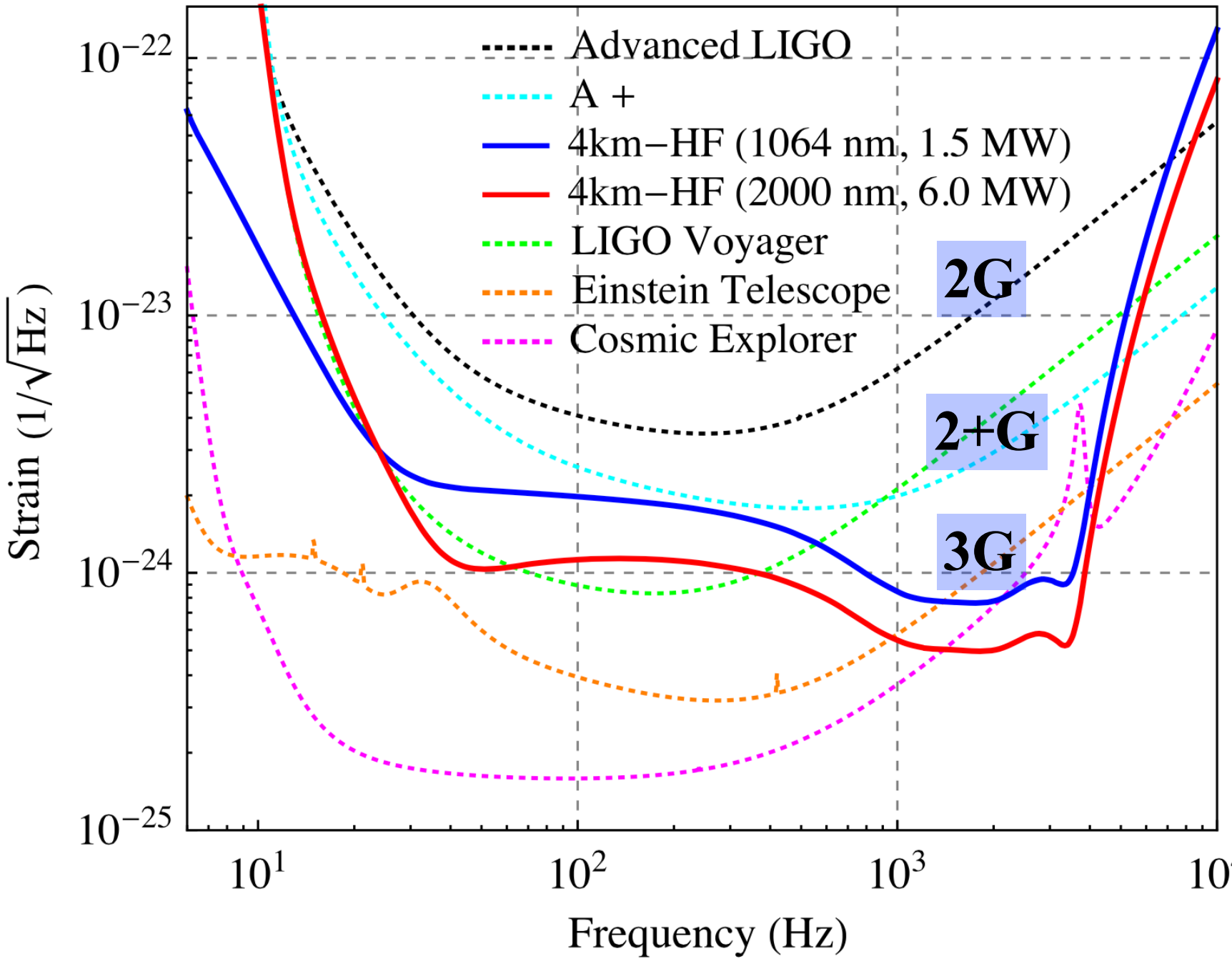

Miao et al (2018)

OzHF 2km High-Frequency GW Detector

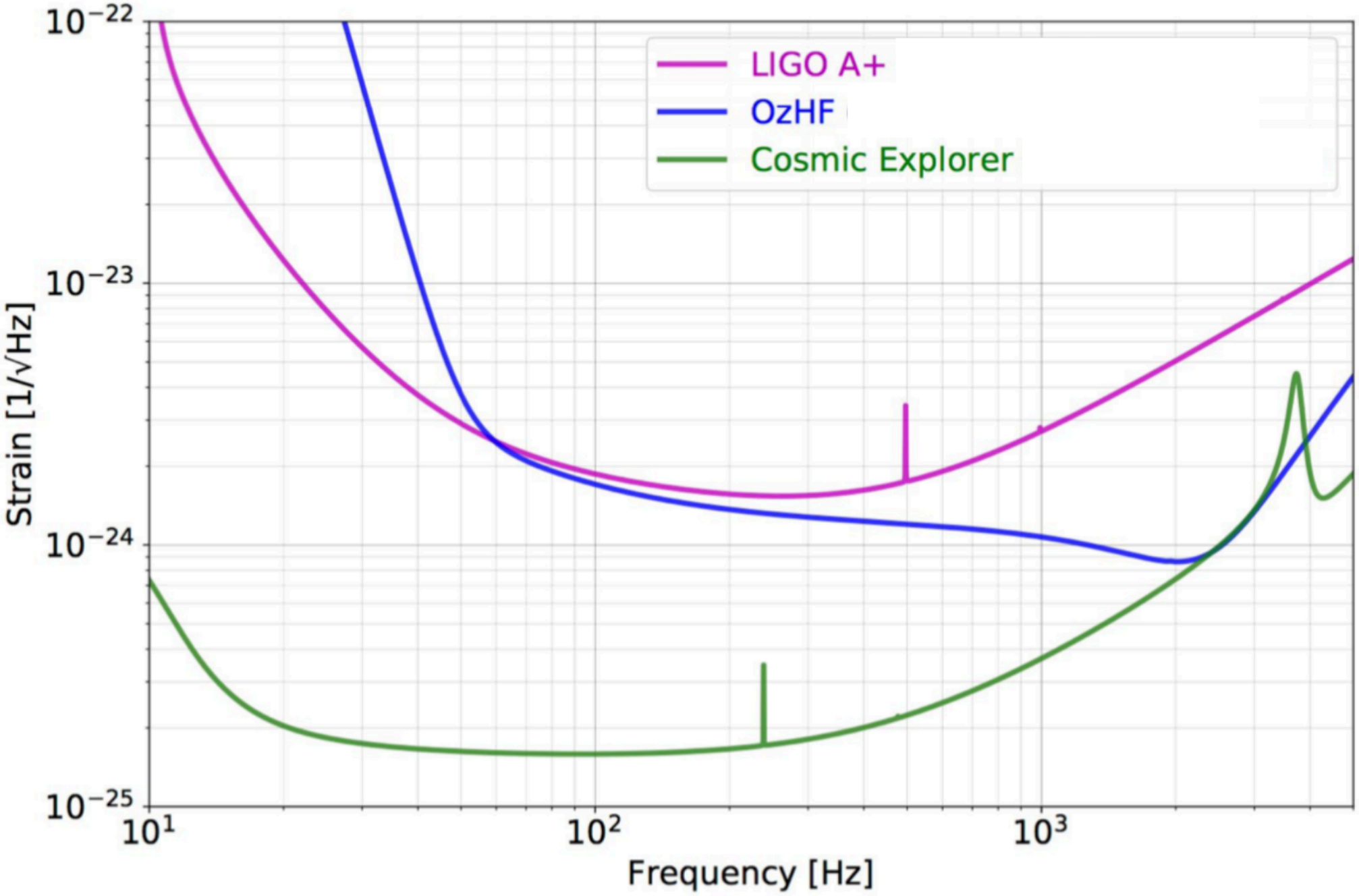

Lasky et al (2019)

Detectability of Post-Merger GWs

Clark, Bauswein, NS, Shoemaker (2016)

PCA template: extracts >80% of signal power.

Single-detector detectability (S/N>5, optimal orientation)

Instrument	$\mathrm{SNR}_{\mathrm{full}}$	$\mathrm{SNR}_{\mathrm{post}}$	D_{hor} [Mpc]	$\dot{\mathcal{N}}_{\mathrm{det}}$ [year^{-1}]	
aLIGO	$2.99^{3.86}_{2.37}$	$1.48^{1.86}_{1.13}$	$29.89^{38.57}_{23.76}$	$0.01^{0.03}_{0.01}$	2G
A+	$7.89^{10.16}_{6.25}$	$4.19^{5.35}_{3.26}$	$78.89^{101.67}_{62.52}$	$0.13^{0.20}_{0.10}$	2G+
LVoyager	$14.06^{18.13}_{11.16}$	$7.28^{9.30}_{5.64}$	$140.56^{181.29}_{111.60}$	$0.41^{0.88}_{0.21}$	
ET-D	$26.65^{34.28}_{20.81}$	$12.16^{15.31}_{9.34}$	$266.52^{342.80}_{208.06}$	$2.81^{5.98}_{1.33}$	3G
CE	$41.50^{53.52}_{32.99}$	$20.52^{25.83}_{15.72}$	$414.62^{535.221}_{329.88}$	$10.59^{22.78}_{5.33}$	

Improvements:

- Network of 5 detectors
- Stacking of several detections (e.g. Bose et al. 2018)
- Improved templates

3G Detectors

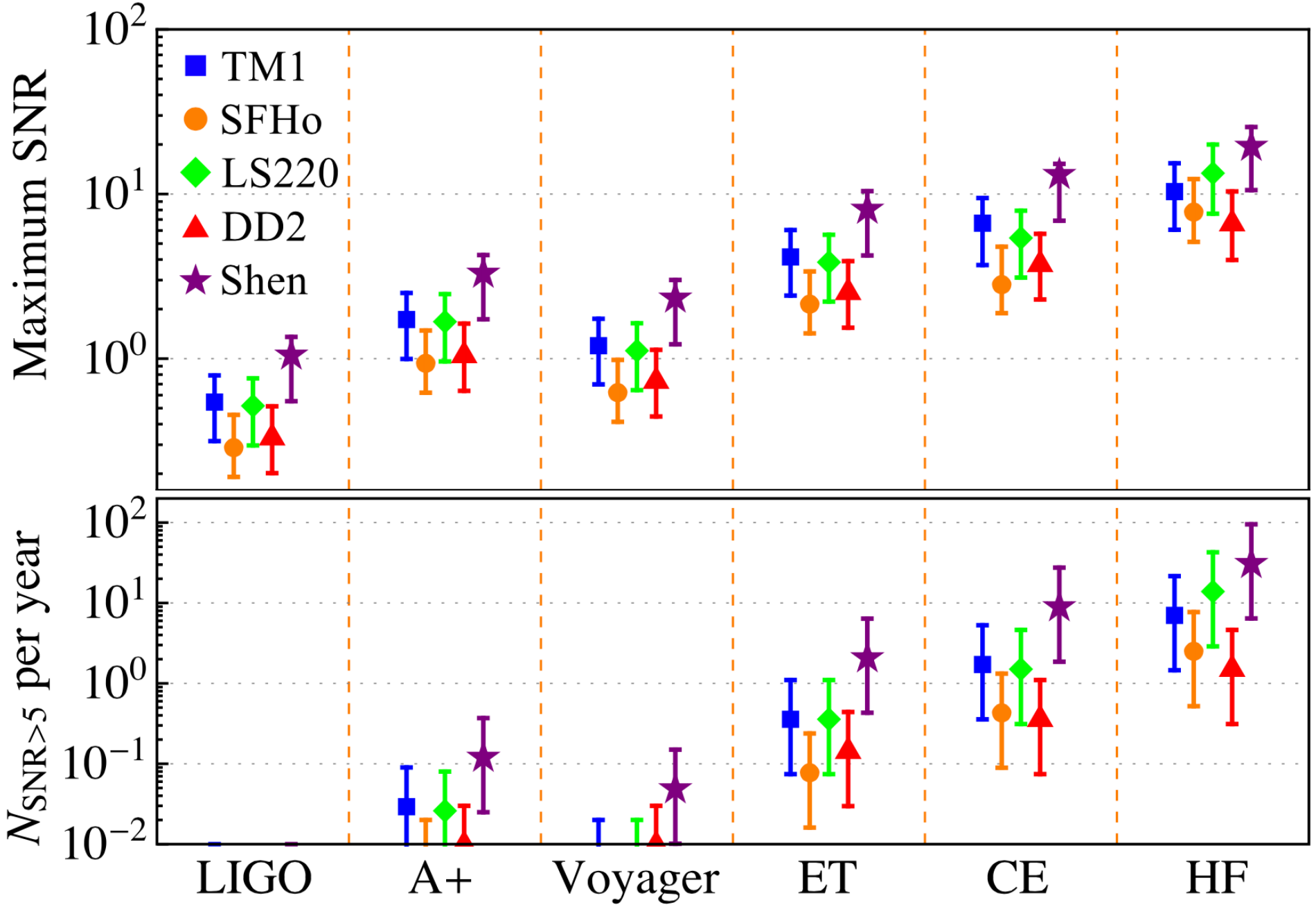

Miao et al (2018)

Inertial Modes!

(Physical Review Letters, 2018)

Convective Excitation of Inertial Modes in Binary Neutron Star Mergers

Roberto De Pietri,[1,2] Alessandra Feo,[3,2] José A. Font,[4,5] Frank Löffler,[6,7] Francesco Maione,[1,2]
Michele Pasquali,[1,2] and Nikolaos Stergioulas[8]

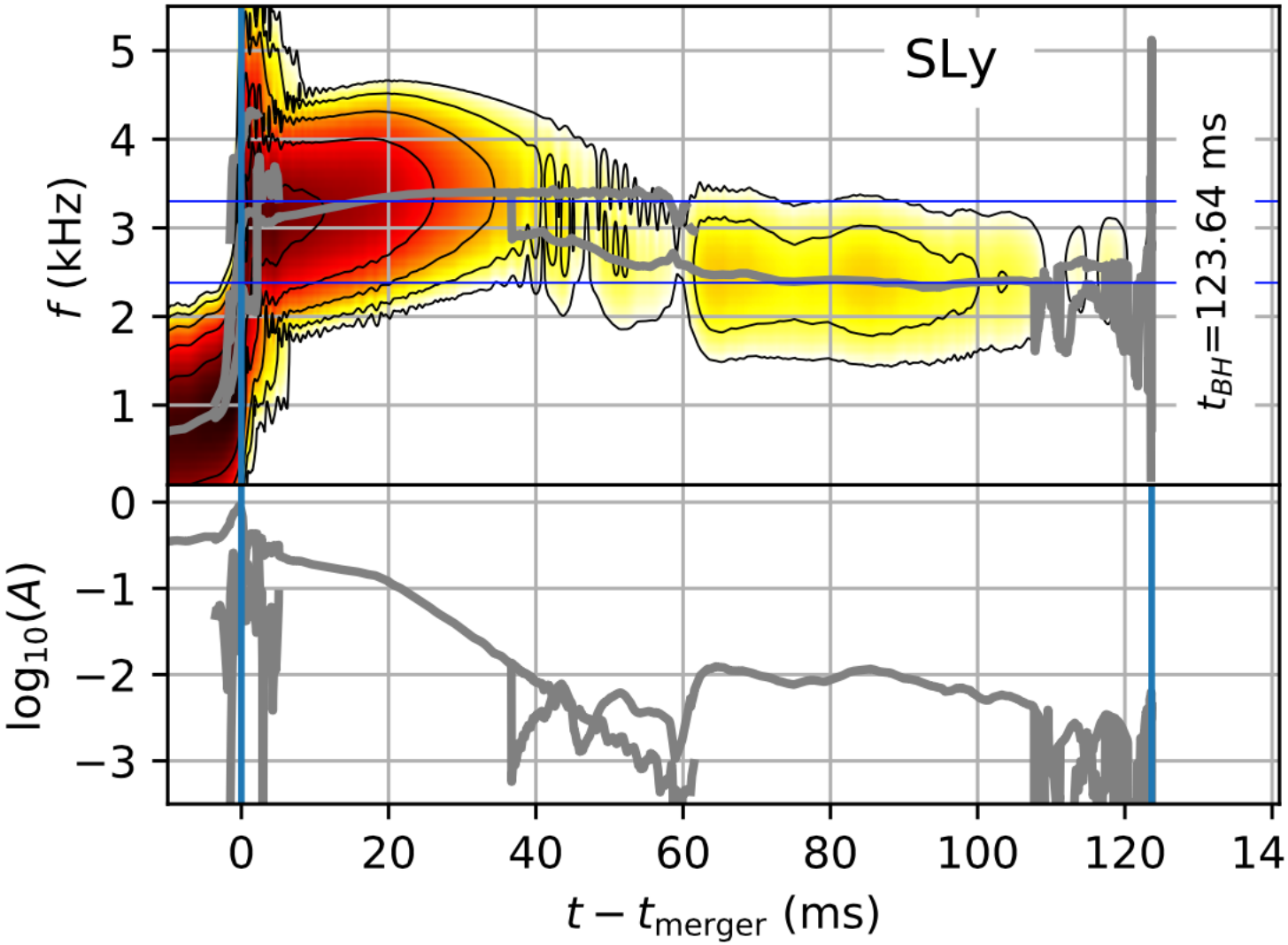

30 million core hours (PRACE)

Convective Instability

The local convective instability depends on the sign of the Schwarzschild discriminant

$$A_\alpha = \frac{1}{\varepsilon + p}\nabla_\alpha \varepsilon - \frac{1}{\Gamma_1 p}\nabla_\alpha p$$

where

$$\Gamma_1 := (\varepsilon + p)/p(dp/d\varepsilon)_s = (d\ln p/d\ln\rho)_s$$

is the adiabatic index.

$A_\alpha < 0$ convective stability

$A_\alpha > 0$ convective instability

For a piecewise-polytropic EOS with a thermal component, we find analytically:

$$\Gamma_1 = \Gamma_{\rm th} + (\Gamma_i - \Gamma_{\rm th})\frac{K_i \rho^{\Gamma_i}}{p}$$

Convective Instability

The sign of A_r in the equatorial plane:

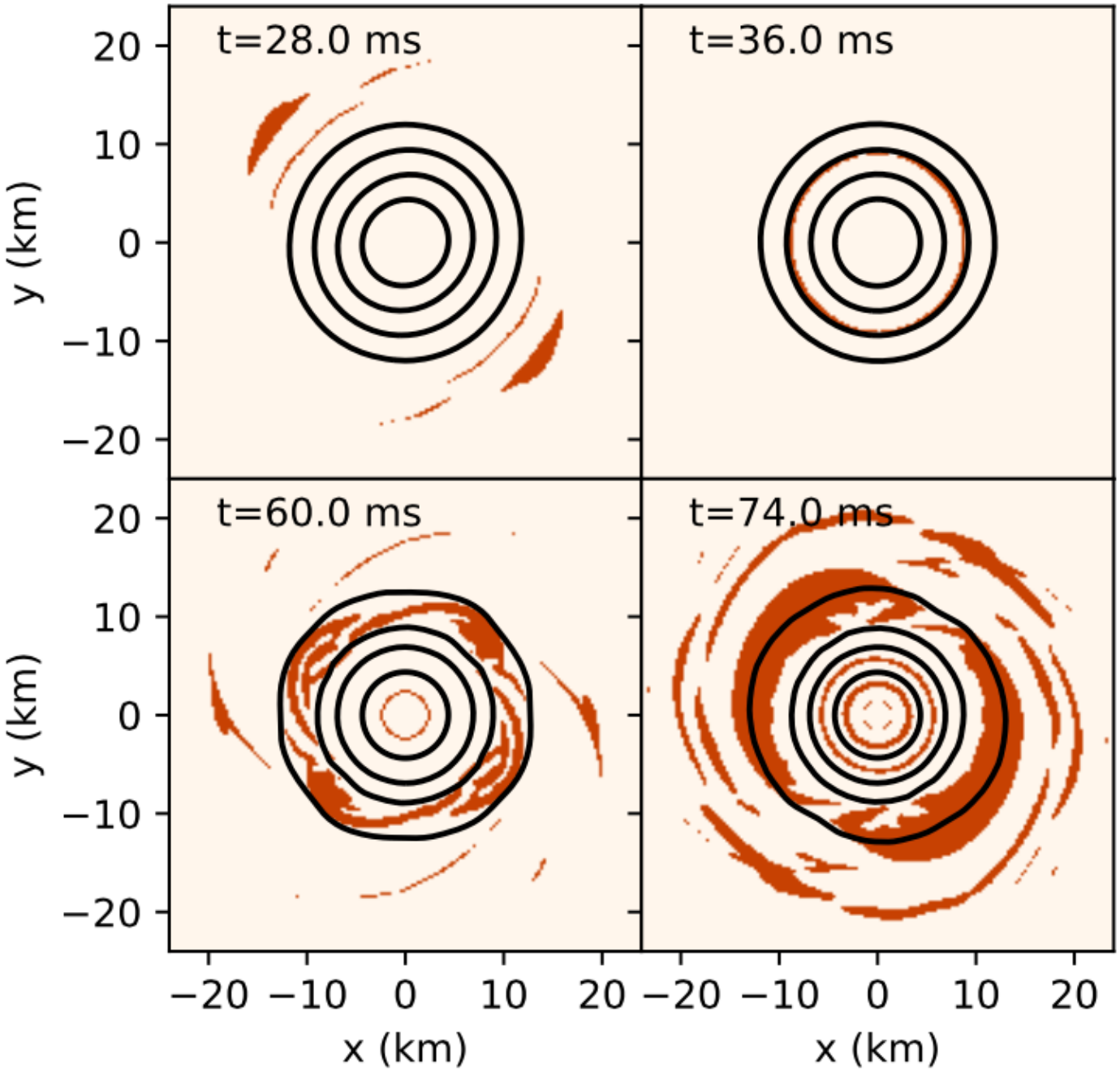

Thermal Evolution

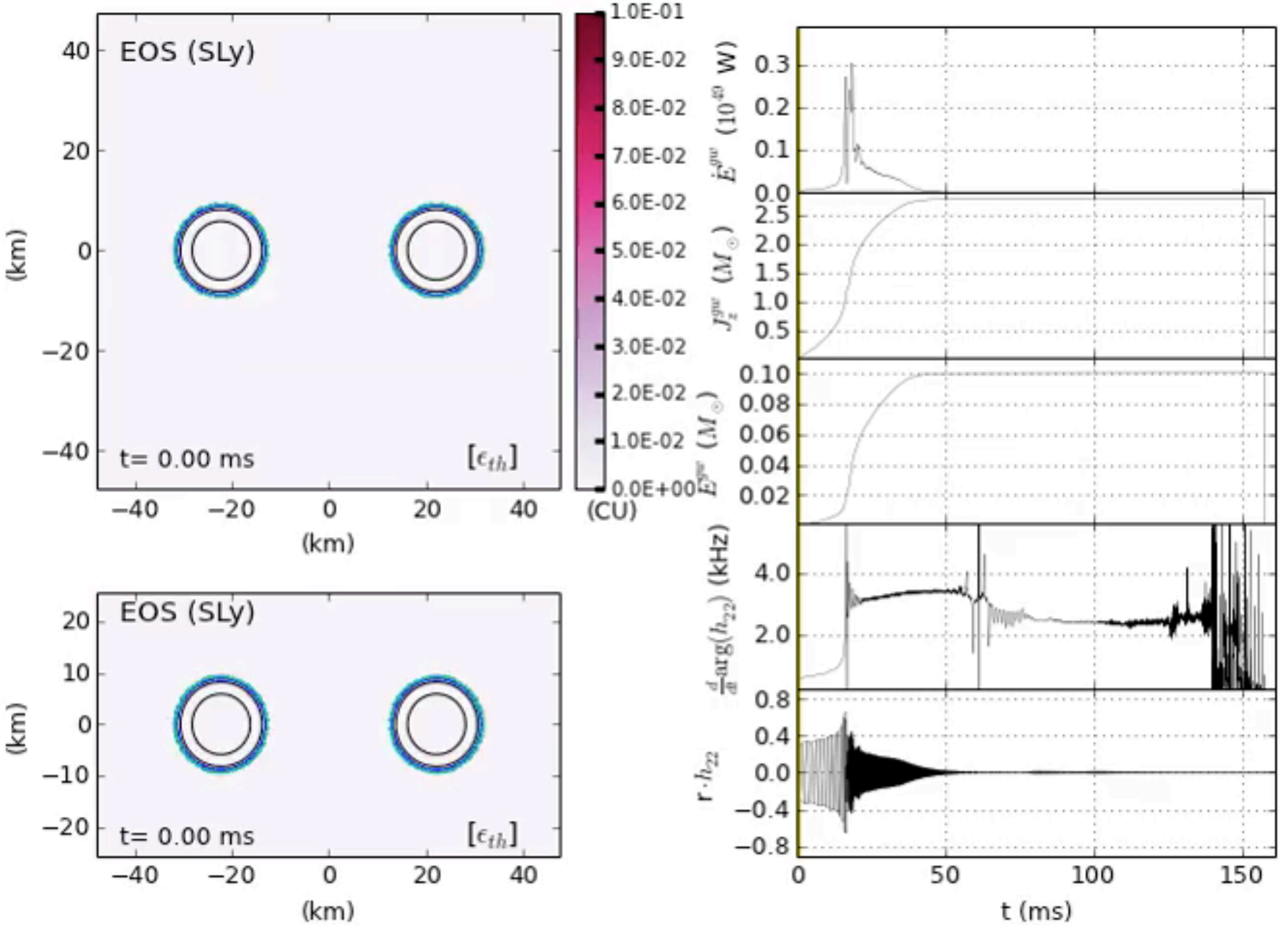

Oscillations

***f*-modes**

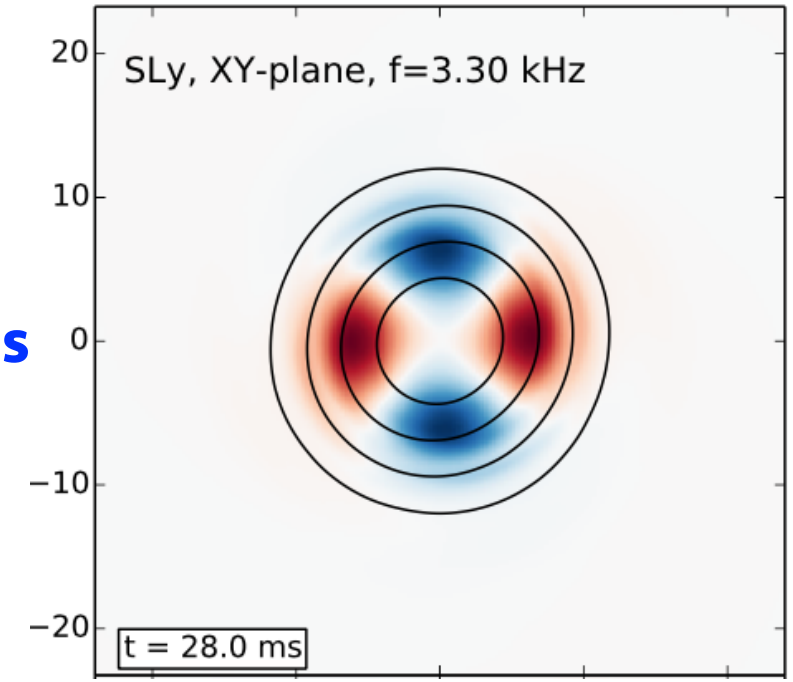

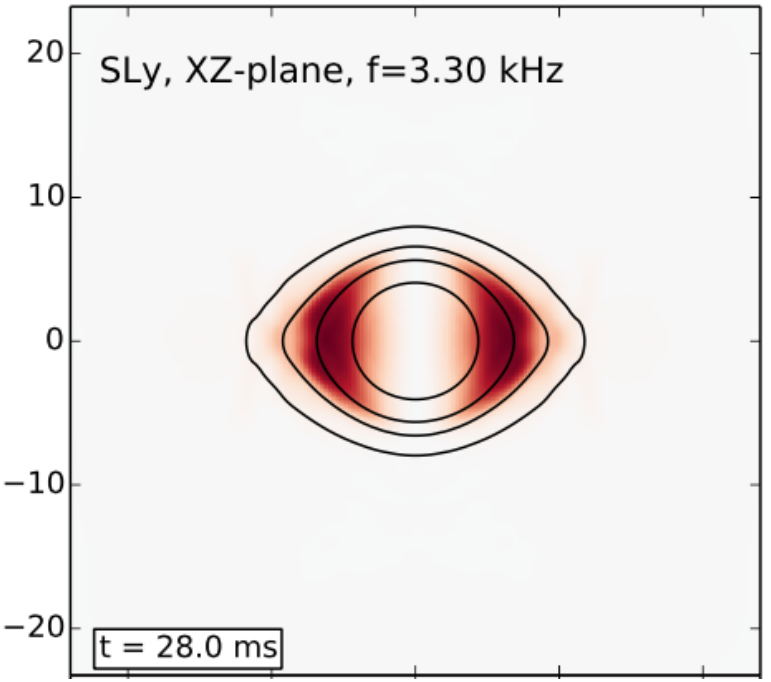

Oscillations

***f*-modes**

***inertial* modes**

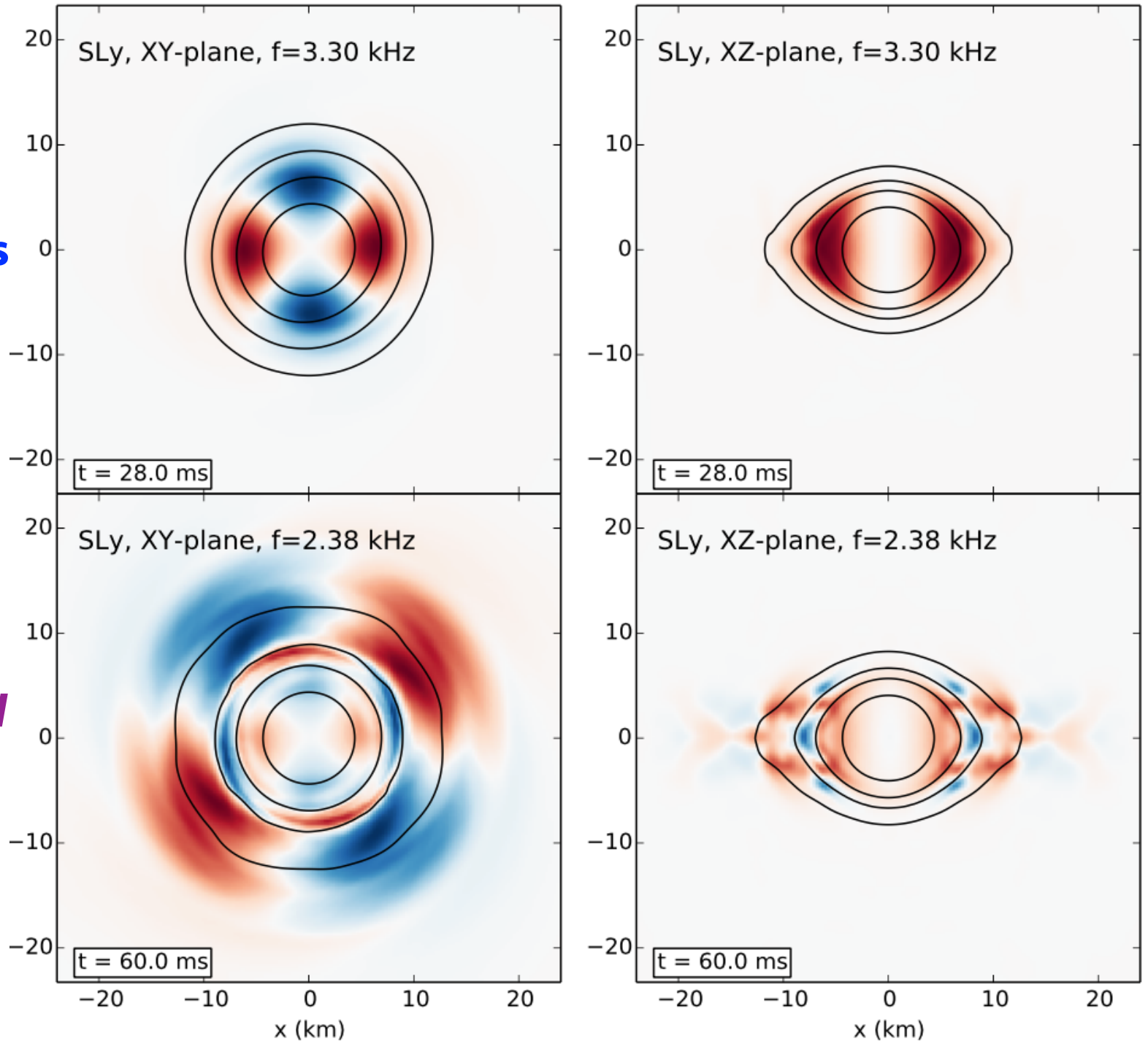

Gravitational Wave Spectrum

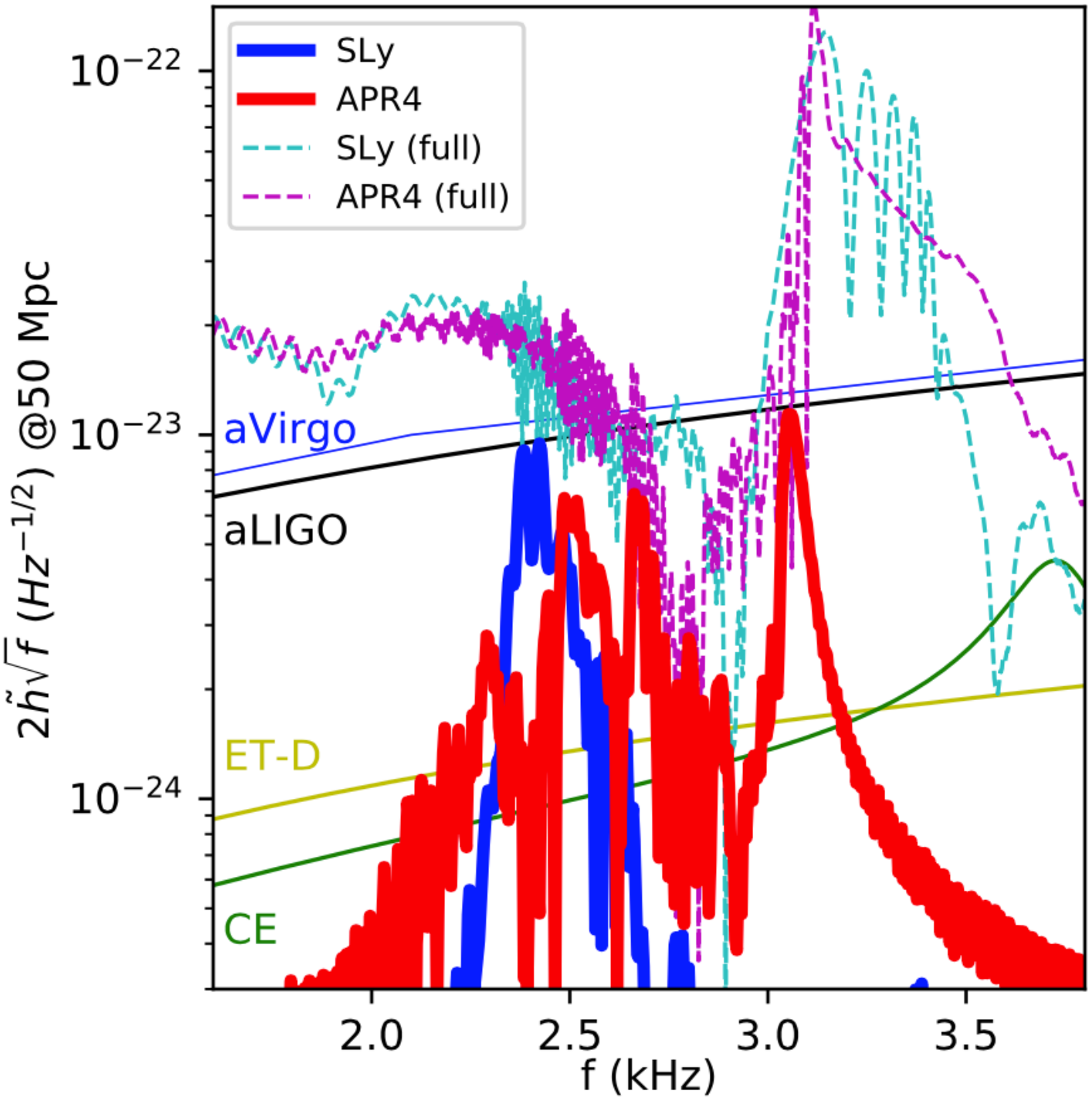

Summary

- Based on a set of minimal assumptions, we set a *strict* lower limit on neutron star radii of 10.7km at $1.6M_{sun}$.
- Gravitational-wave asteroseismology can constrain the neutron star radius to within 0.4km with future observations.
- Principal Component Analysis (PCA) sufficient to reach >80% of optimal signal.
- We discovered *convective instabilities* and *inertial modes* that can probe the thermal part of the EOS.
- Once the EOS is well constrained, one can investigate departures from GR.

Supplementary material

Nonradial Oscillations

$\ell = 0$

$\ell = 1$

$\ell = 2$

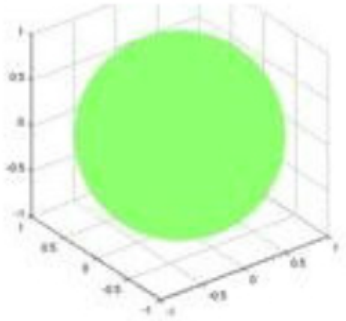

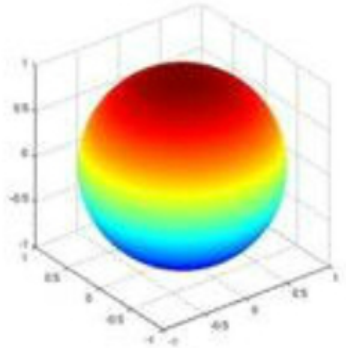

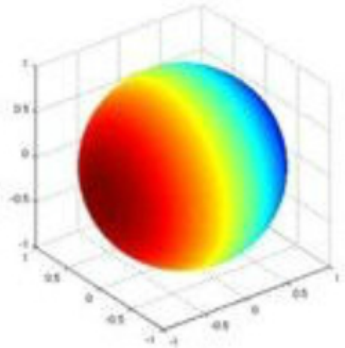

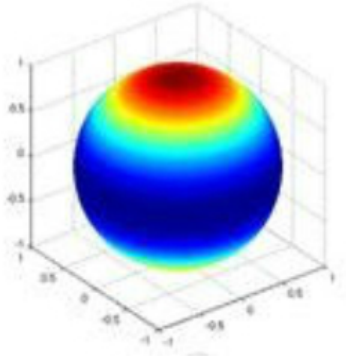

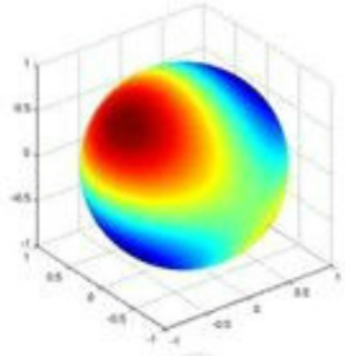

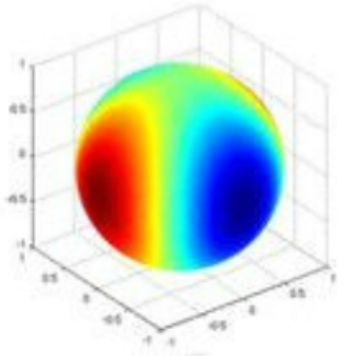

$m = 0$ (zonal)

$m = 1$

$m = 2$

$$\cos(m\phi)\ P_\ell^m(\cos\theta)$$

$l = m$ (sectoral)

$l \neq m$ (tesseral)

Breaking the EOS Degeneracy

Bauswein, NS, Janka (2014)

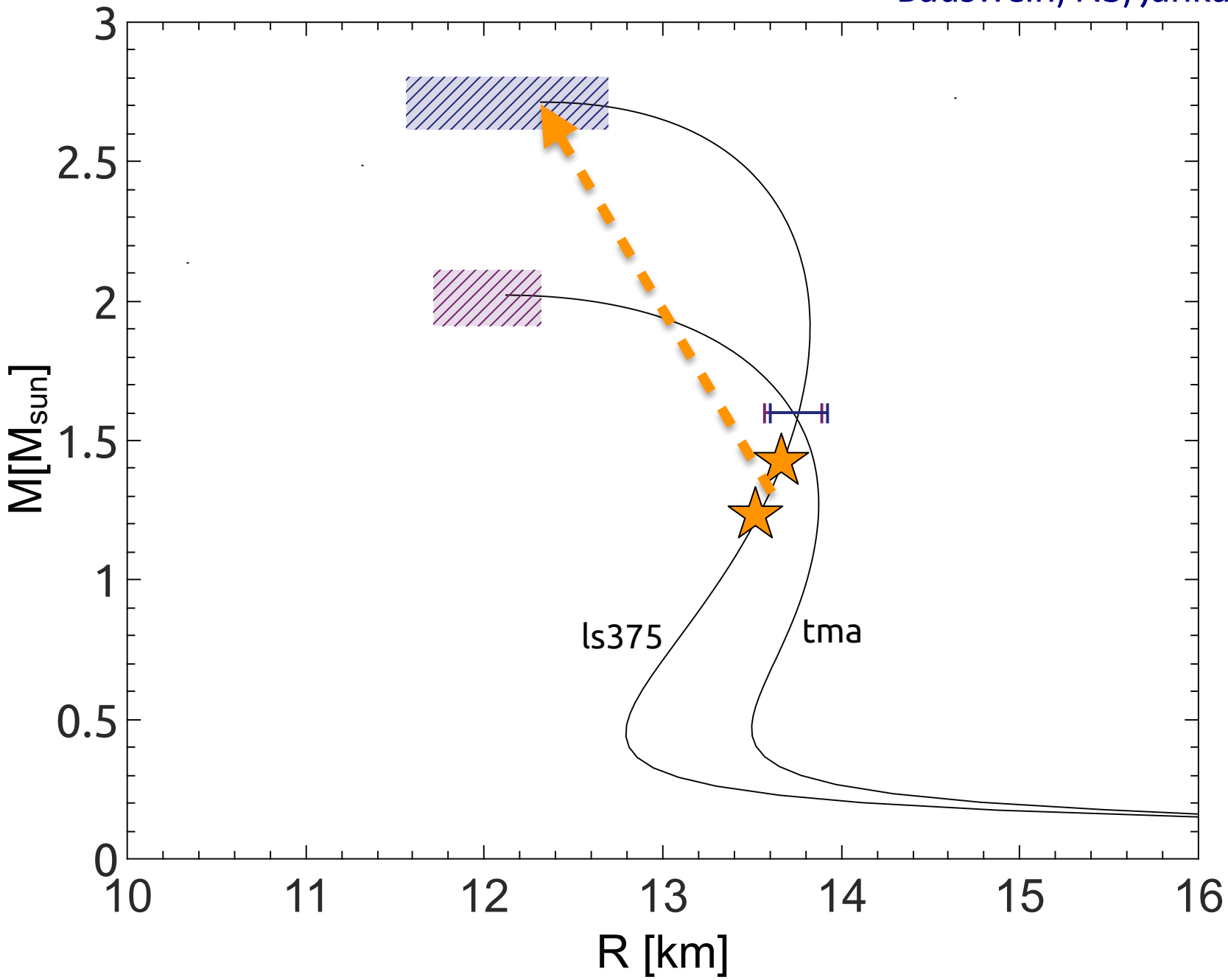

Analytic Model with Physical Parameters

Bauswein, NS & Janka (2016)

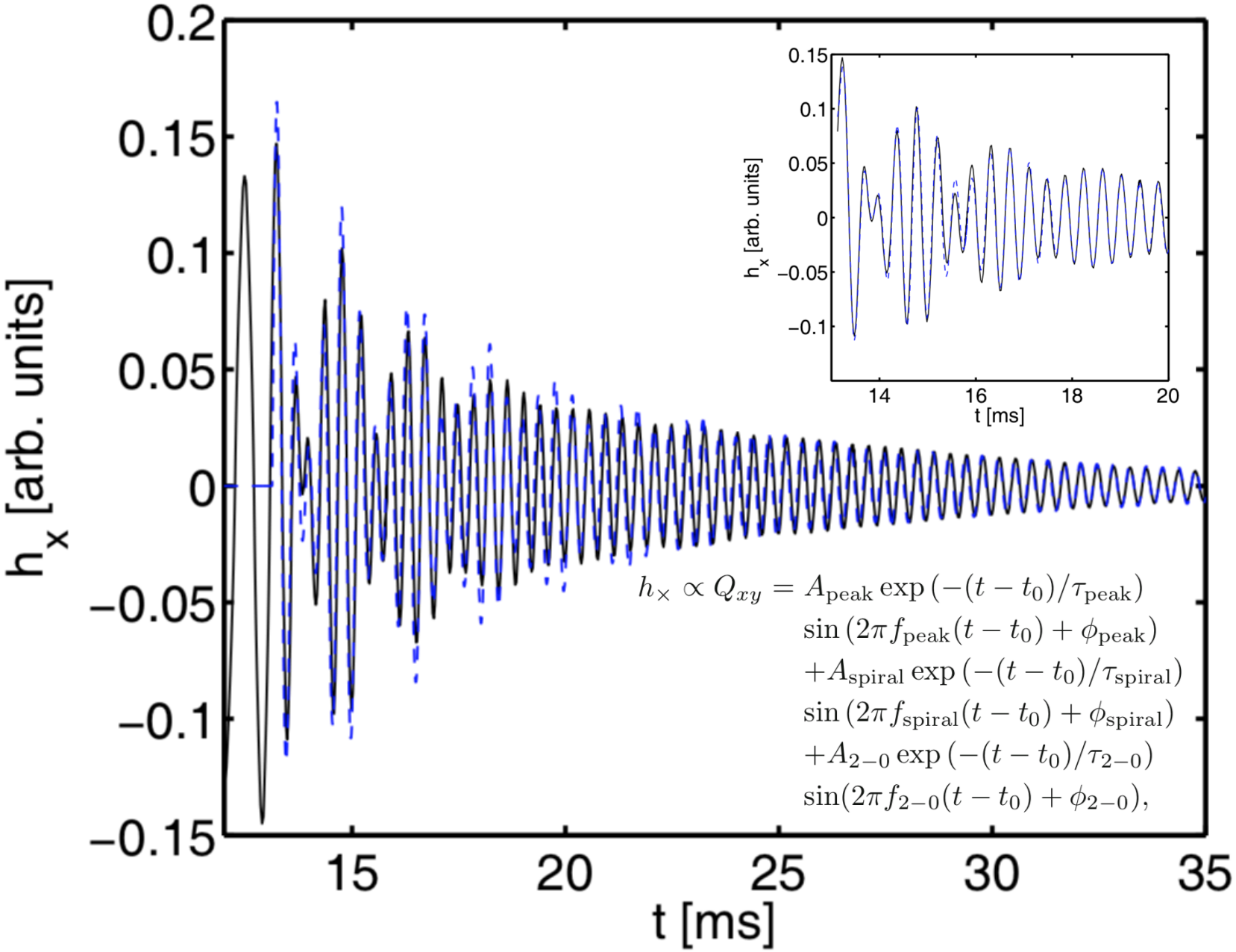

Central Lapse Evolution

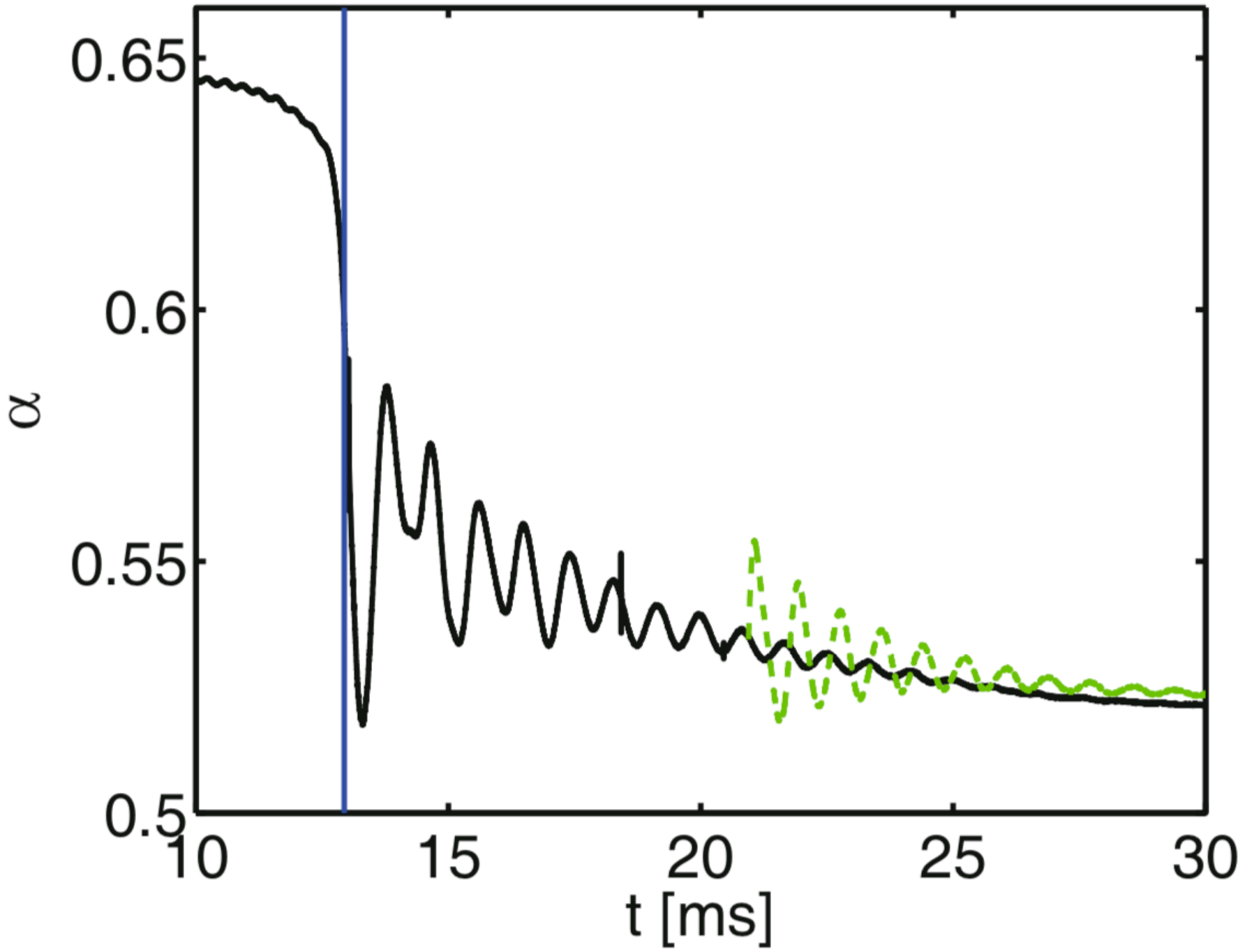

Late-time Excitation of m=2 Mode

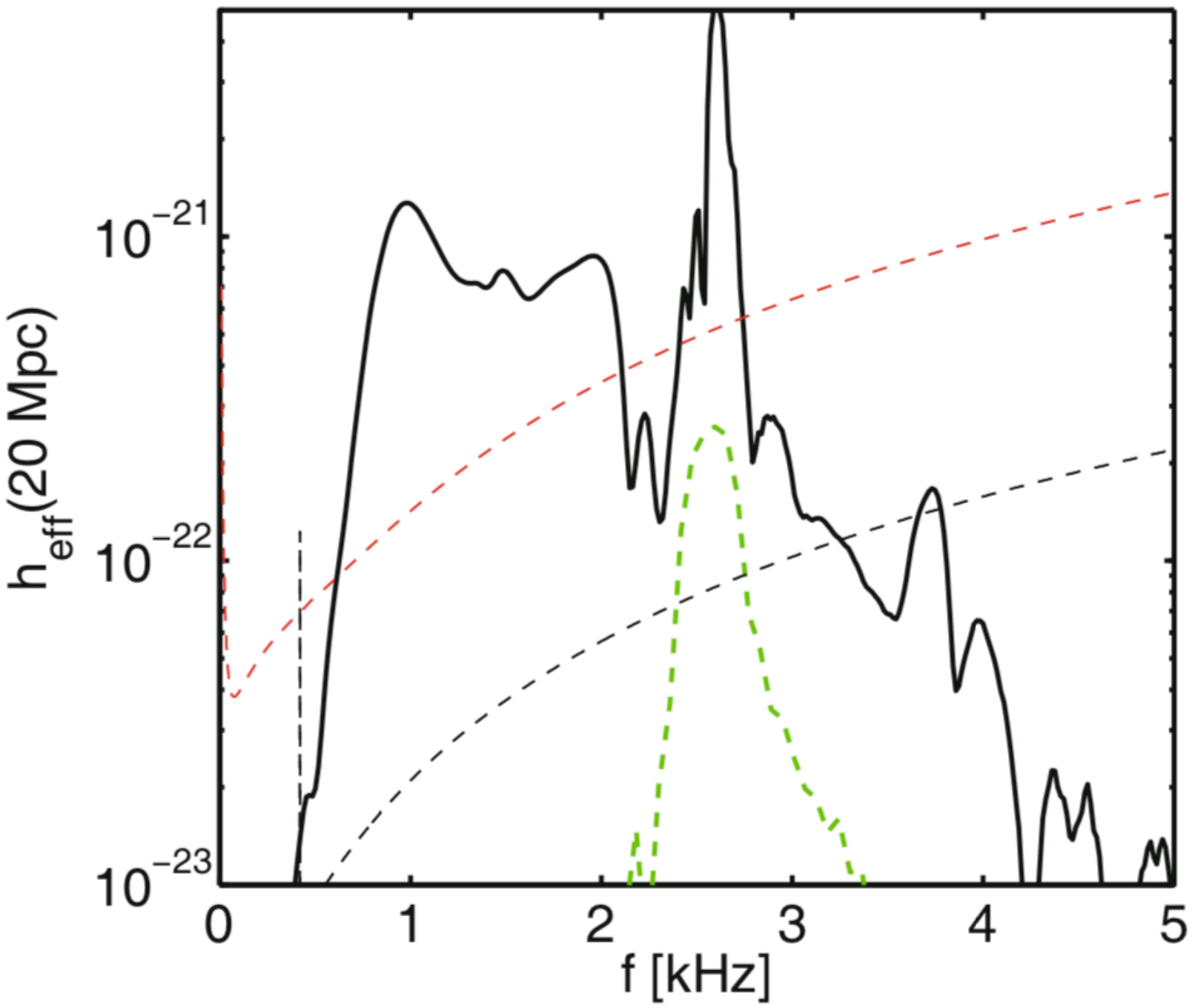

Nonradial Oscillations of Neutron Stars

Main oscillation modes:

1. *f*-modes / *p*-modes

   fluid modes restored by pressure

2. *g*-modes

   restored by gravity/buoyancy in non-isentropic stars

3. inertial modes (*r*-modes)

   restored by the Coriolis force in rotating stars

4. *w*-modes

   spacetime modes (similar to black hole modes)

GW-detection: *f*-, *p*-, *g*-, *r*-modes : stable oscillations

instabilities

Spacetime Evolution

90´s Nakamura, Oohara, Kojima / Shibata, Nakamura / Baumgarte, Shapiro

Definitions

$$\tilde{\gamma}_{ij} = e^{-4\phi}\gamma_{ij}$$

$$e^{4\phi} = \gamma^{1/3} \equiv \det(\gamma_{ij})^{1/3}$$

$$\tilde{A}_{ij} = e^{-4\phi}A_{ij} \quad A_{ij} = K_{ij} - \frac{1}{3}\gamma_{ij}K,$$

$$\tilde{\Gamma}^i := \tilde{\gamma}^{jk}\tilde{\Gamma}^i_{jk} = -\tilde{\gamma}^{ij}{}_{,j}$$

"1+log" lapse function

$$\partial_t \alpha = -2\alpha A$$

$$\partial_t A = \partial_t K$$

"Gamma-driver" shift condition

$$\partial_t \beta^i = B^i$$

$$\partial_t B^i = \frac{3}{4}\alpha\partial_t\tilde{\Gamma}^i - e^{-4\phi}\beta^i$$

Time evolution

$$\frac{d}{dt}\tilde{\gamma}_{ij} = -2\alpha\tilde{A}_{ij}, \qquad \frac{d}{dt} = \partial_t - \mathcal{L}_\beta$$

$$\frac{d}{dt}\phi = -\frac{1}{6}\alpha K.$$

$$\frac{d}{dt}K = -\gamma^{ij}D_iD_j\alpha + \alpha\left[\tilde{A}_{ij}\tilde{A}^{ij} + \frac{1}{3}K^2 + \frac{1}{2}(\rho + S)\right],$$

$$\frac{d}{dt}\tilde{A}_{ij} = e^{-4\phi}[-D_iD_j\alpha + \alpha(R_{ij} - S_{ij})]^{TF}$$

$$+ \alpha(K\tilde{A}_{ij} - 2\tilde{A}_{il}\tilde{A}^l_j),$$

$$\frac{\partial}{\partial t}\tilde{\Gamma}^i = -2\tilde{A}^{ij}\alpha_{,j} + 2\alpha\left(\tilde{\Gamma}^i_{jk}\tilde{A}^{kj} - \frac{2}{3}\tilde{\gamma}^{ij}K_{,j} - \tilde{\gamma}^{ij}S_j + 6\tilde{A}^{ij}\phi_{,j}\right)$$

$$- \frac{\partial}{\partial x^j}\left(\beta^l\tilde{\gamma}^{ij}{}_{,l} - 2\tilde{\gamma}^{m(j}\beta^{i)}_{,m} + \frac{2}{3}\tilde{\gamma}^{ij}\beta^l_{,l}\right).$$

Radius Determination from Post-Merger Signal

Bauswein, Janka, Hebeler & Schwenk (2012)

f_{peak} correlates very well with the radius @ 1.6 Msun (M_{tot} is known from inspiral).

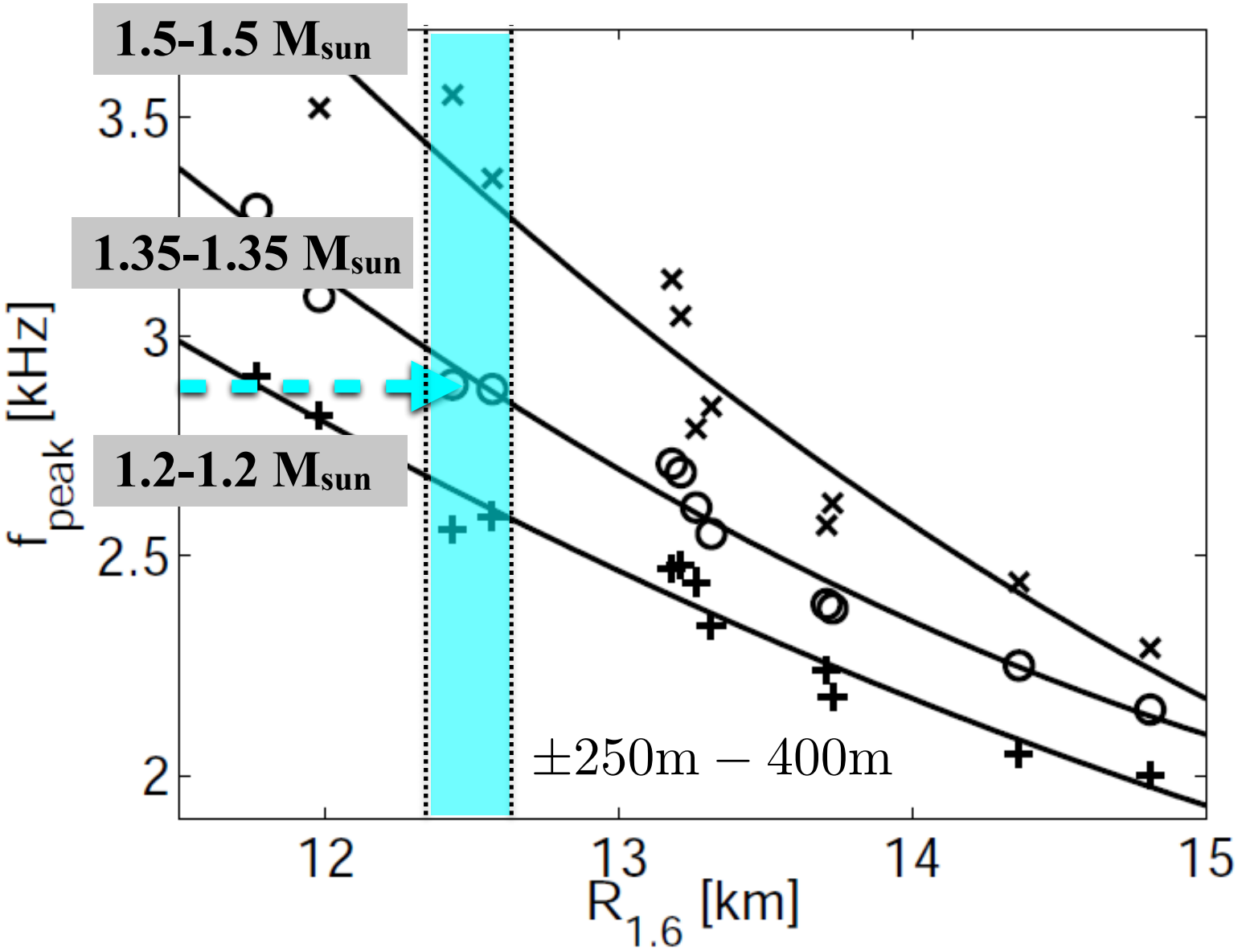

Principal Component Analysis (PCA)

Clark, Bauswein, NS, Shoemaker (2016)

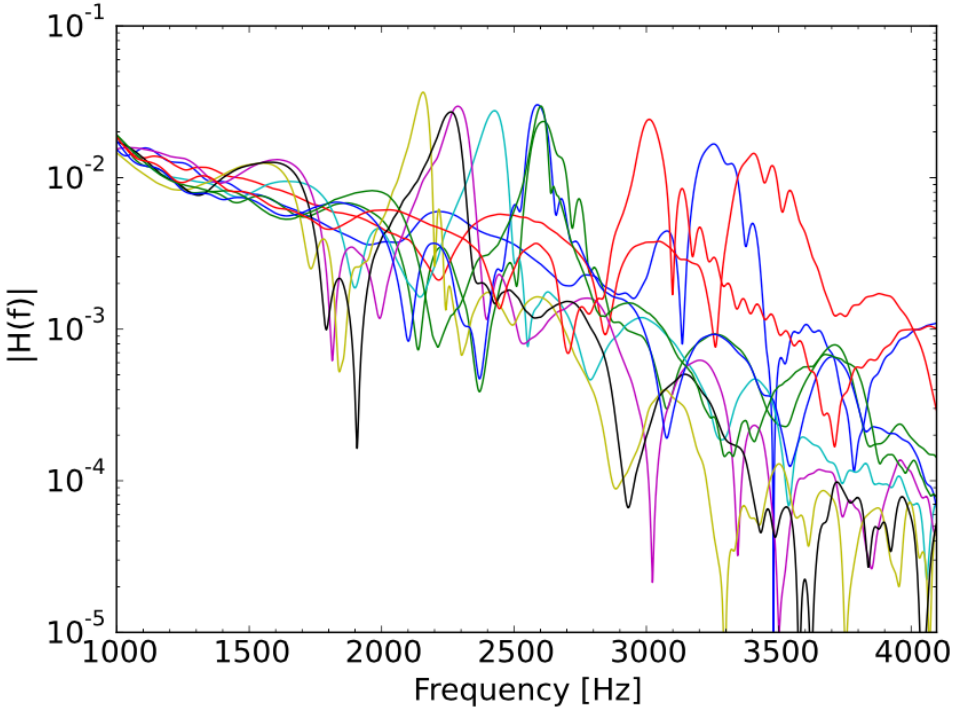

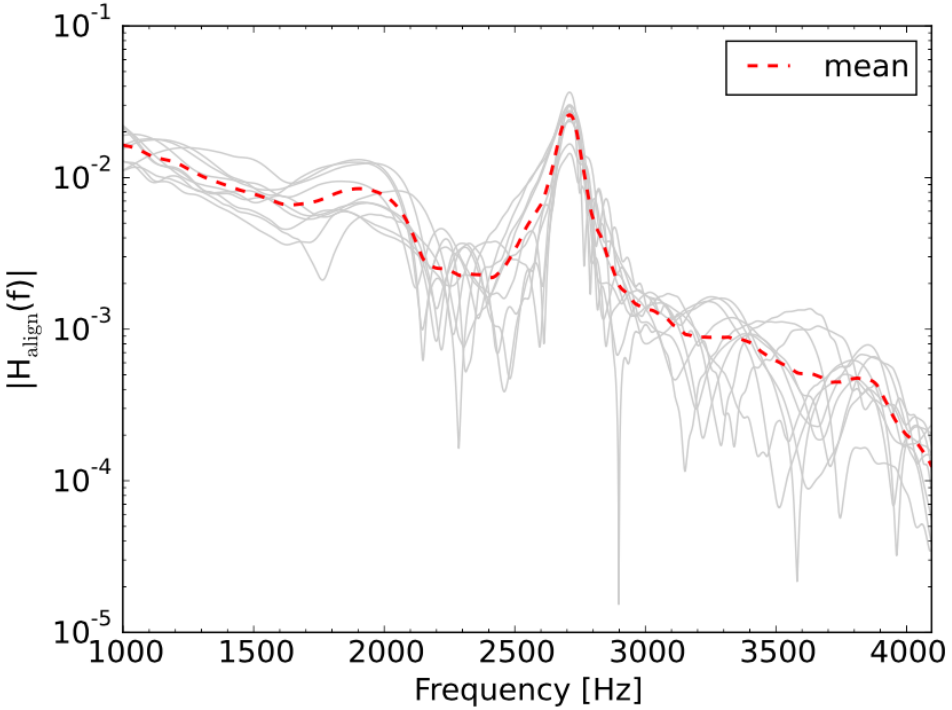

Actual fft's for different models.

Rescaled to common reference model.

Our PCA template extracts >90% of signal power compared to only 40% when using simple burst analysis.